Technical Report

# TURBULENT DIFFUSION IN A SIMULATED VEGETATIVE COVER

by

Motoaki Yano

U.S. Army Research Grant
DA-AMC-28-043-65-G20

Fluid Dynamics and Diffusion Laboratory
College of Engineering
Colorado State University
Fort Collins, Colorado

May 1966



CER66MY25

TABLE OF CONTENTS

TABLE OF CONTENTS - continued

## LIST OF TABLES

## LIST OF FIGURES

LIST OF FIGURES - continued

LIST OF FIGURES - continued

## LIST OF SYMBOLS

| Symbol | Definition | Dimension |
|---|---|---|
| $A(x)$ | Constant of velocity function of superposed wake | |
| $B(x)$ | Constant of velocity function of superposed wake | |
| $B$ | Constant of velocity function of superposed wake | |
| $b$ | Width of Gaussian wake | $L$ |
| $b_{\frac{1}{2}}$ | Half width of Gaussian wake | $L$ |
| $b_i$ | Half width of $i$ combination wakes | $L$ |
| $C$ | Coefficient of Gaussian wake function | |
| $\bar{C}$ | Time mean value of diffusive element | $\frac{M}{L^3}$ |
| $C'$ | Fluctuation value of diffusive element | $\frac{M}{L^3}$ |
| $c_p$ | Coefficient of specific heat at constant pressure | $\frac{L}{t}$ |
| $C_D$ | Drag coefficient of Gaussian wake | |
| $C_{Di}$ | Equivalent drag coefficient on $(i + 1)$ th roughness element | |
| $d$ | Diameter of cylindrical elements | $L$ |
| $\tilde{e}$ | Coefficient of molecular diffusion | $\frac{L^2}{T}$ |

| Symbol | Definition | Dimension |
|---|---|---|
| $\overline{Fx}$ | Flux of turbulent diffusive element | |
| F | Function of maximum velocity of $u_1$ of Gaussian wake in x-direction | |
| f | Function of vertical velocity defect $u_1$ of Gaussian wake | |
| G | Function of equivalent drag coefficient of $C_{Di}$ | |
| h | Height of roughness elements | L |
| K | Coefficient of turbulent diffusion | $\frac{L^2}{T}$ |
| Km | Coefficient of turbulent diffusion concerning momentum | $\frac{L^2}{T}$ |
| $K_H$ | Coefficient of turbulent diffusion concerning heat | $\frac{L^2}{T}$ |
| $K_i$ | Coefficient of turbulent diffusion on (i + 1) th roughness element of the rough surface | $\frac{L^2}{T}$ |
| $K_z$ | Coefficient of turbulent diffusion in vertical z-direction | $\frac{L^2}{T}$ |
| $Kx_i$ | Coefficient of turbulent diffusion in $x_i$-direction | $\frac{L^2}{T}$ |
| k | Karman constant | |
| L | Stability length scale | L |
| $L_*$ | Stability length scale (when $\alpha' = 1$) | L |
| $\ell$ | Scale of turbulence | L |

| Symbol | Definition | Dimension |
|---|---|---|
| Mi | Momentum loss on ith roughness element on the rough surface | $\frac{M}{LT^2}$ |
| $p_1$ | Exponent of power function $C_{Di}$ | |
| $p_2$ | Exponent of power function F(x) | |
| $p_3$ | Exponent of power function b | |
| Q | Strength of point source | $\frac{M}{T}$ |
| q | Vertical heat flux | $\frac{M}{T^3}$ |
| Ri | Richardson number | |
| S(k) | Energy density at given wave number k | |
| T | Temperature | t |
| $T_o$ | Temperature on surface | t |
| T' | Fluctuation of temperature | t |
| $T_*$ | Turbulent shear temperature | t |
| t | Time scale | T |
| $U_o$ | Ambient velocity | $\frac{L}{T}$ |
| $\overline{U}_\epsilon$ | Velocity defect of the completely superposed wake on rough surface | $\frac{L}{T}$ |
| $u_1$ | Velocity of a Gaussian wake ($u_1 = U_o - \tilde{u}$) | $\frac{L}{T}$ |
| $u_*$ | Turbulent shear velocity | $\frac{L}{T}$ |

## LIST OF SYMBOLS - continued

| Symbol | Definition | Dimension |
|---|---|---|
| $u'$ | Fluctuation value of velocity | $\frac{L}{T}$ |
| $\bar{u}$ | Time mean value of velocity | $\frac{L}{T}$ |
| $\tilde{u}_i$ | Velocity defect of i superposed wakes | $\frac{L}{T}$ |
| $u_{1.i}$ | Velocity defect of the wake generated by (i + 1) th roughness element | $\frac{L}{T}$ |
| $\overline{u'w'}$ | Shear turbulence in vertical direction | $(\frac{L}{T})^2$ |
| $w'$ | Vertical fluctuation value of velocity | $\frac{L}{T}$ |
| $w'_i$ | Vertical turbulent fluctuation of i combination wakes | $\frac{L}{T}$ |
| $w'_{(i)}$ | Vertical turbulent fluctuation of wake generated by (i-1) th roughness element | $\frac{L}{T}$ |
| $\bar{X}, \bar{Y}, \bar{Z}$ | Position of released marked particle after time t | L |
| $x_i$, x, y, z | Components of Cartesian coordinate with origin at front base corner of rough surface | L |
| $\alpha, \alpha'$ $\alpha'', \gamma$ | Constant concerning the results given from the turbulent energy balance in shear flow | |
| $\beta$ | Constant concerning Gaussian wake | |
| $\varepsilon$ | Time of dissipation energy of turbulent shear flow | $\frac{ML^2}{T^3}$ |
| $\tau$ | Turbulent shear stress | $\frac{M}{LT^2}$ |

| Symbol | Definition | Dimension |
|---|---|---|
| $\phi$ | Universal function of Eulerian similarity applied to turbulent shear flow | |
| $\lambda$ | Constant concerning vertical turbulent $w'$ | |
| $\sigma_w^2$ | Variance of vertical turbulent fluctuation | $(\frac{L}{T})^2$ |
| $\sigma_y$ | Standard deviation of Gaussian profile in y-direction | L |
| $\bar{\sigma}_y$ | Width between the $\frac{1}{2} C_{max}$ points in the profile of y-direction | L |
| $\bar{\sigma}_z$ | Width between the $C_{max}$ and $\frac{1}{2} C_{max}$ points in the profile of z-direction | L |
| $\delta$ | Height of boundary layer | L |
| $\nu$ | Kinematic viscosity | $\frac{L^2}{T}$ |
| $\Lambda_c$ | Scale of turbulent eddies | L |
| $\psi$ | Probability function of diffusion element | |
| $\Delta$ | Distance between the roughness elements | L |
| $\rho$ | Mass density | $\frac{M}{L^3}$ |

ACKNOWLEDGMENTS

The author wishes to express his special appreciation to his Major Professor, Dr. J. E. Cermak, Professor-in-charge, Fluid Mechanics Program, under whom the author received guidance and advice.

Acknowledgment is also expressed for guidance and advice of the members of the Committee of his graduate studies -- Dean of Engineering College, Professor L. V. Baldwin; Professor H. Bailey; Professor W. E. Marlatt; and Professor R. N. Meroney. (This technical report is also prepared as a Ph. D. dissertation by the author).

The author would like to express his sincere thanks to Mr. J. F. Krakowski, Mr. R. Moore, Mr. W. W. Wallen, Mr. D. Jarmann, and Mr. A. Gorove for technical assistance in the experimental work.

The author is greatful to Mr. T. J. Evatz, and Mr. and Mrs. S. Koehler for instructive suggestions on English composition.

For typing of this dissertation and drawing of the figures, the author is greatful to Mrs. M. Fox, Mrs. S. Yoder, Mrs. S. Murray, Mrs. L. Roberts, Mrs. B. Campen, and Miss H. Akari, and owes a special debt to his wife, Mrs. H. Yano.

Financial support for this study was provided by the Integrated Army Meteorological Wind Tunnel Research Program under Grant DA-AMC-28-043-65-G20.

Chapter I

# INTRODUCTION

Turbulent diffusion is a peculiar kind of phenomena occurring in transport processes. The phenomena of turbulent diffusion can be found in the processes of heat, mass and momentum transfer. The process is produced by the random motion of turbulent eddies contained generally in wind flow. The process of turbulent diffusion may be treated as a stochastic process (13). This process is a random irreversible process. This means that the distribution of a stochastic variable of the process is not related to the initial distribution after sufficiently long times.

The main study of the process of turbulent diffusion is to follow the process until the turbulent diffusive phenomenon reaches its final status.

The basic equation describing turbulent diffusion was developed by Richardson (30) from the macroscopic viewpoint in 1926. Also a famous theory relating the Lagrangian correlation coefficients to the turbulent diffusion process was developed by Taylor (36) in 1921.

On the other hand, the understanding of transport processes has been also advanced by the study of the molecular motion of dilute gases (37, 421)*. Some studies (14, 93) of the interrelation between turbulent and molecular diffusion do exist; however, their results must be used with caution, because turbulent diffusion is associated with mixing on a macro-scale while molecular diffusion refers to the motion of discrete molecules (18, 459).

A more practical way to develop the analogy between transfer by motion of turbulence and individual molecules is to consider the similarity of the flux produced by the molecular diffusion and the small scale turbulent diffusion which are both represented by a mean characteristic velocity and scale length (18, 32) and (34).

When the dispersion time of turbulent diffusive particles is greater than the Lagrangian scale of turbulence. The result of Taylor's theory is considered to be similar to that for Brownian motion developed by Einstein. Since Einstein's result can be obtained from the diffusion law stated by Fick, and considering the turbulent diffusion in an isotropic homogeneous field may be represented by Fick's law, the coefficient of the turbulent diffusion of Fick's law may be represented by Taylor's theory (17, 213).

In this dissertation, the author does not discuss turbulent diffusion from the purely theoretical viewpoint; instead it is considered from the viewpoint of the macroscopic laws of turbulent

---

* The second number in a parentheses refers to a particular page of the reference specified by the first number.

diffusion which are now believed to be valid for turbulent flow (17, 216). Also, this turbulent diffusion is related to the subject of transport processes in the lower atmosphere of the earth. Physical quantities diffused by the turbulence are mass, momentum, and heat.

Predominate factors that influence diffusion in the atmospheric surface layer are shown by Monin (18, 29) to be the following:

1. Nature of the diffusion source whether continuous or instantaneous, constant or variable, point or line or volume source, etc.
2. Characteristics of the turbulent wind, which determines the transporting hydrodynamical process.
3. Interaction of the diffusing quantity with the earth or water surface.

Wind-tunnel model similarity to the prototype of atmospheric surface layer is also very important. Much remains to be learned about the proper similarity criteria; therefore this aspect is still being explored in the Fluid Dynamics and Diffusion Laboratory.

In this paper, the experimental studies are not considered in relation to any specific prototype. The similarity between the laboratory model and the prototype is not discussed here.

A rough surface giving an idealized representation of vegetative cover was installed in the wind tunnel and the characteristics of the turbulent shear flow and of helium gas diffusion above and within this rough surface were studied. The results of this study of turbulent diffusion may be applied to analyze turbulent diffusion phenomena in the atmospheric surface layer having irregular surface conditions by using the concept and procedure of this study.

# Chapter II

## REVIEW OF THE PROBLEM

According to the concept of Reynolds, the turbulent diffusive elements are assumed to consist of the superposition of the mean and fluctuation values.

Adapting this concept to the macroscopic equation of turbulent diffusion of a property $\bar{C}$ whose measure per unit mass of air yields the following equation:

$$\frac{\partial \bar{C}}{\partial t} + \frac{\partial}{\partial x_i}(\bar{u}_i \bar{C}) = \frac{\partial}{\partial x_i}\left(\tilde{e}\frac{\partial \bar{C}}{\partial x_i} + \overline{u_i' C'}\right)$$

$$\frac{\partial \bar{C}}{\partial t} + \frac{\partial}{\partial x_i}(\bar{u}_i \bar{C}) = \frac{\partial}{\partial x_i}\left[\left(\tilde{e} + K_{x_i}^{*}\right)\frac{\partial \bar{C}}{\partial x_i}\right] \qquad (2\text{-}1)$$

where $Kx_i$ is the coefficient of turbulent diffusion or the eddy diffusivity of a property $\bar{C}$. The equation (2-1) is a basic equation of representing the process of turbulent diffusion. In this equation, when the distributions of mean velocities $\bar{u}_i$ and the coefficients of turbulent diffusion $Kx_i$ are obtained, the characteristics of the diffusive property $\bar{C}$ can be obtained. Therefore, these mean

---

* Refer to the following section.

velocities and the coefficient of turbulent diffusion are very important in the studies of turbulent diffusion, and are reviewed in the following sections.

## Coefficient of Turbulent Diffusion

The coefficient of turbulent diffusion is effectively defined by a linear relation of the flux $\bar{F}$ of the turbulent diffusive property $\bar{C}$.

$$\bar{F}_{x_i} = -\rho K_{x_i} \frac{\partial \bar{c}}{\partial x_i} = \overline{(\rho u_i') c'} \qquad (2\text{-}2)$$

The concept of the similarity between molecular and turbulent motion shows that the coefficient of turbulent diffusion K is

$$K = \overline{u' \ell} \qquad (2\text{-}3)$$

where $\ell$ is the scale of turbulent motion analogous to the mean free path of molecular motion.

In the above discussion, the element of the turbulent diffusive property $\bar{C}$ is not limited to any particular one. Therefore, an analogous relation may be expected between the coefficients of the turbulent diffusion and the different elements (28).

Recently, in a Cartesian coordinate, the coefficient of turbulent diffusion has been discussed in the turbulent shear flow in the vertical wind direction only. There are some trial studies of the coefficients in other directions. Classically, when the logarithmic law represents the vertical wind profile of the turbulent shear flow, the coefficient of turbulent diffusion of momentum is given by

$$K_m(z) = k\, u_* z = k^2 z^2 \frac{du}{dz} \tag{2-4}$$

Pasquill (26) suggests several methods for calculating the coefficient of turbulent diffusion of momentum. He classifies it into three types according to the relation between the coefficient and the turbulent energy.

1. <u>The High-Frequency Energy Method (small scale turbulence)</u>

Based on the Kolmogoroff (20) similarity theory of the turbulence on the dimensional grounds, the energy density at a given wave number S(k) in the high frequency range is

$$S(k) = c\,\varepsilon^{2/3} k^{-5/3} \tag{2-5}$$

where $\varepsilon$ is the rate of dissipation

$$\varepsilon \approx \overline{u'w'} \frac{du}{dz} = K_m \left(\frac{du}{dz}\right)^2 \tag{2-6}$$

in a neutral shear flow case. Given measurements of S(k) over the appropriate range of wave numbers, and the vertical gradient of mean wind velocity, the above two equations provide a means of determining K (24).

## 2. The Total Energy Method

In thermally unstable and neutral air, the turbulent velocity corresponds to total energy and the turbulent scale length directly proportional to the height above the ground. Panofsky introduced the above suggestion. Then

$$K_m = A \sigma_w z \qquad (2\text{-}7)$$

where A is constant, and

$$\sigma_w^2 = \int_0^\infty S(n)\, dn \qquad n = ku$$

## 3. The Low-Frequency Energy Method (large scale turbulence)

Using the results of Taylor's theory and assuming the linear relation between the Lagrangian and the Eulerian time scales of turbulence with $\beta'$ being the ratio between the scales, for the time of travel $T = \beta' T'$, the coefficient is $2K = \beta' T [\sigma_w^2]_{T'}$, for large T'. Since T has to be several times greater than the Lagrangian time scale of turbulence, the averaging time T' accordingly has to be several times greater than the Eulerian time scale. Thus, K is determinable from a knowledge of $\beta'$ and of the energy on the low frequency side of the spectrum (since large averaging time spectrum).

In the thermally stratified field, the coefficient of the turbulent diffusion is related to a stability scale length introduced by

Monin and Obukhoff. Therefore, in the following sections which review the similarity hypotheses, the coefficient in the nonneutral case is reviewed at the same time.

## Eulerian Similarity Hypothesis

The concept of similarity in the turbulent shear flow is based on the possibility that the vertical distributions of mean velocities at different downwind distances have the same shape and can be made coincident by appropriate changes in the scale of length and velocity.

There are two basic similarity hypotheses for the study of turbulent diffusion in the lower atmosphere.

One is the Eulerian similarity developed by Monin and Obukhoff (23) in the case of a stationary and horizontally homogeneous turbulence. The hypothesis is that the turbulent regime is completely determined by the parameters $u_* = \sqrt{\frac{\tau}{\rho}}$ and $\frac{q}{C_p \rho}$ which do not vary with altitude in the surface layer, and by the universal parameter $\frac{g}{T_0}$. Therefore, the only scale of velocity in the surface layer is $u_*$ and the only scale of length is the value

$$L = \frac{u_*^3}{\frac{kg}{T_0}\left(-\frac{q}{C_p \rho}\right)}$$

The following results may be obtained from this hypothesis:

$$\frac{du}{dz} = (u_*/kz)\,\phi_1(z/L) \text{ and } u(z) = \frac{u_*}{k}\left[f\left(\frac{z}{L}\right) - f\left(\frac{z_0}{L}\right)\right] \quad (2\text{-}8)$$

$$\frac{dT}{dz} = \frac{T_*}{z}\,\phi_2(z/L) \text{ where } T_* = -\frac{1}{ku_*}\frac{g}{C_p\rho} \quad (2\text{-}9)$$

$$K_m(z) = \frac{ku_*z}{\phi_1(z/L)}, \quad K_H = \frac{ku_*z}{\phi_2(z/L)} \quad (2\text{-}10)$$

Assuming that

$$K_m = K_H \equiv K, \qquad \phi_1\left(\frac{z}{L}\right) = \phi_2\left(\frac{z}{L}\right) \equiv \phi\left(\frac{z}{L}\right)$$

Richardson number is defined for

$$R_i = \frac{g}{T_0}\frac{dT/dz}{\left(\frac{du}{dz}\right)^2} = \frac{z}{L}\frac{1}{\phi\left(\frac{z}{L}\right)}$$

so that K may be expressed as

$$K = k\,u_*\,L\cdot R_i$$

When $\left|\frac{z}{L}\right| \ll 1$

$$\phi\left(\frac{z}{L}\right) \approx 1 + \gamma\frac{z}{L}$$

then

$$u(z) = \frac{u_*}{k}\left(\ln\frac{z}{z_0} + \gamma\frac{z}{L}\right) \quad (2\text{-}11)$$

Utilizing this hypothesis, Monin and Kazansky give the maximum velocity of the vertical propagation of the diffusion (18, 334) as

$$(\overline{w'^2})^{1/2} = \lambda u_* \psi\left(\frac{z}{L}\right) \tag{2-12}$$

where $\lambda$ is constant. Using the turbulent energy balance equation, the following results are obtained

$$\left(\frac{\overline{w'^2}}{u_*^2}\right)^2 \propto (1 - \alpha R_i) \tag{2-13}$$

from which

$$\psi\left(\frac{z}{L}\right) = (1 - \alpha R_i)^{1/4} = \left[1 - 1/f'\left(\frac{z}{L}\right)\right]^{1/4} \tag{2-14}$$

and from

$$\frac{dx}{dt} = u \qquad \frac{dz}{dt} = (\overline{w'^2})^{1/2}$$

$$\frac{dx}{dz} = \frac{1}{k\lambda} \frac{f\left(\frac{z}{L}\right) - f\left(\frac{z_0}{L}\right)}{\left[1 - 1/f'\left(\frac{z}{L}\right)\right]^{1/4}} \tag{2-15}$$

Ellison, Townsend, Monin-Kazansky, Yamamoto, Panofsky and others discussed the above similarity theory, and reached identical results. In this study Yamamoto's results are presented as a representation of all these works. Yamamoto obtains the coefficient of turbulent diffusion by using the energy balance of the turbulent motion. This theory is reexamined by Calder (3) who referred to Richardson's (29) previous formulation

$$K_m = kz\,u_* \,(1 - \alpha R_i)^{1/4} \tag{2-16}$$

Yamamoto (39) also shows that $\phi(\frac{z}{L})$ is defined by

$$\phi^4 + \left(\frac{z}{L}\right)\phi^3 - 1 = 0 \tag{2-17}$$

Panofsky obtains Yamamoto's result by using dimensional analysis. Yamamoto gives the approximate solution of $\phi$ as

$$\phi\left(\frac{z}{L}\right) = \exp\left(-\frac{1}{4}\frac{z}{L}\right) + \frac{\left(\frac{z}{L}\right)^{5/3}}{\left[\left(\frac{z}{L}\right)^2 + 25\right]} \qquad \text{for } \frac{z}{L} > 0 \tag{2-18}$$

$$\phi\left(\frac{z}{L}\right) = \exp\left(-\frac{3}{4}\left|\frac{z}{L}\right|\right) + \left|\frac{z}{L}\right| - \frac{\left|\frac{z}{L}\right|^{5/3}}{\left[\left|\frac{z}{L}\right|^{\frac{12.5}{3}} + 9.87\right]} \qquad \text{for } \frac{z}{L} < 0 \tag{2-19}$$

Hamuro and Shono (33) solved the Yamamoto-Panofsky equation of $\phi$

$$\phi = 1/4\left\{\sqrt{\zeta^2 - \delta^2 + 2\zeta^2(1 + \zeta/\delta)} - \delta - \zeta\right\} \qquad \text{for } \zeta > 0 \tag{2-20}$$

$$\phi = 1/4\left\{\sqrt{\zeta^2 - \delta^2 + 2\zeta^2(1 - \zeta/\delta)} + \delta - \zeta\right\} \qquad \text{for } \zeta < 0 \tag{2-21}$$

where

$$\delta^2 = \tfrac{1}{2}\left\{\left(\sqrt{\zeta^4 + \tfrac{256}{7}} + \zeta^2\right)^{1/3} - \left(\sqrt{\zeta^4 + \tfrac{256}{7}} - \zeta^2\right)^{1/3}\right\}^3 ; \quad \zeta = \frac{z}{L}$$

## Lagrangian Similarity Hypothesis

The second type of similarity is the Lagrangian similarity hypothesis which was developed by Batchelor (1) and (2). He suggests that the similarity concept may be also applied to the turbulent velocity field described in the Lagrangian manner in a nearly neutral condition.

According to the Lagrangian similarity hypothesis, the statistical properties of the velocity of a marked fluid particle at time $t$ after leaving the ground depend only on $u_*$ and $t$. Also, the statistical properties of the velocity of a marked particle at time $t$ after release at height $h$ are the same as those of a particle leaving at the ground ($z = 0$) at the instant $-t_1$, provided $t \gg t_1$, where $t_1$ is expected to be of the order of magnitude of the time-scale of the turbulence at height $h$, that is, of the order $h/u_*$. This hypothesis was discussed by Gifford (11), Cermak (4) and others.

Establishment of an exact relation between the Eulerian and the Lagrangian quantities is usually difficult, but Batchelor suggests that the similarity hypothesis makes this relationship possible. It follows from this hypothesis that the probability distribution of the position of a particle released at the ground at $t = 0$ --defining a kind of "cloud" of marked fluid in probability--retains the same shape at $t$ with an increase of length scale proportional to $u_* t$. The mean horizontal speed of a particle at time $t$ is, by definition, the average of the horizontal speed of an ensemble of marked particles at time $t$ spread about the mean position $(\bar{X}, \bar{Z})$ over a vertical range which increases with $u_* t$; and must remain in a fixed relationship with the mean horizontal speed of the fluid at points between the ground and a height which increases linearly with $t$. There seems to be no reason why the mean speed of particles at time $t$ should be equal to the mean speed of the fluid at the mean position of the particles at time $t$, but it must be equal to the mean speed of the fluid at some constant times the mean height of the particles.

At a time $t$ after being released the mean position of the marked particles is $\bar{X}(t)$, $\bar{Y}(t)$, $\bar{Z}(t)$ and

$$\frac{d^2\bar{Z}}{dt^2} \propto u_*/(t-t_1)$$

$$\bar{Y} = 0$$

$$\frac{d^2\bar{X}}{dt^2} \propto u_*/(t-t_1) \qquad (2\text{-}22)$$

since $\frac{d\bar{Z}}{dt}$ is to be finite for all time

$$\frac{d\bar{Z}}{dt} = b u_*$$

where b is constant

Integration of the last of Eq. (2-22) given

$$\frac{d\bar{X}}{dt} = a u_* \log \frac{t+t_1}{t_0+t_1} \qquad (2\text{-}23)$$

where a is constant

Referring to the above discussion

$$\frac{d\bar{X}}{dt} = u(\bar{Z}) = \frac{u_*}{k} \ln \frac{C\bar{Z}}{Z_0}$$

where C is constant

$$\frac{d\bar{X}}{d\bar{Z}} = \frac{1}{bk} \ln \frac{C\bar{Z}}{Z_0} \qquad (2\text{-}24)$$

The average concentration from the continuous point source of the particle released must be a function of the following

$$C_{cp} = Q_{cp} \int_0^\infty \psi \left( \frac{X-\bar{X}}{\bar{Z}}, \frac{Y}{\bar{Z}}, \frac{Z-\bar{Z}}{\bar{Z}} \right) \frac{dt}{\bar{Z}^3} \qquad (2\text{-}25)$$

on dimensional grounds, where $Q_{cp}$ is strength of the point source. At ground level ( y = 0, z = 0 )

$$C_{cp} \propto \frac{Q_{cp}}{\bar{Z}^2(x)\, \bar{u}(\bar{Z})} \qquad (2\text{-}26)$$

Cermak (4) assumes $C_{cp} \propto x^{m_{cp}}$ and uses a logarithmic profile for the vertical velocity distribution to obtain

$$m_{cp} = -\left(kb\frac{\bar{x}}{z_0}\right)\left(\frac{1 + 2\ln\left(\frac{\bar{z}}{z_0}\right)}{\frac{\bar{z}}{z_0}\ \ln^2\left(\frac{\bar{z}}{z_0}\right)}\right) \qquad (2\text{-}27)$$

in the neutral case.

Also in a thermally stratified case, using Swinbank's (35) velocity distribution, the exponent $m_{cp}$ is

$$m_{cp} = -\frac{bk\left(\frac{\bar{x}}{z_0}\right)}{\left(\frac{\bar{z}}{z_0}\right)}\left\{\frac{2\ln\left(\frac{\bar{z}}{z_0}\right) + \frac{z_0}{L}\left(\frac{\bar{z}}{z_0} - 1\right) + \frac{z_0}{L}\left(\frac{\bar{z}}{z_0}\right) + 1}{\left[\ln\frac{\bar{z}}{z_0} + \frac{z_0}{L}\left(\frac{\bar{z}}{z_0} - 1\right)\right]\left[\ln\frac{\bar{z}}{z_0} + \frac{z_0}{L}\left(\frac{\bar{z}}{z_0} + \frac{1}{4}\frac{\bar{z}}{z_0}\ln\frac{\bar{z}}{z_0} - 1\right)\right]}\right\}$$

(2-28)

## Turbulent Shear Flow

The characteristics of turbulent shear flow have been studied during the last half century, but there are still many difficulties encountered when these characteristics are analyzed.

Classically, there are some concepts concerning the character of the flow; for example, Prandtl's mixing length theory, skin friction law, law of the wall, etc. (21) and (32) which are not well satisfied in the turbulent shear flow, even if the results are used for expedience.

Inoue (15) suggests the following physical structure of the turbulent shear flow on the flat plate in the wind tunnel: the turbulent shear flow is created by the results of the interaction of the energy between the mean ambient uniform flow with velocity and the plate surface. As a result of the interaction, the energy dissipates the magnitude of ($U_0^2 - u^2$), where u is the local velocity of the shear flow. Therefore, it may be considered that momentum loss sources spread on the surface of the plate and that these momentum losses are diffused by turbulent eddies and molecular motion to the region of the turbulent shear flow. Generally, in the turbulent shear flow, the diffusivity of the turbulent eddies is larger than that due to molecular motion.

When the short length of the plate is set in the wind tunnel, this plate is viewed the same as an equivalent line source of momentum loss from far downwind distance, turbulent shear flow is considered a combination of turbulent wakes.

Using the turbulent-energy-balance equation and the scale of large turbulent eddies which seem to determine the energy dissipation, the vertical wind profile is given by

$$\frac{du}{dz} \propto \frac{(\overline{w'^2})^{1/2}}{\Lambda_0(z)} \qquad (2\text{-}29)$$

where $\Lambda_0(z)$ is the scale of the eddies and assumed to be proportional to the height z , also $(\overline{w'^2})^{1/2}$ is assumed constant.

The results of Inoue are the same as those given by the logarithmic law of Prandtl's theory.

Recently, Coles (6) proposed the consideration of turbulent shear flow which is called the law of the wake while as an extension of the law of the wall. He examined practically all available experimental data on turbulent boundary layers in terms of the logarithmic form of the law of the wall, and he concluded that the flow has a wake-like character. A linear combination with the law of the wall is then proposed as an over-all similarity law representing the complete profile for equilibrium and nonequilibrium flows alike.

Hence the vertical wind profiles are given by

$$\frac{u(z)}{u_*} = \frac{1}{k} \ln\left(\frac{u_* z}{\nu}\right) + C + \frac{\Pi(x)}{k}\, \omega\left(\frac{z}{\delta}\right) \tag{2-30}$$

where C is a constant equal to 5.1, $\Pi(x)$ is expressed in the terms of skin friction coefficient $C_f$ and $\omega\left(\frac{z}{\delta}\right)$ is a universal wake function.

In the thermally stratified case, the turbulent shear flow is discussed in many works based on the similarity hypothesis. In the nearly neutral case, Hamuro and Shono (33) show that this case means $\left|\frac{z}{L_*}\right| < 1.755$

where $L_* = \frac{L}{\alpha}$ , $\alpha = \frac{K_H}{K_m}$

and the vertical wind profile is given by

$$u(z) = \frac{u_*}{k}\left(\ln z/z_0 + \frac{\alpha'}{4}\frac{z}{L}\right) \tag{2-31}$$

In the unstable case $\frac{z}{L_*} \gg 1$

$$\frac{ku}{u_*} = -3L_*^{1/3}\left(z^{-1/3} - z_0^{-1/3}\right) + \frac{1}{5}L_*^{1/3}\left(z^{-5/3} - z_0^{-5/3}\right) \tag{2-32}$$

In the stable case $\frac{z}{L_*} << -1$

$$\frac{ku}{u_*} = -\frac{1}{L}(z - z_0) + \frac{L_*^3}{3}\left(z^{-3} - z_0^{-3}\right) \tag{2-33}$$

These results are given by Shono and Hamuro (33) who solved the Yamamoto-Panofsky equation for $\phi(\frac{z}{L})$ and substituted it into the basic equation of the similarity hypothesis.

These results also coincide with the solutions of Kazansky-Monin and Yamamoto.

The analysis of the turbulent shear flow with a change in rough surfaces in the downwind distance was studied by Elliott (9). He concluded that there were two turbulent shear flows -- one for each surface.

Recently, Elliott (9), Miyake (22) and Panofsky-Townsend (25) discussed the growth of a new turbulent boundary layer generated by the downwind rough surface (called an internal boundary layer). In the thermally neutral case, the thickness of the boundary layer $\delta$ is

$$\delta = (0.75 - 0.03 \ln \frac{z_0}{z_0'}) z_0^{0.2} x^{0.8} \qquad \text{by Elliott} \qquad (2\text{-}34)$$

or

$$x = \frac{1}{kAD} \frac{u_*'}{u_*} \delta [\ln \frac{\delta}{z_0'} - 1] \qquad \text{by Miyake} \qquad (2\text{-}35)$$

or

$$\delta = [1 + 0.28 (\frac{z_0}{z_0'})^{0.3}] z_0^{0.2} x^{0.8} \qquad \text{by Panofsky-Townsend} \qquad (2\text{-}36)$$

where $z_0'$ is the roughness length of the upstream surface, $z_0$ is the roughness length of the downstream surface, and

$$\frac{dz}{dt} = D\sigma_w = DAu_*$$

where D and A are constant.

Classically, almost the same study was developed by Jacobs (19) who assumed the shear stress distribution, and analyzed the wind profile.

Miyake (22) analyzed the growth of the internal boundary layer in the thermally stratified case also.

# Chapter III

# EXPERIMENTAL EQUIPMENT AND TECHNIQUES

The object of the experimental studies was to obtain data on mean wind velocity, temperature, and helium gas concentration over the elements of a rough surface and also between them in a wind tunnel, in order to analyze the process of turbulent diffusion. Helium gas was used as a tracer for this diffusion process.

Experimental equipment and techniques used in the study are described in this chapter. The equipment and techniques are discussed separately in two sections titled as Equipment of Wind Tunnel, and Measuring Equipment and Techniques. Experimental techniques for determining the wake of a cylinder are also described in the last section of this chapter. This experiment is the preliminary study of turbulent diffusion over the rough surface.

## Equipment of Wind Tunnel

The large wind tunnel of the Fluid Dynamics and Diffusion Laboratory of Colorado State University was used for the experimental studies of turbulent diffusion discussed later in this dissertation.

The structure of this wind tunnel of circulating type is shown in Fig. 1. The dimensions of the test section of the wind tunnel are:

| | | |
|---|---|---|
| 80 ft | in | x-direction |
| 6 ft | in | y-direction |
| 6 ft | in | z-direction |

where the reference coordinators (x, y, z) of the experimental studies are shown in Fig. 2. A turbulence stimulator consisting of a sawtooth strip and a sheet of gravel are placed at the test section entrance. The upstream 40 ft length of test section is a thermally neutral floor. The downstream 40 ft length of test section is a thermally controlled floor which can be heated by electric heaters or cooled by circulating cold brine. The entire wind tunnel is thermally insulated. Ambient air temperature in the wind tunnel can be controlled by passing the air through cooling and heating coils placed in the return flow section. The slope of the test section roof is adjustable in order to produce the condition of zero pressure gradient in the flow direction.

The rough surface that was used to simulate vegetative cover was placed over the downwind 40 ft length of the test section of the wind tunnel as shown in Fig. 3. Therefore, the upstream 40 ft of the test section was a smooth surface. The simulated rough surface was comprised of ten roughness plates. Each roughness plate consisted of a base aluminum plate (1/4 in. x 4 ft x 6 ft) and the small vertical wooden cylinders corresponding to roughness elements were 3/16 in. in diameter and 1 3/4 in. in height. The separation distances $\Delta$ between the cylinders were 1 in. in the downwind direction (x-direction) and in the lateral direction (y-direction). The air speed in the wind tunnel can be adjusted in the range of 5 to 60 ft/sec. However, all experiments employed a mean ambient wind velocity of 10 ft/sec. Also the pressure gradient in the downwind direction was adjusted to zero by adjustment of the roof slope.

## Measuring Equipment and Techniques

The mean wind speeds were obtained by using a pitot tube. The pitot tube was installed on a vertical carriage so that the vertical position of the pitot tube could be changed continuously by the driving action of a small DC motor. The output of pressures from the pitot tube was connected to a "transonic" electric pressure transducer. The two electric signals from the vertical position potentiometer and the pressure difference (dynamic and static) of the pitot tube, formed the input to an x-y plotter. The vertical pressure difference profiles were obtained directly in graphical form from the x-y plotter. Between the pressure difference $\Delta p$ and wind velocity $u$, there is the following relation based on Bernoulli's equation

$$u = K\sqrt{\Delta p}$$

where K is a constant dependent on air temperature and atmospheric pressure. These two quantities were measured in each experimental study. The Transonic error is less than 1% (pressure) when compared with an alcohol tilting pressure tube. The position error of the vertical carriage signal is less than 1/16 in. The mean velocity profiles were taken over and between the elements of the rough surface along the center line (y = 0) of the mid-point between elements. The wind tunnel flow was adjusted to be thermally neutral, stable, or unstable cases. The ambient air and floor temperatures during heating or cooling of the air are described in the following discussion concerning the experiments with temperature gradients.

Mean temperature was measured with a copper-constantan thermo-couple and a Honeywell Type 153 recorder having a range of $0^0 \sim 350^0$F. The error of this equipment was $\pm\ 1^0$F. The time-response of this thermo-couple was not sufficiently sensitive. Therefore, the temperature in the turbulent diffusion field was measured point by point over and between the rough surface elements. The mean temperature data were obtained for vertical profiles taken along the centerline (y = 0) of the wind tunnel. The temperature conditions of the wind tunnel were:

stable case -- $\left\{ \begin{array}{l} \text{floor temperature was } 20^{0}\text{F and the} \\ \text{ambient air temperature was } 160^{0}\text{F} \end{array} \right.$

unstable case -- $\left\{ \begin{array}{l} \text{floor temperature was } 300^{0}\text{F and the} \\ \text{ambient air temperature was } 40^{0}\text{F} \end{array} \right.$

Pure helium gas (Grade A, AIRCO nearly 100% $(\frac{\text{vol.}}{\text{vol.}})$) was used as a tracer for the turbulent diffusion experiment. Experimental equipment for the diffusion measurements included such equipment as a gas injection unit, gas suction unit, and gas detector unit. A continuous point source of gas was made from a 1/16 in. nozel attached to the tube of the gas injection unit. The suction unit employed the same type of tube as did the injection unit. The gas flow rates of both units were measured by flow meter and controlled. Gas flow rate for most experiments was 100 cc/min (0.56 in./sec). In the experiments where measurements were made of gas concentration at a large distance from the source, the injection flow rate was 900 cc/min (5.04 in./sec) or more. The flow rate of gas into the sampling system was 200 cc/min (1.12 in./sec) in both of the above cases. The gas detector was a mass spectrometer, model MS9AS of the Vacuum-Electronics Corp. (Vecco). The horizontal and vertical gas concentration profiles were obtained at several sections in the downwind direction from each continuous point source which was placed at several positions along the centerline ($y = 0$) of the test section. Positions of the source and the profile are in the experimental data. The time-response of this whole equipment was insufficient to measure concentration fluctuations. The concentration was obtained point by point over and between the elements of the rough surface. The mass-spectrometer was not stable for continuous use. Therefore it was necessary to calibrate the mass-spectrometer for each run of the experiment. Standard mixing gases of nitrogen and helium of three types (N: 99.5%, He: 0.5%; N: 99.8%, He: 0.2%; N: 99.95%, He: 0.05%) were used for this calibration.

## Measuring Equipment and Techniques to Study Wakes of Cylinders

In order to confirm the concept of combination of wakes generated by aligned cylinders, the following equipment and techniques of measurement were considered. The concept of combination of wakes was applied to analyze the characteristics of turbulent shear flow on the rough surface, as shown in Fig. 3.

### (A) Horizontal Cylinders Aligned in Horizontal Plane

In the uniform flow zone (outside of boundary layer) of the wind tunnel, each lateral (y-direction) wooden cylinder having 3/16 in. diameter (the same diameter of the roughness element of the rough surface as shown in Fig. 3) and 2 ft length in the y-direction (simulated enough to infinite length cylinder of the experiment) was placed in the horizontal plane (x-y place, z = 3 ft) with separation distance $\Delta$ = 1 in. between each cylinder. Each horizontal cylinder (y-direction) was normal to wind direction as shown in Fig. 4. First, a cylinder was placed in its position and the velocity profile, a two-dimensional Gaussian wake, was measured in the vertical sections along downwind direction behind the center point of the cylinder. After measuring the first cylinder's wake, a second cylinder was placed in its position and the velocity profile of the combination wake for the first and second cylinders was measured at the same vertical section where the wake of the first cylinder was measured. This measuring technique for combination wakes of two cylinders was repeated for the cases of three cylinders, four cylinders, and so on, up to six cylinders.

(B) Irregularly Aligned Horizontal Cylinder

The cylinders in the above case (A) were placed in a horizontal section. In this case (B), the same cylinders used for case (A) were aligned in two horizontal planes in the uniform flow. The cylinders were placed alternately in each horizontal place. In the downwind direction, the separation distance of each cylinder was 1 in. ( $\Delta$ = 1 in.). The two horizontal planes were separated by a distance of 0.35 in. in one case, and by 0.75 in. in the other case, as shown in Fig. 10. Behind these cylinders, two-dimensional combination wakes were measured by using the same technique as described for case (A).

(C) Semi-Infinite Aligned Cylinders

In order to examine the wakes generated by the ends of the aligned cylinders for case (A), the ends of the cylinders were aligned on a straight line along the downwind direction (x-direction) in a uniform flow. The combination wakes were measured downstream from the ends of the cylinders by using the same technique as described in case (A).

(D) Finite Cylinders in Turbulent Shear Flow

Only along the base center line (x-direction, $y = z = 0$), finite vertical cylinders were aligned on this centerline with the separation distance $\Delta = 1$ in. in turbulent shear flow. The cylinders were the same as the cylinders comprising the rough surface, as shown in Fig. 3. Behind the cylinders, velocity profiles in the three-dimensional wakes were measured by using the same technique as described for case (A).

(E) Rows of Cylinders in the y-direction in Turbulent Shear Flow

In case (D), ends of the cylinders were aligned only on a straight line along the x-direction. In this case (E), each row of cylinders (aligned on a line in the y-direction) was aligned in x-direction, with a separation distance $\Delta = 1$ in. in turbulent shear flow. Each cylinder was the same as the cylinders of the rough surface. The combination wake was measured by using the same procedure used for case (A).

# Chapter IV

## THEORETICAL STUDY

The process of turbulent diffusion is related to the random motion of turbulent eddies (or vortices) contained in a turbulent diffusive medium. The motion of these turbulent eddies is determined by the energy they contain. The energy balance of turbulent eddies is discussed from two different aspects. One aspect is the local energy balance of turbulent motion. The other is the energy balance among different sizes of turbulent eddies.

Concerning stationary turbulent shear flow in a thermally neutral condition, the above two basic concepts of the energy of turbulent motion are discussed briefly as follows (3). Local energy balance of turbulent motion for two-dimensional mean motion in unit time and unit mass may be represented by Eq. (4-1)

$$\underbrace{-\overline{u'w'}\frac{\partial \bar{u}}{\partial z}}_{(\mathrm{I})} \underbrace{- \frac{\partial}{\partial z}\left\{\frac{1}{2}\overline{(u'^2+v'^2+w'^2)w'}+\frac{1}{\rho}\overline{p'w'}\right\}}_{(\mathrm{II})} = \underbrace{\varepsilon}_{(\mathrm{III})} \qquad (4\text{-}1)$$

The meaning of each term of Eq. (4-1) is as follows: term (I) is energy production obtained from mean wind flow by the shear stress; term (II) is energy diffusion which transports the energy from one point to another, and term (III) is energy dissipation transformed to heat through viscosity of the fluid flow. This equation is valid when the flow is essentially invariant in the x-direction. Equation (4-1) may be rewritten as follows, as shown in Ref. (26).

$$-\overline{u'w'}\,\frac{\partial \bar{u}}{\partial z} = \varepsilon$$

or (4-2)

$$K_m \left(\frac{\partial \bar{u}}{\partial z}\right)^2 = \varepsilon$$

This form is approximately valid for the lower 10% of a turbulent boundary layer. The time rate of energy dissipation $\varepsilon$ is represented by Eq. (4-3), except for regions very close to the wall.

$$\varepsilon = \nu \left[ 2\overline{\left(\frac{\partial u'}{\partial x}\right)^2} + 2\overline{\left(\frac{\partial v'}{\partial y}\right)^2} + 2\overline{\left(\frac{\partial w'}{\partial z}\right)^2} + \overline{\left(\frac{\partial u'}{\partial y} + \frac{\partial v'}{\partial x}\right)^2} \right.$$

$$\left. + \overline{\left(\frac{\partial u'}{\partial z} + \frac{\partial w'}{\partial x}\right)^2} + \overline{\left(\frac{\partial v'}{\partial z} + \frac{\partial w'}{\partial y}\right)^2} \right] \qquad (4\text{-}3)$$

When the motion of the part of turbulence which is responsible for the viscous dissipation is isotropic, the expression for the turbulent energy dissipation, Eq. (4-3) can be simplified. Using the continuity equation and the definition of isotropy, Eq. (4-3) reduces to

$$\varepsilon = 15\nu\overline{\left(\frac{\partial u'}{\partial x}\right)^2} = 15\nu\frac{\overline{u'^2}}{\lambda}$$
$$= \frac{15\nu}{2}\overline{\left(\frac{\partial u'}{\partial z}\right)^2} \tag{4-4}$$

where $\lambda$ is the size of the smallest turbulent eddies (micro-scale).

Concerning the energy of each size of the turbulent eddies, the fundamental physical concept of turbulent flow was developed by Kolmogoroff (20) and Obukhov (24). A turbulent flow at large Reynolds number is considered to be the result of imposing disturbances of all possible scales of turbulent eddies. In these turbulent eddies, the largest eddies arise directly from the instability of the mean flow. The motion of turbulent eddies is unstable except the eddies of the smallest size of which characteristic Reynolds number is less than the critical value of the stability condition of viscous flow. The unstable condition of the turbulent eddies produces the subdividing action of turbulent eddies to the eddies having smaller scale of the second order, and energy of the large eddies transfers to the smaller eddies. However, energy of the smallest size eddies is dissipated as heat. The motion of turbulent eddies, except for the largest ones, may be assumed locally homogeneous isotropic and also quasi-stationary. And for all eddies except the smallest ones, the characteristic Reynolds number is large and the viscosity has no appreciable effect on their motion.

## Superposition Concept for Momentum Defect of Wakes

In order to study the turbulent diffusion over the rough surface described in Chapter III, first it is necessary to obtain the characteristics of the turbulent shear flow. Observing the geometrical structure of the rough surface, as shown in Fig. 3, turbulent shear flow on the rough surface is considered to be produced by effects from each roughness element. These effects on turbulent shear flow may be considered to have wake characteristics. Because, considering each roughness element of the rough surface, the element should produce a wake in the downwind direction. Turbulent shear flow on the rough surface may be considered as a combination of the wakes generated by each roughness element of the surface. If a valid combination principle and the flow characteristics of the wakes of the element can be found, turbulent shear flow may be analyzed by methods of wake combination.

Consider first a problem of greater simplicity, the case of a two-dimensional wake having a Gaussian profile which is created by a circular cylinder of infinite length placed normal to a uniform flow. If an array of infinite cylinders is formed in the downwind direction with a separation distance $\Delta$ between the cylinders, and is placed in a horizontal plane in the uniform flow as seen in Fig. 4, a turbulent shear flow is expected. This experimental arrangement was utilized for the exploratory study of combination of wake characteristics in this chapter.

The following two questions finally evolve when the second cylinder is set in the wake of the first cylinder. What is the wake created by the second cylinder? What is the wake formed from combination of the wakes of the first and second cylinders?

At long downwind distance, the two cylinders look like a single equivalent cylinder, therefore, the wind flow should be a two-dimensional wake having a Gaussian profile. The first cylinder, of course, has a two-dimensional wake having a Gaussian profile. Therefore, the wake generated by the second cylinder can be assumed to be a two-dimensional wake having a Gaussian profile.

The next question is, what is the combination law for the wakes produced by the first and second cylinders? A simple combination may be a superposition of the wake. The elements for the superposition may be momentum defect flux of the wakes.

It is generally assumed that the turbulence of the turbulent diffusion field is not influenced by the existence of the diffusion source. In the case of the wake, however, the turbulence is transformed by the source from the original isotropic to the nonisotropic turbulence. However, it may be still assumed that the wake turbulence is quasi-isotropic. Therefore, time rate of energy dissipation of a wake in unit mass is represented by (Townsend, 1949)

$$\varepsilon \propto 15\nu \frac{\overline{u'^2}}{\lambda}$$

The energy is equal to $\frac{1}{2}(\overline{u'^2}+\overline{v'^2}+\overline{w'^2})$ in unit mass. Assuming quasi-isotropy, this energy is proportional to $\frac{3}{2}\overline{u'^2}$

then
$$\frac{d}{dt}\left(\frac{3}{2}\overline{u'^2}\right) \propto -15\nu \frac{\overline{u'^2}}{\lambda}$$

When two wakes are mixed and the largest turbulent eddies of each wake are assumed to be created independently by instability of mean flow of each wake, then

$$\overline{u'^2}_{\text{two wakes}} = \overline{u'^2}_{\text{first wake}} + \overline{u'^2}_{\text{second wake}}$$

The energy of eddies for both wakes only transfers to eddies of the smaller size and there is little interaction between the same size of eddies. The total energy dissipation for two wakes is considered, therefore assumed to be a direct superposition of the energy dissipation for each wake

$$\varepsilon_{\text{two wakes}} = \varepsilon_{\text{first wake}} + \varepsilon_{\text{second wake}} \qquad (4\text{-}5)$$

The turbulent intensity $\overline{u'^2}$ of a wake has a characteristic similar to that of the momentum defect $(U_0 - u)^2 \equiv \tilde{u}^2$ for the wake (38, 135).

$$\overline{u'^2} \propto (U_0 - u)^2 \equiv \tilde{u}^2$$

Then the following relation should exist

$$\tilde{u}^2_{two\ wakes} = \tilde{u}^2_{first\ wake} + \tilde{u}^2_{second\ wake} \qquad (4\text{-}6)$$

On the other hand, from Eq. (4-2) locally,

$$-\overline{u'w'}\frac{\partial u}{\partial z} \propto -\overline{w'^2}\frac{\partial u}{\partial z} = -\overline{w'^2}\frac{\partial(U_0 - \tilde{u})}{\partial z}$$

$$\overline{w'^2}\frac{\partial \tilde{u}}{\partial z} \propto \varepsilon_{turbulent\ shear\ flow}$$

where $\qquad \varepsilon_{\text{turbulent shear flow}} = \sum \varepsilon_{\text{wake}}$

$$\sum \varepsilon_{wake} \propto \frac{d}{dt}(\sum \overline{u'^2_{wake}}) = 2(\sum \overline{u'^2_{wake}})^{1/2}\frac{d}{dt}(\sum \overline{u'^2_{w}})^{1/2}$$

then

$$\varepsilon_{t.s.f.} \propto \frac{d}{dt}\sum \overline{u'^2_{w.}} = (\overline{w'^2})^{1/2}_{t.s.f.}\frac{d}{dz}(\sum \overline{u'^2_{w.}})$$

where

$$\overline{w'^2}_{t.s.f.} \propto \sum \overline{w'^2_{w.}} \propto \sum \overline{u'^2_{w}}$$

then

$$\varepsilon_{t.s.f.} \propto \overline{w'^2}_{t.s.f.}\frac{d}{dz}(\sum \overline{u'^2_{w}})^{1/2}$$

$$\left(\overline{w'^2}\frac{\partial \tilde{u}}{\partial z}\right)_{t.s.f.} \propto \overline{w'^2}_{t.s.f.}\frac{d}{dz}(\sum \overline{u'^2_{w.}})^{1/2}$$

Therefore, locally

$$\tilde{u}^2_{t.s.f.} \propto (\Sigma\, \overline{u'^2_{w.}})^{1/2} \propto (\Sigma\, \tilde{u}^2_{w.})^{1/2}$$

The mean velocity defect $\tilde{u} = u_1$ of a wake having a two-dimensional Gaussian profile is defined as the following (31, 601)

$$u_1(x, z) = u_{1max}(x) \cdot \left\{1 - \left(\frac{z}{b_{1/2}}\right)^{3/2}\right\}^2 \equiv u_{1max} \cdot f \qquad (4\text{-}7)$$

$$b_{1/2}(x) = \sqrt{10}\,\beta\sqrt{C_D}\, d \left(\frac{x}{d}\right)^{1/2} \equiv C_2 \cdot \frac{1}{F(x)} \qquad (4\text{-}8)$$

$$u_{1max}(x) = U_0 \frac{\sqrt{10}}{18\beta}\sqrt{C_D}\left(\frac{x}{d}\right)^{-1/2} \equiv U_0\, C_1 F(x) \qquad (4\text{-}9)$$

and

$$C\,F(0^+) \equiv 1 \qquad \text{for } x = 0^+$$

$$f \equiv 1 \qquad \text{for } z = 0$$

The concept of superposition of the momentum defect of wakes is applied to two-dimensional wakes for the cylinders aligned in a horizontal plane. First, considering two cylinders, the combination of momentum defects of wakes $(\tilde{u}_1)^2$ is

$$(\tilde{u}_1)^2 = (u_{1,0})^2 + (u_{1,1})^2$$

where $(u_{1,0})^2$ is the momentum defect of the wake of the first cylinder and $(u_{1,1})^2$ is the momentum defect of the second cylinder.

$$(\tilde{u}_1)^2 = [u_{1,0\,max}(x) \cdot f]^2 + [u_{1,1\,max}(x-\Delta) \cdot f]^2$$

$$= [U_0 C_1 F(x) \cdot f]^2 + [U_1 C_1 F(x-\Delta) \cdot f]^2$$

$$\text{for } x > \Delta$$

along the wake axis

$$[\tilde{u}_1(x,0)]^2 = [\tilde{u}_{1max}]^2 = [u_{1,0\,max}(x)]^2 + [u_{1,1\,max}(x-\Delta)]^2$$

$$= [U_0 C_1 F(x)]^2 + [U_1 C_1 F(x-\Delta)]^2$$

at $\quad x = \Delta + 0^+$

$$[\tilde{u}_{1max}(\Delta)]^2 = [U_0 C_1 F(\Delta)]^2 + [U_1 C F(0^+)]^2$$

also

$$[\tilde{u}_{1max}(\Delta)]^2 = U_0^2$$

then

$$U_0^2 = [U_0 C_1 F(\Delta)]^2 + U_1^2$$

and

$$U_1^2 = U_0^2 [1 - C_1^2 F^2(\Delta)]$$

The function F(x) and $f(b_{1/2}(x), z)$ for the wake are assumed the same for each wake by the discussion of this section. The coefficient $C_1$ includes the drag coefficient $C_D$, therefore, $C_1$ for the first cylinder is not equal to that for the second cylinder. However, in the following relationship $C_1$ for any cylinder is assumed to be the same as for the first cylinder. If $C_1$ is only dependent on the apparent ambient velocity $U_i$ of the cylinder, then $U_i \approx U_0$ and

$$C_D \propto U_i^{-1/4} \qquad (U_i = 1 \sim 10 \text{ ft/sec.}) \text{ -- } (31,\ 16)$$

Therefore, the above assumption may be valid.

Considering three cylinders, the momentum defect of combination wake $\tilde{u}_2$ is

$$(\tilde{u}_2)^2 = (u_{1,0})^2 + (u_{1,1})^2 + (u_{1,2})^2$$

$$= [U_0 C_1 F(x) \cdot f]^2 + [U_1 C_1 F(x-\Delta) \cdot f]^2 + [U_2 C_1 F(x-2\Delta) \cdot f]^2$$

$$\text{for } x > 2\Delta$$

Along the wake axis, at $x = 2\Delta + 0^+$

$$[\tilde{u}_{2max}(2\Delta)]^2 = [U_0 C_1 F(2\Delta)]^2 + [U_1 C_1 F(\Delta)]^2 + U_2^2$$

$$[\tilde{u}^2_{max}(2\Delta)]^2 = U_0^2$$

$$U_2^2 = U_0^2 - [U_0 C_1 F(2\Delta)]^2 - [U_1 C_1 F(\Delta)]^2$$

Therefore, the combination of wakes behind (n + 1) cylinders

$$(\tilde{u}_n)^2 = \sum_0^n [U_i C_1 F(x - i\Delta) \cdot f]^2 \tag{4-10}$$

$$(\tilde{u}_{n\,max})^2 = \sum_0^n [U_i C_1 F(x - i\Delta)]^2 \tag{4-11}$$

$$\text{for } x > n\Delta$$

and

$$U_i^2 = U_0^2 - \sum_0^{i-1} [U_r C_1 F(\overline{i - r\Delta})]^2$$

$$= U_0^2 - \sum_0^{i} [U_r C_1 F(\overline{i - r\Delta})]^2 + U_i^2$$

$$U_0^2 = \sum_0^{i} [U_r C_1 F(\overline{i - r\Delta})]^2 \tag{4-12}$$

Equation (4-10) and Eq. (4-12) are the equations which determine the velocity profile perpendicular to the plane of aligned cylinders.

Before further discussion about the velocity profile perpendicular to the plane of aligned cylinder, the width of the combined wakes which corresponds to the boundary layer thickness and the coefficient of turbulent diffusion are discussed. This is necessary because the wake function $f(b_{1/2}(x), z)$ includes the wakes widths.

## Coefficient of Turbulent Diffusion

From the conservation of momentum of the air flow behind (i + 1) aligned cylinders (x-direction) of the cylinder surface in a uniform flow is obtained

$$\rho \int_{-\infty}^{\infty} \tilde{u}_i (U_0 - \tilde{u}_i)\, dz = \frac{\rho}{2} C_{Di} U_0^2 d \tag{4-13}$$

where $C_{Di}$ is the equivalent drag coefficient of these (i + 1) cylinders. Considering (i + 1) cylinders in the uniform flow, and observing the flow in the downwind distance from (i + 1) cylinders, the wind flow can be represented by a two-dimensional Gaussian wake. But in this expression of the flow the drag coefficient $C_{Di}$ is not a constant and $C_{Di}$ should be a function of $(x - i\Delta)$.

$$\tilde{u}_{i\,max} = const. \cdot U_0 [C_{Di} (x - i\Delta)]^{1/2} F(x - i\Delta) \tag{4-14}$$

$$\text{for } x > i\Delta$$

On the other hand, according to the concept of superposition of momentum defect of wakes, from Eq. (4-11)

$$\tilde{u}_{i\,max} = [\sum_0^i (U_r C_1 F(x - r\Delta))^2]^{1/2}$$

$$= U_0 \cdot C \cdot \sqrt{C_D} \, [\sum_0^i (\frac{F(x-r\Delta)}{F(x-i\Delta)} \frac{U_r}{U_0})^2]^{1/2} \cdot F(x-i\Delta)$$

$$= U_0 \cdot C \cdot \sqrt{C_D \, G(x-i\Delta)} \cdot F(x-i\Delta) \tag{4-15}$$

where $$G(x-i\Delta) = \sum_0^i [\frac{F(x-r\Delta)}{F(x-i\Delta)} \frac{U_r}{U_0}]^2$$

Equations (4-14) and (4-15) should be identical. Therefore, $C_{Di}$ is

$$C_{Di} = C_D \sum_{0}^{i} \left[ \frac{F(x-r\Delta)}{F(x-i\Delta)} \frac{U_r}{U_0} \right]^2$$

$$= C_D \, G(x-i\Delta) \qquad (4\text{-}16)$$

At $x \gg i\Delta$, $\quad \dfrac{F(x-r\Delta)}{F(x-i\Delta)} \approx 1$

$$C_{Di} = C_D \sum_{0}^{i} \left( \frac{U_r}{U_0} \right)^2$$

when $(x-i\Delta) \ll 1$, $\quad F(x-r\Delta) \approx F(\overline{i-r\Delta})$

$$\left[ \sum_{0}^{i} \left( U_r C_1 F(\overline{i-r\Delta}) \right)^2 \right]^{1/2} = U_0$$

$$C_{Di} = C_D$$

At the short distance x from the ith cylinder, the wakes generated by each cylinder of ith, (i - 1) th ..., and (i - n) th position do not superpose on the wake completely. This wake is a completely superposed wake generated by the first (i - n) cylinders. The widths of wakes generated by the ith, (i - 1) th, ... (i - n) th cylinders are not the same width as the wake generated by the first (i - n) cylinders. The combination of the wakes behind the ith cylinder is considered to be the superposition of the (i - n) wake, the (i - n + 1) wake ... the (i + 1) wake in vertical direction perpendicular to the surface of cylinders as shown in Fig. 34. Therefore, Eq. (4-11) can be understood as Eq. (4-17)

$$\tilde{u}_i^2 = \sum_{i-n}^{i} [U_r C_1 F(x - r\Delta) \cdot f]^2 + \tilde{u}^2_{i-(n+1)}(x, z) \tag{4-17}$$

where $\tilde{u}_{i-(n+1)}$ is the completely superposed wake which has a Gaussian profile on the first (i - n) cylinders. And also at each vertical superposed zone of wakes, the corresponding vertical velocity fluctuation $(\overline{w_i'^2})^{1/2}$ can be assumed to be the superposition of the vertical velocity fluctuation for each wake $(\overline{w_{(r)}'^2})^{1/2}$

$$(\overline{w_i'^2}) = \sum_{0}^{i} (\overline{w_{(r)}'^2})$$

The width of wake $b_i$ can be determined by the vertical velocity fluctuation of $(\overline{w_{i\,max}'^2})^{1/2}$ (10, 342)

$$(\overline{w_{i\,max}'^2})^{1/2} \propto \frac{db_i}{dt} \propto U_0 \frac{db_i}{dx}$$

considering that

$$(\overline{w_{i\,max}'^2})^{1/2} \propto \tilde{u}_{i\,max}$$

then
$$b_i \propto \frac{1}{U_0} \int \tilde{u}_{i\,max}\, dx$$

For the zone of the ith superposed wake from Eq. (4-15)

$$(\overline{w'^2_{imax}})^{1/2} \propto v_0 \sqrt{C_D G(x-i\Delta)}\; F(x-i\Delta)$$

The function $G(x-i\Delta)$ may be expressed by a power function of $(x-i\Delta)$, also the function $F(x-i\Delta)$ is $(x-i\Delta)^{1/2}$. Finally, the width of the wake generated by ith cylinder $b_i$ is

$$\begin{aligned} bi &= \text{const.} \cdot \sqrt{C_D G(x-i\Delta)}\; (x-i\Delta)^{1/2} \\ &= \text{const.} \cdot \sqrt{C_D G(x-i\Delta)} \cdot d \cdot \frac{1}{F(x-i\Delta)} \end{aligned} \qquad (4\text{-}18)$$

Prandtl (refer 31, 603) suggests that the relation concerning the coefficient of the turbulent diffusion K for a wake is proportional to the production of maximum velocity defect and width of wake. This may be expected as $K \propto u_{imax} \cdot b$. The maximum defect velocity and width of the flow for combined wakes can be represented by a wake flow function through Eqs. (4-15) and (4-18). The coefficient of turbulent diffusion of the flow of combination wakes is

$$K_i = \text{const.} \cdot \tilde{u}_{imax} \cdot b_i \qquad (4\text{-}19)$$

in (i + 1) wakes combination zone.

The results of numerical calculation corresponding to each equation of combined wakes are shown in the following figures.

| | |
|---|---|
| Fig. 7 | Eq. (4-11) |
| Fig. 37 | Eq. (4-12) |
| Fig. 35 | Eq. (4-18) |
| Fig. 40 | Eq. (4-17) |
| Fig. 36 | Eq. (4-19) |

The theoretical study for combined wakes in this chapter is discussed only concerning the two-dimensional wake. The combination of wakes of three-dimensional (generated by spheres) can be treated the same as the case of two-dimensional wakes when the sources of wakes are only arranged on a straight line in x-direction. The characteristics of three-dimensional Gaussian wakes may be represented as the following -- (31, 595).

$$u_{1max} \propto U_0 (\beta^{-2} C_D)^{1/3} \left(\frac{x}{d}\right)^{-2/3} \equiv U_0 C_1 F(x) \tag{4-20}$$

$$b_{1/2} \propto (\beta C_D)^{1/3} \cdot d \cdot \left(\frac{x}{d}\right)^{1/3} \equiv C_2 \int F(x)\, dx \tag{4-21}$$

$$u_1(x,z) \equiv U_0 C_1 F(x) \cdot f(b_{1/2}, z) \tag{4-22}$$

By using the above relation, the results of calculation corresponding to the case of two-dimensional wakes are shown in each corresponding figure described in the above discussion. The treatment of this concept of combination of wakes on a general rough surface are discussed in Chapter VI of this dissertation.

Using the velocity profile and the coefficient of turbulent diffusion of momentum, the shear turbulence $\overline{u'w'}$ and the length scale of the turbulence $\ell$ can be calculated. In stationary turbulent shear flow with a thermally neutral condition, dissipation energy is equal to production energy

$$\frac{(\overline{w'^2})^{3/2}}{\ell} \propto \overline{u'w'} \frac{\partial u}{\partial z}$$

and $$\overline{u'w'} = K_m \left(\frac{\partial u}{\partial z}\right) \approx (\overline{w'^2})^{1/2} \ell \cdot \frac{\partial u}{\partial z}$$

then $$\frac{(\overline{w'^2})^2}{\overline{u'w'}} = \text{const.}$$

also $$\ell \propto \frac{K_m}{(\overline{u'w'})^{1/2}}$$

The calculated value of the shear turbulence $\overline{u'w'}$ and the length scale of the turbulence $\ell$ are shown in Figs. 41 and 42.

A surface consisting of an arrangement of heated cylinders which are the same as case (A) in Chapter III may be used to simulate the surface of unstable turbulent shear flow.

From the motion equation, the Reynolds stress in the wake of a heated cylinder is (32, 35)

$$\tau = -\bar{\rho}\,\overline{u'w'} + \bar{\rho}\,\frac{U_o}{\overline{\overline{T}}}\,\overline{T'w'} \qquad (4\text{-}23)$$

Assuming that the characteristics of the wake's temperature profile is the same as that of the velocity profile and that the coefficient of the turbulent heat diffusion is similar to the momentum, the Reynolds stress may be represented by

$$\tau = -\bar{\rho}\,\overline{u'w'}\,(1-\alpha'') \tag{4-24}$$

where

$$\alpha'' = \frac{U_0}{\bar{T}} \cdot \frac{\overline{T'w'}}{\overline{u'w'}} = -\frac{U_0}{\bar{T}} \cdot \frac{K_H}{K_m} \frac{\partial T/\partial z}{\partial u/\partial z} \tag{4-25}$$
$$= const.$$

Therefore, the coefficient of the turbulent diffusion of momentum in a thermally stratified wake is

$$K_{(\text{thermal wake})} = K_{(\text{neutral wake})}(1-\alpha'') \tag{4-26}$$

where $K \propto C_D$

Therefore, the coefficient of wake $C_l$ is

$$C_{l(\text{thermal wake})} = C_{l(\text{neutral wake})} \cdot \text{const.} \tag{4-27}$$

In the theoretical calculation of combination of wakes, when the coefficient of wake coefficient $C_l$ is taken to have a different value than for the neutral wake, the results can be obtained concerning the stratified combination wakes. The characteristic difference of the coefficients of the turbulent diffusion $K_i$ in a thermally stratified case is shown in Fig. 43. In this figure, if $K_2$ is assumed to correspond to the neutral case, then $K_3$ corresponds to the stable case and $K_1$ corresponds to the unstable case.

# Chapter V

## EXPERIMENTAL RESULTS OF COMBINATION OF WAKES

The purpose of the experiments for combined wakes generated by cylinders is to confirm the concept of superposition of momentum defect of wakes. Two- and three-dimensional Gaussian wakes were measured as described in Chapter III of this dissertation. Following the cases described in Chapter III, the characteristics of these wakes are discussed.

### Two-Dimensional Wakes

First, in order to obtain the coefficient of $C_1$ in Eq. (4-9) and $C_2$ in Eq. (4-8), that means $\beta$ and $C_D$ of the Schlichting's solution, single cylinder in uniform wind flow whose velocity was 10 ft/sec was examined. The Reynolds number concerning this cylinder in this case is 975, then $C_D = 1$ by using the reference graph of ($C_D$ & Re) (31, 16), and $\beta$ is 0.18 given by Schlichting (31, 602). Therefore,

$$C_1 = \frac{\sqrt{10}}{18\beta}\sqrt{C_D} = 0.975$$

$$C_2 = \sqrt{10}\,\beta\,\sqrt{C_D}\cdot d = 0.107 \text{ (in.)}$$

The results of the experiments concerning $u_{1\,max}$ and $b_{1/2}$ as shown in Figs. 5 and 6 were

$$C_1 = 0.83$$

$$C_2 = 0.048 \cdot \frac{b_{1/2}}{\sigma_z} = 0.048 \cdot \frac{0.5}{0.183} = 0.13$$

Even if the experimental results were satisfied with the function form of $u_1$ and $b_{1/2}$, the coefficients were slightly different from Schlichting's results. In the following discussion of this chapter, these values of $C_1 = 0.83$ and $C_2 = 0.13$ (in.) are used.

The experiment of case (A) described in the subsection of Chapter III gave the following results. Each experimental result satisfied the theoretical results.

| | | |
|---|---|---|
| Maximum velocity defect of combination of wake ($\tilde{u}_{i\,max}$) | in Fig. 7, | Eq. (4-11) and Eq. (4-12) |
| Maximum velocity defect of each wake in combination of wakes ($u_{1.i\,max}$) | in Fig. 8, | Eq. (4-9) with $U_i$ |
| Velocity profile of $u_{1.i}$ | in Fig. 9-A, | Eq. (4-7) |
| $u_{1.i}$ in Gaussian scale | in Fig. 9-B, | Eq. (4-7) |

Half width of combination of wakes $(b_i)$ in Fig. 35, Eq. (4-18)

From these results of theories and experiments, the momentum flux defect superposition of the wakes for aligned cylinders may satisfy the characteristics of the flow on aligned cylinders.

However, the superposition of wakes for the aligned cylinders is not a general case in the superposition of the wakes. The reason is that each cylinder is located at the maximum velocity position of $u_{1.i}$ of the upstream wake. Furthermore, the turbulent shear $\overline{u'w'}$ for the front wake is zero.

Two types of irregularly aligned cylinders are considered for the general combination of the wakes shown in Fig. 10 and in case (B) of Chapter III. The results of the combination of the wakes of the above irregular cylinders are shown in Figs. 11 and 12. It still seems that the concept of momentum flux defect superposition is satisfied in the case of irregularly aligned cylinders.

## Three-Dimensional Wakes

Next in uniform flow, the aligned cylinders of case (C) in Chapter III were used as the elements of the wakes.

Behind the cylinder, the cylinder appears to have infinite length except near the end zone of the cylinder. There, the wake should be a two-dimensional wake that is horizontal to the cylinder.

The wake behind the top edge zone of the cylinder may have a three-dimensional wake having a Gaussian profile of half. This wake connects to the two-dimensional wake generated by the central part of the cylinder. The wake behind the cylinder may transform from the combination of the two- and three-dimensional profiles to a three-dimensional wake in the downwind direction when the length of the cylinder is finite.

Interesting wakes for the turbulent shear flow are the wakes on the surface which are produced by the ends of the aligned cylinders. These wakes are the three-dimensional wakes generated by the top ends of the cylinders.

Concerning the wake generated by the top edge zone of the cylinder, it was confirmed that the wake has three-dimensional Gaussian characteristics by the experimental studies as shown in Figs. 13 and 14. From the experimental data, the coefficient of $C_1$ and $C_2$ which is related to the drag coefficient $C_D$ can be expressed as

$$\frac{u_1}{U_0} = 0.9 \left(\frac{x}{d}\right)^{-2/3} \qquad b_{1/2} = 0.22 \left(\frac{x}{d}\right)^{1/3} \quad (m)$$

These three-dimensional vertical wakes having a Gaussian profile of half are connected to the two-dimensional horizontal wakes generated by the central part of the cylinder, as shown in Fig. 15. Along the downwind distance, the position of the three-dimensional wake having a half Gaussian profile moves downward.

This means that the position of maximum velocity of $u_{1.0}$ transforms downward in the downwind direction, but the wake boundary (where the wake velocities are equal to the ambient velocity) also transforms downward in the downwind direction. However, the wake boundaries which are behind the second cylinder do not show clearly this movement in the downwind direction. These ends are located almost at the same height of the cylinder in the downwind direction, as shown in Fig. 16.

As shown in Fig. 17, the momentum flux defect superposition is satisfied in relation to these three-dimensional wakes having Gaussian profiles of half, even if the position in (vertical direction) are different between two wakes.

Next, when the cylinders of case (D) in Chapter III were set in the turbulent shear flow, the wakes behind the cylinder were again examined.

As described in Chapter IV, if the turbulent shear flow can be considered as a combination of wakes which are generated by each roughness element on the surface, it is possible to apply the concept of momentum flux defect superposition between turbulent shear flow and the wake generated by the cylinder set in the turbulent shear flow.

The single roughness element of the rough surface (as shown in Fig. 3) is selected for the experimental study of the wake in the turbulent shear flow. The results of the experiment of this wake are shown in Fig. 18. The three-dimensional wake, having a Gaussian profile of half, may exist behind the top edge zone of the cylinder element.

Applying the concept of momentum flux defect superposition to the combination wake with the turbulent shear flow, where the shear flow is assumed to have the same profile (decay characteristics were not obtained) in the downwind direction, the maximum velocity defect of $u_{1.0}$, and the half width $b_{1/2}$ of the wake generated by the top edge of the cylinder can be obtained as shown in Figs. 19 and 20. The data show that the wake is a three-dimensional Gaussian profile.

The concept of superposition is also confirmed by the experiments of the combined wakes of two and three cylinders. These results are shown in Figs. 21 and 22, and the drag coefficients of the wake of the second and third cylinders are found to have the same values as the case of uniform flow.

The vertical position of the end of the wakes relative to the cylinder does not vary much in short distances.

At a far downwind distance, it seems that the vertical position of the maximum value of $u_{1.i}$ of the wake finally reaches the base surface or some balancing position, and afterwards the ends of the wakes are developed upward.

At a far downwind distance from the cylinder element, it is rather difficult to distinguish the point of maximum three-dimensional wake velocity defect, because the transition between the three-dimensional and two-dimensional wakes is not clear. Therefore, the maximum velocity defect of $u_{1.i}$ of the three-dimensional wake shows the characteristics of the two-dimensional type, as shown in Fig. 19.

Behind the central part of the cylinder (this is the excluded parts of both end zones of the cylinder), the horizontal two-dimensional wake can be observed as shown in Figs. 23 and 24. In this case, the turbulent shear flow affected by the wake of a cylinder is also assumed to have the same profile in the downwind direction.

The vertical profile of the wind in this two-dimensional wake zone has a uniform profile as shown in Fig. 18. Referring to Fig. 25, the ratio of the velocities (under the concept of superposition of momentum defect) at different heights is

$$\frac{\overline{u_1^2}(x_0)}{\overline{u_2^2}(x_0)} = \frac{u_1'^2(x_0) + u_1''^2(x_0)}{u_2'^2(x_0) + u_2''^2(x_0)} = \frac{u_1'^2(x_0) + U_1^2 C_1^2 F^2(x_0)}{u_2'^2(x_0) + U_2^2 C_1^2 F^2(x_0)}$$

$$= \frac{u_1'^2(x_0) + [U_0^2 - u_1'^2(0)]\, C_1^2 F^2(x_0)}{u_2'^2(x_0) + [U_0^2 - u_2'^2(0)]\, C_1^2 F^2(x_0)}$$

$$= \frac{[u_1'^2(x_0) - u_1'^2(0)\, C_1^2 F^2(x_0)] + U_0^2 C_1^2 F^2(x_0)}{[u_2'^2(x_0) - u_2'^2(0)\, C_1^2 F^2(x_0)] + U_0^2 C_1^2 F^2(x_0)}$$

when $x_0$ is not a large distance as compared with $\Delta$

$$U_0^2 C_1^2 F^2(x_0) \gg [u_1'^2(x_0) - u_1'^2(0) C_1^2 F^2(x_0)]$$

$$U_0^2 C_1^2 F^2(x_0) \gg [u_2'^2(x_0) - u_2'^2(0) C_1^2 F^2(x_0)]$$

$$\bar{u}_1(x_0) = \bar{u}_2(x_0)$$

Therefore, the vertical profile of the velocity defect over the two-dimensional wake region is uniform.

The lower zone of the wind behind the cylinder is small and also combines two types of flow conditions which are the eddy wake flow and the shear flow. This eddy wake flow is generated by the downward flow along the front surface of the cylinder. Shear flow is regenerated by the smooth base boundary behind the element. The wake generated by the downward flow seems to be a three-dimensional wake.

Summarizing, the wake generated by a single roughness element in the turbulent shear flow is shown in the schematic diagram of Fig. 26.

The general characteristics of the wind profile behind the fifth cylinder are shown in Fig. 27. From this result, the top position of the combined three-dimensional wake is higher than that of the single element case, and is constant in height for a short distance. Therefore, it may be possible to suggest that the top edge position of these wakes is dependent on the initial wind characteristics and that the position of the maximum velocity defect of the wake finally reaches the equilibrium height with the eddy wake of the base. Afterwards the end of the wake advances upward.

The experimental results of case (E) in Chapter III are not much different from wakes generated by the single elements, at short downwind distances. In Figs. 28, 29, 30, and 31, the results of the experimental characteristics of the wakes of single and five rows are shown. Midway between two cylinders, the general wind profile of a wake generated by a single row of aligned cylinders is shown in Fig. 32.

From these experimental results, at far downwind distances, the wakes generated by a row of aligned cylinders are combined in the lateral direction. The wakes seem to show the same characteristics as the two-dimensional wakes of the infinite cylinder in the y-direction.

The general velocity profile behind the cylinder at the 188th row (24 ft.) aligned cylinder is shown in Fig. 33. The relative position of the maximum velocity defect $\tilde{u}$ of three-dimensional edge wakes is almost the same as the wake generated by a single element in the downwind direction.

# Chapter VI

## EXPERIMENTAL RESULTS OF TURBULENT DIFFUSION

The horizontal roughness plates described in Chapter III were used for the experimental studies of turbulent diffusion in the wind tunnel. The experimental data were obtained over and between the rough surface by following the techniques described in Chapter III. In the following section, the experimental results are discussed.

### Turbulent Shear Flow

In the downwind distance the transformation of the wind velocity profiles in the y- and the z-directions are shown in Figs. 44, 45, 46, 47 and 48.

From these vertical wind profiles, it may be possible to separate the profile into several zones that seem to have different flow characteristics.

Referring to Fig. 45, zone 1 is a region at the bottom of the roughness elements and near the leading edge of the rough surface. This zone is very small as compared with the other zones. The wind profile may be affected by the smooth base plate of roughness elements and the eddy flow generated by downward flow along the front surface of each roughness element. This zone decays in the downwind direction.

Zone 2 is also between the roughness elements. The wind velocity profiles have a uniform distribution in this zone. This zone corresponds to the horizontal two-dimensional wake zone of the vertical cylinder. The magnitudes of wind velocity and zone height decay in wind direction.

Zone 3 is a type of transition zone which connects zone 2 and zone 4. There is a question as to whether it is necessary to set this zone in the wind profiles. When the logarithmic or power law is applied to the wind velocity profile in zone 4, it is necessary to set this transition zone. There is not, however, much physical meaning to this zone. Inoue in 1965 (16) used lower atmospheric field wind data to suggest that the wind profile was of the exponential type. The zone's upper limit is not clear and it exists around the roughness top.

Zone 4 is the turbulent shear flow zone. The wind characteristic has been discussed by numerous papers (21) (30) and (32). The logarithmic or power law theory satisfies the experimental data in this zone. Zone 3 and zone 4 are considered and discussed by the combination of wakes in this dissertation.

Zone 5 is the outer turbulent shear flow zone. In this author's experiment this zone is another turbulent shear zone affected by front smooth bed. Therefore, the internal boundary layer exists between zone 4 and zone 5 .

Referring to Fig. 44, the horizontal wind velocity profiles are of the trigonometric function curve type corresponding between the roughness elements. Over the roughness element's zone, the profiles are uniform. In zone 3 of the vertical profile the horizontal wind profile shows a transition from the trigonometric profile to the uniform.

Even if the data of velocity profiles were obtained under the condition of stratified air, the experimental data could not obtain any remarkable differences between the data. It should be noted that there is a large temperature gradient between the top of the base roughness plate and the floor of the wind tunnel. This fact means that the actual thermal effect between the rough surface and the ambient wind flow is small. Also, the mechanical turbulence created by the rough surface is large when compared with the lesser thermal turbulence generated in the turbulent shear flow. Therefore, the thermal effects on turbulent diffusion are not apparent clearly in experimental results.

## Temperature Distribution

The data of the mean vertical temperature profiles of the experiments are taken by using the copper-constantan thermo-couple.

The measured vertical temperature profiles are shown in Figs. 49 and 50. At the corresponding vertical wind profile zones of Fig. 45 the temperature profiles have similar characteristics. In order to make clear the similarity between the wind profile and the temperature profile, the relations between the velocities and the temperatures at the same height $z$ are plotted in Figs. 51 and 52. It can be seen from these results that each zone of the vertical velocity profile has a linear relation between the velocity and temperature. Also, the above linear relations in zones 3 and 4 show the same characteristics.

From these experimental data of the velocity and the temperature profile, the considerable coefficients of the turbulent diffusion of momentum or heat are

| | | |
|---|---|---|
| Zone 1 | $K(z)$ | (linear) |
| Zone 2 | $K(z)$ | const. |
| Zone 3 | $K(z)$ | linear |
| Zone 4 | $K(z)$ | linear |
| Zone 5 | $K(z)$ | linear |

The same results were also found by Denmead (8) in the lower atmospheric field.

The stability length given by Monin and Obukhoff can be calculated by using the experimental data

$$L = \frac{u_*^3}{\frac{kg}{T_0}\left(-\frac{q}{C_p \rho}\right)} = \frac{u_*}{\frac{kg}{T_0}} \frac{K_m}{K_H} \frac{\partial u/\partial z}{\partial T/\partial z}$$

From the experimental data $\partial u/\partial z \Big/ \partial T/\partial z$ = constant

Therefore, $L \propto u_*(x)$

In Fig. 53, the above relation is shown by using the experimental data of zone 4 where the velocity profile is assumed to have the logarithmic profile for obtaining of $u_*$.

## Gas Concentration

Typical diffusion profiles and the longitudinal traces of the position of the maximum gas concentration are shown in Figs. 54 and 55. In the above experiment, the gas point sources are set on the rough surface at different distances from the leading edge of the rough surface. The profiles of the gas concentration in horizontal and vertical directions are shown in Figs. 56, 57 and 58. In the horizontal direction, the concentration profiles are of the Gaussian type. In the vertical direction, the profiles do not show the Gaussian type but do show approximately the half Gaussian profiles. The standard deviation and the width between the half maximum concentration points are shown in Figs. 59, 60 and 61.

A strong injection flow rate must be issued from the continuous point source in order to measure the concentration at the far distances from the source. Therefore, the concentration profiles near the source are affected by jet gas flow from the source.

From the experimental data (standard deviation and the concentration profile), it seems that the turbulence of the diffusion field over the rough surface is homogeneous horizontally.

When the concentration profiles in the horizontal and vertical directions show the Gaussian profiles, the decayed characteristics of the maximum concentrations (27, 190) in the longitudinal direction x is represented by

$$\bar{C}_{max}(x) \propto \frac{Q}{2\pi \bar{u} \tilde{\sigma}_y \tilde{\sigma}_z}$$

where the standard deviation $\tilde{\sigma}_y$ and $\tilde{\sigma}_z$ of the profile can be obtained from the experimental data which seem to satisfy the above condition over the rough surface approximately.

$$\tilde{\sigma}_y \propto x^{0.5}$$

$$\tilde{\sigma}_z \propto x^{0.8}$$

and $\tilde{u}$ is assumed independent of x locally. Therefore,

$$\bar{C}_{max}(x) \propto x^{-1.3}$$

This result is confirmed by the experimental studies shown in Figs. 62 and 63 over the rough surface.

Between the cylinders of the rough surface, the experimental data concerning maximum concentration of gas can be also obtained in the same way as the data over the rough surface, as shown in Figs. 60, 61 and 63.

$$\sigma_y \propto x^{0.5} \qquad \sigma_z \propto x^{0.8}$$

$$\bar{C}_{max}(x) \propto x^{-1.3}$$

When the point source is placed at x = 15 ft , the characteristics of turbulent diffusion are the same as the characteristics over the rough surface, because the flow zones 2 and 3 seem to be very small. On the other hand, when the point source is placed at x = 0 ft (the leading edge of the rough surface), the velocity and the coefficient of turbulent diffusion are functions of (x, y, z) even if these profiles seem to be uniform locally. Therefore, analyses of the data of maximum concentration of gas may contain more difficulties, even if the data show the same result over the rough surface.

# Chapter VII

# DISCUSSION

Theoretical studies based on the concept of combined wakes and the experimental studies in the wind tunnel made clear the characteristics of the turbulent diffusion on the rough surface.

In this chapter, the characteristics of turbulent shear flow are discussed by theories and experimental results. The characteristics of gas diffusion are also discussed by using the above shear flow characteristics.

## Turbulent Shear Flow

The velocity profile $\tilde{u}(x, z)$ of combined wakes described in Chapter IV is from Eq. (4-17)

$$\tilde{u}(x,z) = \left[ \sum_{i-n}^{i} [(U_r C_i F(x - r\Delta)) \cdot f]^2 + \tilde{u}^2_{i-(n+1)} \right]^{1/2}$$

$$i\Delta < x < \overline{i+1}\,\Delta$$

$$\approx \left[ \int_{\epsilon x}^{x} [U(\zeta) C_i F(x-\zeta)\, f]^2 d\zeta + \bar{U}_\epsilon^2(x,z) \right]^{1/2} \qquad (7\text{-}1)$$

where $U_r$ is defined as

$$U_0 = \left[\sum_{0}^{i} \left(U_r C_1 F(\overline{i - r\Delta})\right)^2\right]^{\frac{1}{2}}$$

$$\approx \left[\int_0^{\xi} [U(\xi) C_1 F(\xi - \zeta)]^2 d\zeta\right]^{\frac{1}{2}} \qquad (7\text{-}2)$$

$\epsilon x$ is an effective distance that corresponds to the distance of $x = (i - n)\Delta$, and $\overline{U_\epsilon}(x, z)$ is the completely superposed Gaussian profile wake generated by the front zone of rough surface which corresponds to the zone of the first $i-(n+1)$ cylinders. The velocity $U_i$ is defined by

$$Const = \int_0^{\xi} \frac{U^2(\zeta)}{(\xi - \zeta)} d\zeta \qquad (7\text{-}3)$$

in the combination of two-dimensional wakes.

The exact solution of equation (7-3) is unknown but the numerical solution is shown in Fig. 37. The velocity $U(\xi)$ seems to have a constant value locally in the downwind direction.

The application of the concept of combined wakes to the analysis of turbulent shear flow on a general rough surface is rather difficult. This difficulty arises because the roughness elements of the surface are generally scattered randomly the lateral y and the longitudinal x directions, the initial flow is not always uniform, etc.

On the rough surface described in Chapter III, the combination of wakes generated by each roughness element should be considered to superpose in the x and y directions. At the far downwind distance, the combination of wakes in the y-direction has a constant lateral velocity profile as follows. This wake is generated by each roughness element aligned as a lateral row of the front zone of the rough surface.

$$\int_{-\infty}^{\infty} u_{1,s}(y)\, dy \approx const.$$

Thus, the roughness elements in a front zone row seem to have the characteristics of the infinite cylinder laid in the y-direction. The combined wakes in the y-direction of this front zone of the rough surface can be considered to be a two-dimensional wake, and the velocity profile $\bar{U}_e(x, z)$ in Eq. (7-1) has the characteristics of a two-dimensional Gaussian wake.

On the other hand, at the short downwind distance from a roughness element, it is not necessary to consider the combination in the y-direction. Therefore, the wake function F(x) transforms from a two-dimensional to a three-dimensional wake in the x-direction.

As described in Chapter V, the vertical relative position of wakes generated by each roughness element does not have a constant height in the downwind direction as shown in Fig. 18. Thus, in the calculation of $U_i$ , the decaying function $F(x - i\Delta)$ should be some suitable function of the wakes. Also for the calculation of the combined wakes, it is necessary to consider the vertical displacement of each wake.

The initial wind flow, which is generally considered to be a turbulent shear flow, also affects the combined wakes. From the result of the experiment probing of the turbulent shear flow as shown in Figs. 38 and 39, the velocity $U_i$ is obtained locally as a constant, and the vertical displacement position of $\tilde{u}_{i\,max}$ is also obtained as a local constant.

The initial turbulent shear flow is considered to be a combined wakes flow. The effect of this initial flow should decay some distance from the leading edge of the rough surface.

On the basis of the above discussion, except for the front zone of the rough surface, Eq. (7-1) with constant $U_i$ can represent the vertical velocity profile of the turbulent shear flow. Assuming that

$$F(x) \propto x^{-P_2} \qquad f = \left(1 - \left(\frac{z}{(C_2 x^{P_3})}\right)^{3/2}\right)^2$$

that is

$$b \propto x^{P_3}, \quad \text{and} \quad C_1 F(0^+) = 1, \quad f_{b=0^+} = 1$$

then Eq. (7-1) is reduced,

$$\tilde{u}^2(x,z) = \int_{\epsilon x}^{x} [U C_1 (x-\zeta)^{-P_2} [1 - (\frac{z}{C_2 (x-\zeta)^{P_3}})^{3/2}]^2]^2 d\zeta + \bar{U}_\epsilon^2(x,z)$$

Let $x - \zeta \equiv \xi$ then

$$\tilde{u}^2 = \int_{0^+}^{(1-\epsilon)x} [U C_1 \xi^{-P_2} (1 - (\frac{z}{C_2 \xi^{P_3}})^{3/2})^2]^2 d\xi + \bar{U}_\epsilon^2$$

When $P_2 \neq 1/2$

$$\bar{u}^2 = [U^2 C_1^2 \frac{1}{1-2P_2} \xi^{1-2P_2} \{ [1 - (\frac{z}{C_2 \xi^{P_3}})^{3/2}]^4 - [\frac{6P_3}{1-2P_2-\frac{3}{2}P_3} (\frac{z}{C_2 \xi^{P_3}})^{3/2}$$

$$- \frac{18P_3}{1-2P_2-3P_3} (\frac{z}{C_2 \xi^{P_3}})^3 + \frac{18P_3}{1-2P_2-\frac{9}{2}P_3} (\frac{z}{C_2 \xi^{P_3}})^{9/2} - \frac{6P_3}{1-2P_2-6P_3}$$

$$\times (\frac{z}{C_2 \xi^{P_3}})^6 ] \} ]_{0^+}^{(1-\epsilon)x} + \bar{U}_\epsilon^2$$

At $\xi = 0^+$, $(\frac{z}{C_2 \xi^{P_3}}) = 0$

the first term on the right had side of the above equation is

$$U^2 C_1 \frac{1}{1-2P_2} (0^+)^{1-2P_2} \equiv B^2(0^+)$$

At $\xi = (1-\epsilon)x$,

$b = C_2 \xi^{p_3}$ should be equal to the thickness of the boundary layer $\delta$ . Therefore,

$$\tilde{u}^2 = B^2(x)[1-(\frac{z}{\delta})^{3/2}]^4 - g(\frac{z}{\delta}) + \bar{U}_e^2 \qquad (7\text{-}4)$$

where
$$B^2(x) = \frac{U^2 C_1^2}{1-2p_2}(1-\epsilon)x^{1-2p_2} ,$$

$$g(\frac{z}{\delta}) = B^2(x)[\frac{6p_3}{1-2p_2-\frac{3}{2}p_3}(\frac{z}{\delta})^{3/2} - \frac{18p_3}{1-2p_2-3p_3}(\frac{z}{\delta})^3$$
$$+ \frac{18p_3}{1-2p_2-\frac{9}{2}p_3}(\frac{z}{\delta})^{9/2} - \frac{6p_3}{1-2p_2-6p_3}(\frac{z}{\delta})^6] + B^2(0^+)$$

The first and the third terms on the right hand side of the above Eq. (7-4) have the same functional form concerning the height z . Therefore,

$$\tilde{u} = [[A(x)[1-(\frac{z}{\delta})^{3/2}]^2]^2 - g(\frac{z}{\delta})]^{1/2}$$

From the boundary conditions,

$$\text{at } z=0 \qquad \tilde{u}^2 = \tilde{u}^2_{max} \approx U_0^2 \qquad A^2(x) - B^2(0^+) = U_0^2$$

$$\text{at } z=\delta \qquad \tilde{u}^2 = 0 \qquad g(1) = 0$$

It is apparent from the above result that the velocity profile shows the Gaussian profile when z approaches zero and $\delta$ .

On the other hand, by using the Eqs. (4-10) and (4-18), the velocity profile can be obtained by numerical calculation. This numerical result is shown in Fig. 40. But these two theoretical analyses of the vertical velocity profiles are calculated in the zone of the vertical wakes generated by each roughness element (zone 3 and 4 described in Chapter III). Therefore, the height $z$ is not taken from the base plate of the roughness elements but is taken from the height of the maximum velocity of $\tilde{u}$ of the combined wakes. There is a uniform velocity profile under this height. At the far downwind distance on the rough surface, this height approaches the base plate. If it is possible to consider the same form of vertical velocity profile in the x-direction over the rough surface, the experimental results can be satisfied with these results as shown in Fig. 40.

Experimental data of the vertical wind velocity profiles are taken at the center position among four roughness cylinders. The lower part of the velocity profile is not independent of the measured position. As shown in Fig. 33, the velocity profiles directly behind the roughness cylinders are clearly not the same as the velocity profiles at the center position, even if the profiles are taken at a very far downwind distance from the leading edge of the surface. However, over the rough surface this profile difference is negligible since it seems that the velocity profiles are independent of the measuring position.

From the analytical calculation of turbulent shear flow profile based on the concept of combined wakes, both ends of the vertical velocity profile show the characteristics of the wake flow as shown in Fig. 40. This is a confirmation of the wake law suggested by Coles (6). Also the upper part of the velocity profile shows the same characteristics as the studies by Hama (12), Clauser (5), et. al.

At present, the most utilized concepts of the turbulent shear flow characteristics in lower layers of the atmosphere are:

1. The vertical velocity profile is given by the logarithmic law.
2. The coefficient of the turbulent diffusion in the vertical direction is proportional to the height $z$.
3. The vertical shear turbulence $\overline{u'w'}$ is constant.
4. The scale of the turbulence in the vertical direction $\ell$ is proportional to the height $z$.

Referring to the theoretical and experimental results of Figs. 40, 41 and 42, at the middle lower part of the vertical velocity profile. ( $z/\delta = 0.25 \sim 0.45$ ), the above characteristics of the factors are almost proved by the momentum defect superposition of wakes. Comparing the analytical velocity profiles with the experimental data in Fig. 40, it is difficult to distinguish whether two- or three-dimensional wake combinations satisfy the experimental data.

When the two-dimensional wakes combination is applied to turbulent shear flow, the relation between the momentum of turbulent shear flow and the equivalent drag coefficient is shown as Eq. (4-16) and also

$$\frac{dM_i}{d(i\Delta)} \propto \frac{dC_{Di}}{d(i\Delta)} \propto \frac{\tau_{wi}}{\frac{1}{2}\rho U_o^2}$$

where

$$C_{Di} = C_D \sum_{o}^{i} \left(\frac{U_r}{U_o}\right)^2 \approx C_D \int_0^{i\Delta} \left(\frac{U_r}{U_o}\right)^2 d(r\Delta)$$

$$\frac{\tau_{wi}}{\frac{1}{2}\rho U_o} \propto C_D \left(\frac{U_i}{U_o}\right)^2$$

$$u_* \propto U_i$$

The experimental data of $u_*$ in Fig. 66 are obtained from the velocity profile (from the part of the logarithmic profile). Comparing the experimental data of $U_i$ (Fig. 38) with the analytical calculation values, it is found that they have the same characteristics.

The development of the thickness of the boundary layer $\delta$ (internal) over the rough surface can be analyzed by taking the width envelope of the combined wakes of Fig. 35, as shown in Fig. 64. The experimental data of this $\delta$ are shown in the same figure. The development of the internal boundary layer can not be represented by a power function as $x^{\beta_3}$, but as the local zone of the far downwind distance from the leading edge of the rough surface, the thickness of the layer $\delta$ is approximately represented by the function of $x^{\beta}$ where $\beta \approx 0.8$ . The equivalent drag coefficient at the height of internal boundary layer appears to be $C_{Di} = C_D\, G(x - i\Delta) \propto x^{0.8-0.5} = x^{0.3}$ Variation of this drag coefficient in the longitudinal x-direction is shown in Fig. 65.

Stratified Turbulent Shear Flow

Concerning the coefficient of the turbulent diffusion, in a thermally stratified case, the result of the analytical study of the Eulerian similarity hypothesis shows (39),

$$\frac{K(\text{stratified})}{K(\text{neutral})} \propto (1 - \alpha R_i)^{1/4}$$

where Ri is the Richardson number, and $\alpha \approx \frac{K_H}{K_m}$. The Richardson number is nondimensional. However, when the temperature profile is similar to the velocity profile, then

$$R_i = \frac{g}{T_0} \frac{\partial T/\partial z}{(\partial u/\partial z)^2} \Rightarrow \frac{g}{T_0} \frac{1}{\partial u/\partial z}$$

so that

$$R_i \propto 1/\partial u/\partial z$$

and

$$\left[ \frac{K(\text{stratified})}{K(\text{neutral})} \right]^4 - 1 \propto 1/\partial u/\partial z$$

Using the ratio of $K_1$ and $K_2$ in Fig. 44, and the velocity gradient $\partial u / \partial z$ (the values are given by the concept of combined wakes), the above relation is confirmed analytically as shown in Fig. 67. Also the experimental data of the gas diffusion concentration, as shown in Fig. 59, show the thermal effect on the coefficients of the gas turbulent diffusion in the horizontal direction, but the thermal effect in the vertical direction is not clear from experimental data shown in Fig. 61.

## Concentration Profile

The equation for the diffusion from a continuous point source in a steady state is given by

$$u \frac{\partial \bar{c}}{\partial x} = \frac{\partial}{\partial y}\left(K_y \frac{\partial \bar{c}}{\partial y}\right) + \frac{\partial}{\partial z}\left(K_z \frac{\partial \bar{c}}{\partial z}\right) \qquad (7\text{-}5)$$

where $\bar{C}$ is the helium gas concentration of the diffusion.

The results of the analytical vertical velocity profile shown in Fig. 40, and the coefficient of the turbulent diffusion in Fig. 36 (the coefficient of momentum is assumed to be similar to the coefficient of the helium gas) are used for the analysis of the concentration profile. (These $K$ and $\tilde{u}$ are assumed zero at $z/\delta = 0$ ). When the point source position is at the far downwind distance from the leading edge, locally, it is possible to consider that approximately (40)

$$\delta = const.$$
$$u = u(z)$$
$$K_z = K_z(z)$$
$$K_y \propto K_z$$
$$= K_y(z)$$

The boundary condition is

1. $\bar{c} = 0$ as $x, z \Rightarrow \infty$
2. $\bar{c} \Rightarrow \infty$ as $x = z = 0$
3. $K_z \dfrac{\partial \bar{c}}{\partial z} = 0$ as $z = 0, \ x > 0$
4. $K_y \dfrac{\partial c}{\partial y} = 0$ as $y = y_0, \ x > 0$ $(y \Leftarrow c(y) = max)$

and with the source strength

$$\int_0^\infty dz \int_{-\infty}^{\infty} u\bar{c}\, dy = Q$$

Rewriting Eq. (7-5) to the following finite difference equation, then it is possible to obtain the numerical solution of the mean profile of the helium gas concentration from the equation.

The equivalent finite difference equation of Eq. (7-5) is

$$\bar{c}(x+\Delta x, y, z) = \bar{c}(x,y,z) + \frac{\Delta x}{u z}\Big\{\frac{K_y(z)}{(\Delta y)^2}[\bar{c}(x,y+\Delta y,z) - 2\bar{c}(x,y,z) + \bar{c}(x,y-\Delta y z)] + \frac{1}{\Delta z^2}[K_z(z+\Delta z)[\bar{c}(x,y,z+\Delta z) - \bar{c}(x,y,z)] - K_z(z)[\bar{c}(x,y,z) - \bar{c}(x,y,z-\Delta z)]]\Big\} \qquad (7\text{-}6)$$

At the vertical section of the maximum concentration Eq. (7-5) is

$$\bar{C}(x+\Delta x, z) = \bar{C}(x,z) + \frac{\Delta x}{u(z)(\Delta z)^2}\left\{K_z(z+\Delta z)\left[\bar{C}(x, z+\Delta z)\right.\right.$$

$$\left.\left.-\bar{C}(x,z)\right] - K_z(z)\left[\bar{C}(x,z) - \bar{C}(x, z-\Delta z)\right]\right\}. \qquad (7\text{-}7)$$

In the numerical calculation of equation (7-6) and (7-7), the boundary condition 2 is reconsidered to have a finite pulse or a Gaussian profile (40).

Using one of the experimental concentration profiles as the initial value for the calculation, the difference of this concentration profile and the profile of the following section $\Delta\bar{C}(z) = \bar{C}(x+\eta\Delta x, z) - \bar{C}(x,z)$ is calculated by dividing the distance $\eta\Delta x$ into five steps instead of the complete calculation of equation (7-6) or (7-7) by using an electronic digital computer. The calculated values and the experimental results of $\Delta\bar{C}$ are shown in Figs. 68 and 69. Except the lower zone of the profile that is inside the roughness element, the calculation values satisfy the experimental data.

Considering Eq. (7-7), when the coefficient $K_z$ and the velocity $u$ are constant, the difference of the concentration $\Delta\bar{C}(z)$ is symmetrical in relation to the axis of the maximum concentration if the initial concentration distribution is symmetrical, as in a Gaussian profile. The profile of $\Delta\bar{C}(z)$ is the difference between two Gaussian profiles with different $C_{max}$ s and widths.

When the coefficient $K_z$ is a large value, the value of $|\Delta\bar{C}(z)|$ is also a large value, and when the coefficient $K_z$ is small, the value of $|\Delta\bar{C}|$ is small. Also, the value of $|\Delta\bar{C}|$ is proportional to the term of $\frac{1}{u}$ . When the velocity profile has a positive gradient, in the vertical direction, the value of $|\Delta\bar{C}|$ becomes a small value along the height as compared with the case of uniform flow.

On the other hand, when the coefficient of the turbulent diffusion $K_z$ has a positive gradient in the upward direction, the value of $|\Delta\bar{C}|$ becomes large in the vertical direction as compared with the case of the constant coefficient.

As shown in Fig. 70, at the leading edge zone of the roughness surface, the coefficient of turbulent diffusion $K_z$ is nearly constant, but the velocity gradient is rather large. Therefore, when the point source of the diffusion is located at the leading edge on the rough surface (the difference value of $\Delta\bar{C}$ has the negative value at the surrounding part of the maximum concentration of its profile), the negative value $\Delta\bar{C}$ has a large lower part and a small upper part concerning the axis of the maximum concentration. This means that the position of the maximum concentration transforms upward in the downwind direction.

When the point source is located in the far downwind distance, both of the coefficients $K_z$ and the velocity $u$ have a positive gradient in the vertical direction. Therefore, the transferred position of the maximum concentration cannot be understood directly.

The result of the calculation of Eq. (7-7) shows that the position of the maximum concentration transfers downward in the downwind direction as shown in Fig. 68. These transformation are confirmed experimentally as shown in Figs. 54 and 55.

It seems that the transformation of the positions of the maximum concentration are determined by the gradients of the coefficient of the turbulent diffusion and the velocity profile.

# Chapter VIII

# CONCLUSIONS

The study of the turbulent diffusion over a rough surface in the wind tunnel was utilized with the concept of momentum defect superposition in the wakes of an array of roughness elements. Based on this concept, the characteristics of each factor of turbulent diffusion are analyzed and the results are confirmed experimentally. From agreement between theory and experiment, the concept, the turbulent shear flow consists of the combination of the individual wake flows, is confirmed and forms the conclusion of this study.

The results of this study may suggest a method for predicting diffusion in the lower layer of the atmosphere. When the thickness of the internal boundary layer $\delta$ and the distance from the leading edge of the rough surface to the observation point are known, the equivalent drag coefficient at the height of the internal boundary layer can be analyzed by using Fig. 65 and the value of the initial drag coefficient. From this coefficient, the coefficient of turbulent diffusion is calculated, and in all z-directions the coefficient of turbulent diffusion can be obtained from Fig. 36. Therefore, the diffusion profile may be calculated by numerical Eq. (7-6) using the velocity profiles of Fig. 40.

If the height of the internal boundary layer is large compared to the plume height, the results which are already discussed in many studies ( $K \propto Z$, $u \propto \ln Z$ etc.) may be satisfactory.

# BIBLIOGRAPHY

# BIBLIOGRAPHY


1. Batchelor, G. K., Diffusion from sources in a turbulent boundary layer. Archiwum Mechaniki Stosowanej 16:661-670, 1964.

2. Batchelor, G. K., Diffusion in free turbulent shear flows. Journal of Fluid Mechanics 3:67-80, 1957.

3. Calder, K. L., The criterion of turbulence in a fluid of variable density, with particular reference to conditions in the atmosphere. Quarterly Journal of the Royal Meteorological Society 75:71-88, 1949.

4. Cermak, J. E., Lagrangian similarity hypothesis applied to diffusion in turbulent shear flow. Journal of Fluid Mechanics 15:49-64, 1963.

5. Clauser, F. H., The turbulent boundary layer. Advances in Applied Mechanics 4:1-51, Academic Press, New York, 1956.

6. Coles, D., The law of the wake in the turbulent boundary layer. Journal of Fluid Mechanics 1:191-226, 1956.

7. Courant, R. and Hilbert, D., Methods of Mathematical Physics. Interscience Publishers, New York, 1962, 2v.

8. Denmead, O. T., Evaporation sources and apparent diffusivities in a forest canopy. Journal of Applied Meteorology 3:383-389, 1964.

9. Elliott, W. P., The growth of the atmospheric internal boundary layer. Transactions, American Geophysical Union 39:1048-1054, 1958.

10. Fujimoto, T., Ryutai Rikigaku (Fluid Mechanics). 6th edition, Yoken-do, Tokyo, 1960, 390 p.

11. Gifford, F. A., Diffusion in the diabatic surface layer. Journal of Geophysical research 67:3207-3212, 1962.

12. Hama, F. R., Boundary layer characteristics for smooth and rough surfaces. Transactions of the Society of Naval Architects and Marine Engineers 62:333-358, 1954.

13. Hayami, S., Kozuiryu no Riron ni stuite, Suikogaku no Saikin no Shinpo (Theory of flood flow, Advances in hydraulic engineerings). Japan Society of Civil Engineers, Tokyo, 1953, 288 p.

14. Huang, K., Statistical Mechanics. John Wiley and Sons, New York, 1963, 470 p.

15. Inoue, E., Ranryu Kyokaiso ni stuite (On the structure of turbulent boundary layer). Oyo Rikigaku (Applied Mechanics) 4:53-58, 1951.

16. Inoue, E., On the turbulent structure of airflow within crop canopies. Journal of the Meteorological Society of Japan 41:317-325, 1963.

17. International Symposium on Transport Processes in Statistical Mechanics. Proceedings, Interscience Publishers, New York, 1958, 436 p.

18. International Union of Theoretical and Applied Mechanics and International Union of Geodesy and Geophysics. Atmospheric Diffusion and Air Pollution, Academic Press, New York, 1959, 471 p. (Advances in Geophysics 6).

19. Jacob, W., Variation in velocity profile with change in surface roughness of boundary. NACA Technical Memorandum 951, 1940, 26 p.

20. Kolmogoroff, A. M., Dissipation of energy in the locally isotropic turbulence in: Turbulence 159-161, Interscience Publishers, New York, 1961, 187 p.

21. Kutateladze, S. S. and Leont'ev, A. I., Turbulent boundary layers in compressible gases. Academic Press, New York, 1964, 170 p.

22. Miyake, M., Transformation of atmospheric boundary layer induced by inhomogeneous surface (Growth of internal boundary layer). M. S. Thesis, University of Washington, Seattle, 1961, 65 p.

23. Monin, A. S. and Obukhov, A. M., Fundamentale Gesetzmassigkeiten der turbulenten Vermischung in der budennahen Schicht der Atmosphare (The basic laws of turbulent transport in the ground layer of the atmosphere). in: Statistische Theorie der Turbulenz, 199-226, Akademie-Verlag, Berlin, 1958, 228 p.

24. Obukhov, A. M. and Yaglom, A. M., The microstructure of turbulent flow. NACA Technical Memorandum 1350, 1953, 41 p.

25. Panofsky, H. A. and Townsend, A. A. Change of terrain roughness and the wind profile. Quarterly Journal of the Royal Meteorological Society 90:47-55, 1964.

26. Pasquill, F., The determination of eddy diffusivity from measurements of turbulent energy. Quarterly Journal of the Royal Meteorlogical Society 89:95-106, 1963.

27. Pasquill, F., Atmospheric Diffusion. Van Nostrand, London, 1961, 297 p.

28. Priestley, C. H. B. and Sheppard, P. A., Turbulence and transfer process in the atmosphere. Quarterly Journal of the Royal Meteorological Society 78:488-529, 1952.

29. Richardson, L. F., The supply of energy from and to atmospheric eddies. Proceedings of the Royal Society A 97:354-373, 1920.

30. Richardson, L. F., Atmospheric diffusion shown on a distance neighbour graph. Proceedings of the Royal Society A 110: 709-737, 1926.

31. Schlichting, H., Boundary Layer Theory. McGraw-Hill, New York, 1960, 647 p.

32. Schubauer, G. B. and Tchen, C. M., Turbulent flow. Princeton University Press, Princeton, 1961, 23 p.

33. Shono, S. and Hamuro, M., Note on the wind-profile in the lower layer of a diabatic atmosphere. Journal of the Meteorological Society of Japan 40:1-12, 1962.

34. Sutton, O. G., Wind structure and evaporation in a turbulent atmosphere. Proceedings of the Royal Society A 146: 701-722, 1934.

35. Swinbank, W. C., The exponential wind profile. Quarterly Journal of the Royal Meterological Society 90:119-135, 1964.

36. Taylor, G. I., Diffusion by continuous movement. Proceedings of London Mathematical Society 20:196-212, 1921.

37. Tokyo Kogyo Daigaku, Tokei Kogaku Hando Buku (Handbook of Statistical Mechanics). Gihodo, Tokyo, 1953, 1262 p.

38. Townsend, A. A., The structure of turbulent shear flow. Cambridge University Press, London, 1956, 315 p.

39. Yamamoto, G., Theory of turbulent transfer in non-neutral conditions. Journal of the Meteorological Society of Japan 37:60-69, 1959.

40. Yamamoto, G. and Shimanuki, A., The determination of lateral diffusivity in diabatic conditions near the ground from diffusion experiments. Journal of Atmospheric Sciences 21:187-196, 1964.

TABLES

TABLE 1 Numerical Calculation of Eqs. (4-11) and (4-12) $u_{1.0\,max} = 1 \cdot 0.83 \cdot (x/d)^{-\frac{1}{2}}$

| x/Δ | x/d | $u_{1.0\,max}$ | $u_{1.1\,max}$ | $\tilde{u}_{1\,max}$ | $u_{1.2\,max}$ | $\tilde{u}_{2\,max}$ | $u_{1.3\,max}$ | $\tilde{u}_{3\,max}$ | $u_{1.4\,max}$ | $\tilde{u}_{4\,max}$ | $u_{1.5\,max}$ | $\tilde{u}_{5\,max}$ | $u_{1.6\,max}$ | $\tilde{u}_{6\,max}$ |
|---|---|---|---|---|---|---|---|---|---|---|---|---|---|---|
| 0 | 0 | 1 | | | | | | | | | | | | |
| 1 | 5.33 | 0.360 | 0.933 | 1 | | | | | | | | | | |
| 2 | 10.67 | 0.254 | 0.336 | 0.421 | 0.907 | 1 | | | | | | | | |
| 3 | 16.00 | 0.207 | 0.237 | 0.314 | 0.326 | 0.453 | 0.892 | 1 | | | | | | |
| 4 | 21.33 | 0.180 | 0.193 | 0.264 | 0.230 | 0.350 | 0.321 | 0.475 | 0.880 | 1 | | | | |
| 5 | 26.67 | 0.161 | 0.168 | 0.233 | 0.188 | 0.299 | 0.226 | 0.375 | 0.317 | 0.490 | 0.871 | 1 | | |
| 6 | 32.00 | 0.147 | 0.150 | 0.210 | 0.163 | 0.266 | 0.185 | 0.324 | 0.224 | 0.393 | 0.314 | 0.504 | 0.863 | 1 |
| 7 | 37.33 | 0.136 | 0.137 | 0.193 | 0.146 | 0.242 | 0.161 | 0.291 | 0.182 | 0.343 | 0.221 | 0.408 | 0.311 | 0.513 |
| 8 | 42.67 | 0.127 | 0.127 | 0.179 | 0.133 | 0.223 | 0.144 | 0.265 | 0.158 | 0.309 | 0.180 | 0.358 | 0.219 | 0.419 |
| 9 | 48.00 | 0.120 | 0.118 | 0.167 | 0.123 | 0.208 | 0.131 | 0.245 | 0.142 | 0.283 | 0.157 | 0.323 | 0.179 | 0.370 |
| 10 | 53.33 | 0.114 | 0.112 | 0.160 | 0.115 | 0.197 | 0.121 | 0.231 | 0.129 | 0.265 | 0.140 | 0.300 | 0.156 | 0.337 |
| 11 | 58.67 | 0.108 | 0.106 | 0.155 | 0.109 | 0.187 | 0.113 | 0.218 | 0.120 | 0.249 | 0.128 | 0.280 | 0.139 | 0.312 |
| 12 | 64.00 | 0.104 | 0.101 | 0.145 | 0.103 | 0.178 | 0.107 | 0.208 | 0.112 | 0.236 | 0.119 | 0.264 | 0.127 | 0.293 |
| 13 | 69.33 | 0.0996 | 0.0970 | 0.139 | 0.0980 | 0.170 | 0.102 | 0.198 | 0.106 | 0.225 | 0.111 | 0.250 | 0.118 | 0.276 |
| 14 | 74.67 | 0.0961 | 0.0930 | 0.134 | 0.0940 | 0.164 | 0.0962 | 0.190 | 0.100 | 0.217 | 0.105 | 0.238 | 0.110 | 0.262 |
| 15 | 80.00 | 0.0927 | 0.0897 | 0.129 | 0.0904 | 0.158 | 0.0927 | 0.183 | 0.0950 | 0.206 | 0.0993 | 0.229 | 0.104 | 0.251 |
| 16 | 85.33 | 0.0898 | 0.0865 | 0.125 | 0.0872 | 0.152 | 0.0888 | 0.176 | 0.0915 | 0.199 | 0.0941 | 0.220 | 0.0984 | 0.239 |
| 17 | 90.67 | 0.0873 | 0.0838 | 0.121 | 0.0841 | 0.147 | 0.0857 | 0.171 | 0.0876 | 0.192 | 0.0906 | 0.212 | 0.0933 | 0.231 |
| 18 | 96.00 | 0.0849 | 0.0851 | 0.118 | 0.0792 | 0.142 | 0.0826 | 0.164 | 0.0845 | 0.185 | 0.0867 | 0.204 | 0.0898 | 0.223 |
| 19 | 101.33 | 0.0820 | 0.0792 | 0.114 | 0.0768 | 0.138 | 0.0801 | 0.159 | 0.0815 | 0.179 | 0.0837 | 0.197 | 0.0860 | 0.215 |
| 20 | 106.67 | 0.0781 | 0.0765 | 0.109 | 0.0744 | 0.132 | 0.0779 | 0.154 | 0.0791 | 0.173 | 0.0807 | 0.191 | 0.0803 | 0.208 |

| x/Δ | x/d | $u^2_{1.0\,max}$ | $u^2_{1.1\,max}$ | $\tilde{u}^2_{1\,max}$ | $u^2_{1.2\,max}$ | $\tilde{u}^2_{2\,max}$ | $u^2_{1.3\,max}$ | $\tilde{u}^2_{3\,max}$ | $u^2_{1.4\,max}$ | $\tilde{u}^2_{4\,max}$ | $u^2_{1.5\,max}$ | $\tilde{u}^2_{5\,max}$ | $u^2_{1.6\,max}$ | $\tilde{u}^2_{6\,max}$ |
|---|---|---|---|---|---|---|---|---|---|---|---|---|---|---|
| 0 | 0 | 1 | 0 | | | | | | | | | | | |
| 1 | 5.33 | 0.130 | 0.870 | 1 | 0 | | | | | | | | | |
| 2 | 10.67 | 0.0645 | 0.113 | 0.178 | 0.823 | 1 | 0 | | | | | | | |
| 3 | 16.00 | 0.0430 | 0.0560 | 0.0990 | 0.107 | 0.206 | 0.795 | 1 | | | | | | |
| 4 | 21.33 | 0.0324 | 0.0373 | 0.0697 | 0.0530 | 0.123 | 0.103 | 0.226 | 0.774 | 1 | | | | |
| 5 | 26.67 | 0.0259 | 0.0283 | 0.0542 | 0.0354 | 0.0896 | 0.0510 | 0.141 | 0.100 | 0.241 | 0.759 | 1 | | |
| 6 | 32.00 | 0.0216 | 0.0225 | 0.0441 | 0.0266 | 0.0707 | 0.0241 | 0.105 | 0.0500 | 0.155 | 0.0987 | 0.254 | 0.747 | 1 |
| 7 | 37.33 | 0.0185 | 0.0188 | 0.0373 | 0.0213 | 0.0586 | 0.0258 | 0.0844 | 0.0332 | 0.118 | 0.0488 | 0.166 | 0.0965 | 0.263 |
| 8 | 42.67 | 0.0161 | 0.0161 | 0.0322 | 0.0177 | 0.0499 | 0.0206 | 0.0705 | 0.0215 | 0.0956 | 0.0324 | 0.128 | 0.0480 | 0.176 |
| 9 | 48.00 | 0.0144 | 0.0140 | 0.0280 | 0.0151 | 0.0431 | 0.0171 | 0.0602 | 0.0201 | 0.0803 | 0.0247 | 0.105 | 0.0321 | 0.137 |
| 10 | 63.33 | 0.0130 | 0.0126 | 0.0256 | 0.0132 | 0.0388 | 0.0147 | 0.0535 | 0.0167 | 0.0702 | 0.0196 | 0.0898 | 0.0242 | 0.114 |
| 11 | 58.67 | 0.0117 | 0.0112 | 0.0229 | 0.0119 | 0.0348 | 0.0128 | 0.0476 | 0.0143 | 0.0619 | 0.0164 | 0.0783 | 0.0193 | 0.0976 |
| 12 | 64.00 | 0.0108 | 0.0102 | 0.0210 | 0.0106 | 0.0316 | 0.0115 | 0.0431 | 0.0125 | 0.0556 | 0.0141 | 0.0697 | 0.0161 | 0.0858 |
| 13 | 69.33 | 0.00992 | 0.00942 | 0.0193 | 0.00960 | 0.0289 | 0.0103 | 0.0392 | 0.0111 | 0.0503 | 0.0122 | 0.0625 | 0.0138 | 0.0763 |
| 14 | 74.67 | 0.00924 | 0.00865 | 0.0179 | 0.00885 | 0.0267 | 0.00925 | 0.0360 | 0.0101 | 0.0461 | 0.0109 | 0.0570 | 0.0120 | 0.0690 |
| 15 | 80.00 | 0.00862 | 0.00805 | 0.0167 | 0.00818 | 0.0249 | 0.00860 | 0.0335 | 0.00903 | 0.0425 | 0.00985 | 0.0523 | 0.0107 | 0.0630 |
| 16 | 85.33 | 0.00808 | 0.00747 | 0.0156 | 0.00760 | 0.0232 | 0.00788 | 0.0310 | 0.00837 | 0.0394 | 0.00885 | 0.0483 | 0.00920 | 0.0575 |
| 17 | 90.67 | 0.00753 | 0.00703 | 0.0147 | 0.00705 | 0.0217 | 0.00735 | 0.0291 | 0.00767 | 0.0367 | 0.00822 | 0.0450 | 0.00872 | 0.0537 |
| 18 | 96.00 | 0.00720 | 0.00665 | 0.0139 | 0.00628 | 0.0201 | 0.00682 | 0.0270 | 0.00715 | 0.0341 | 0.00752 | 0.0416 | 0.00805 | 0.0497 |
| 19 | 101.33 | 0.00672 | 0.00628 | 0.0130 | 0.00590 | 0.0189 | 0.00641 | 0.0253 | 0.00665 | 0.0320 | 0.00700 | 0.0390 | 0.00740 | 0.0464 |
| 20 | 106.67 | 0.00610 | 0.00585 | 0.0120 | 0.00555 | 0.0175 | 0.00607 | 0.0236 | 0.00625 | 0.0298 | 0.00652 | 0.0363 | 0.00688 | 0.0432 |

TABLE 1 - Continued

| $x/\Delta$ | $u_{1.7\,max}$ | $\tilde{u}_{7\,max}$ | $u_{1.8\,max}$ | $\tilde{u}_{8\,max}$ | $u_{1.9\,max}$ | $\tilde{u}_{9\,max}$ | $u_{1.10\,max}$ | $\tilde{u}_{10\,max}$ | $u_{1.11\,max}$ | $\tilde{u}_{11\,max}$ | $u_{1.12\,max}$ | $\tilde{u}_{12\,max}$ | $u_{1.13\,max}$ | $\tilde{u}_{13\,max}$ | $u_{1.14\,max}$ |
|---|---|---|---|---|---|---|---|---|---|---|---|---|---|---|---|
| 0 | | | | | | | | | | | | | | | |
| 1 | | | | | | | | | | | | | | | |
| 2 | | | | | | | | | | | | | | | |
| 3 | | | | | | | | | | | | | | | |
| 4 | | | | | | | | | | | | | | | |
| 5 | | | | | | | | | | | | | | | |
| 6 | | | | | | | | | | | | | | | |
| 7 | 0.858 | 1 | | | | | | | | | | | | | |
| 8 | 0.309 | 0.521 | 0.853 | 1 | | | | | | | | | | | |
| 9 | 0.218 | 0.429 | 0.307 | 0.528 | 0.849 | 1 | | | | | | | | | |
| 10 | 0.178 | 0.381 | 0.217 | 0.438 | 0.305 | 0.534 | 0.845 | 1 | | | | | | | |
| 11 | 0.155 | 0.349 | 0.177 | 0.391 | 0.216 | 0.447 | 0.304 | 0.541 | 0.842 | 1 | | | | | |
| 12 | 0.138 | 0.324 | 0.154 | 0.359 | 0.176 | 0.400 | 0.214 | 0.453 | 0.303 | 0.545 | 0.839 | 1 | | | |
| 13 | 0.126 | 0.304 | 0.138 | 0.333 | 0.153 | 0.366 | 0.175 | 0.407 | 0.213 | 0.459 | 0.302 | 0.548 | 0.836 | 1 | |
| 14 | 0.117 | 0.288 | 0.126 | 0.314 | 0.137 | 0.342 | 0.152 | 0.374 | 0.174 | 0.413 | 0.213 | 0.464 | 0.301 | 0.553 | 0.833 |
| 15 | 0.109 | 0.274 | 0.116 | 0.297 | 0.125 | 0.322 | 0.136 | 0.350 | 0.152 | 0.381 | 0.174 | 0.418 | 0.212 | 0.470 | 0.300 |
| 16 | 0.103 | 0.251 | 0.108 | 0.282 | 0.116 | 0.215 | 0.124 | 0.329 | 0.136 | 0.356 | 0.151 | 0.387 | 0.173 | 0.424 | 0.212 |
| 17 | 0.0978 | 0.252 | 0.103 | 0.271 | 0.108 | 0.292 | 0.115 | 0.314 | 0.124 | 0.337 | 0.135 | 0.364 | 0.151 | 0.394 | 0.173 |
| 18 | 0.0927 | 0.241 | 0.0973 | 0.260 | 0.102 | 0.279 | 0.107 | 0.299 | 0.115 | 0.321 | 0.123 | 0.343 | 0.135 | 0.369 | 0.150 |
| 19 | 0.0893 | 0.233 | 0.0921 | 0.251 | 0.0968 | 0.268 | 0.102 | 0.287 | 0.107 | 0.306 | 0.114 | 0.327 | 0.123 | 0.349 | 0.134 |
| 20 | 0.0855 | 0.225 | 0.0887 | 0.241 | 0.0917 | 0.258 | 0.0963 | 0.276 | 0.101 | 0.294 | 0.107 | 0.313 | 0.114 | 0.332 | 0.123 |

| $x/\Delta$ | $u^2_{1.7\,max}$ | $\tilde{u}^2_{7\,max}$ | $u^2_{1.8\,max}$ | $\tilde{u}^2_{8\,max}$ | $u^2_{1.9\,max}$ | $\tilde{u}^2_{9\,max}$ | $u^2_{1.10\,max}$ | $\tilde{u}^2_{10\,max}$ | $u^2_{1.11\,max}$ | $\tilde{u}^2_{11\,max}$ | $u^2_{1.12\,max}$ | $\tilde{u}^2_{12\,max}$ | $u^2_{1.13\,max}$ | $\tilde{u}^2_{13\,max}$ | $u^2_{1.14\,max}$ |
|---|---|---|---|---|---|---|---|---|---|---|---|---|---|---|---|
| 0 | | | | | | | | | | | | | | | |
| 1 | | | | | | | | | | | | | | | |
| 2 | | | | | | | | | | | | | | | |
| 3 | | | | | | | | | | | | | | | |
| 4 | | | | | | | | | | | | | | | |
| 5 | | | | | | | | | | | | | | | |
| 6 | | | | | | | | | | | | | | | |
| 7 | 0.737 | 1 | | | | | | | | | | | | | |
| 8 | 0.0955 | 0.272 | 0.729 | 1 | | | | | | | | | | | |
| 9 | 0.0476 | 0.185 | 0.0945 | 0.279 | 0.721 | 1 | | | | | | | | | |
| 10 | 0.0317 | 0.146 | 0.0468 | 0.193 | 0.0930 | 0.286 | 0.715 | 1 | | | | | | | |
| 11 | 0.0242 | 0.122 | 0.0312 | 0.153 | 0.0467 | 0.200 | 0.0925 | 0.292 | 0.708 | 1 | | | | | |
| 12 | 0.0191 | 0.105 | 0.0236 | 0.129 | 0.0310 | 0.160 | 0.0458 | 0.205 | 0.0918 | 0.297 | 0.723 | 1 | | | |
| 13 | 0.0159 | 0.0922 | 0.0189 | 0.111 | 0.0234 | 0.135 | 0.0307 | 0.165 | 0.0453 | 0.211 | 0.0910 | 0.302 | 0.699 | 1 | |
| 14 | 0.0137 | 0.0826 | 0.0158 | 0.0984 | 0.0187 | 0.117 | 0.0232 | 0.140 | 0.0303 | 0.171 | 0.0454 | 0.216 | 0.0905 | 0.307 | 0.695 |
| 15 | 0.0119 | 0.0749 | 0.0135 | 0.0884 | 0.0156 | 0.104 | 0.0185 | 0.123 | 0.0229 | 0.145 | 0.0302 | 0.176 | 0.0450 | 0.221 | 0.0900 |
| 16 | 0.0106 | 0.0681 | 0.0117 | 0.0797 | 0.0133 | 0.0930 | 0.0154 | 0.108 | 0.0184 | 0.127 | 0.0228 | 0.150 | 0.0300 | 0.180 | 0.0448 |
| 17 | 0.00957 | 0.0632 | 0.0105 | 0.0737 | 0.0117 | 0.0854 | 0.0132 | 0.0986 | 0.0153 | 0.114 | 0.0183 | 0.132 | 0.0227 | 0.155 | 0.0298 |
| 18 | 0.00860 | 0.0583 | 0.00947 | 0.0677 | 0.0104 | 0.0781 | 0.0115 | 0.0896 | 0.0131 | 0.103 | 0.0151 | 0.118 | 0.0181 | 0.136 | 0.0225 |
| 19 | 0.00800 | 0.0544 | 0.00847 | 0.0628 | 0.00940 | 0.0722 | 0.0103 | 0.0825 | 0.0115 | 0.0940 | 0.0130 | 0.107 | 0.0151 | 0.122 | 0.0180 |
| 20 | 0.00730 | 0.0505 | 0.00787 | 0.0584 | 0.00843 | 0.0668 | 0.00930 | 0.0761 | 0.0102 | 0.0863 | 0.0114 | 0.0977 | 0.0129 | 0.111 | 0.0150 |

TABLE 1 - Continued

| $x/\Delta$ | $\tilde{u}_{14\,max}$ | $u_{1,15\,max}$ | $\tilde{u}_{15\,max}$ | $u_{1,16\,max}$ | $\tilde{u}_{16\,max}$ | $u_{1,17\,max}$ | $\tilde{u}_{17\,max}$ | $u_{1,18\,max}$ | $\tilde{u}_{18\,max}$ | $u_{1,19\,max}$ | $\tilde{u}_{19\,max}$ | $\tilde{u}_{20\,max}$ |
|---|---|---|---|---|---|---|---|---|---|---|---|---|
| 0 | | | | | | | | | | | | |
| 1 | | | | | | | | | | | | |
| 2 | | | | | | | | | | | | |
| 3 | | | | | | | | | | | | |
| 4 | | | | | | | | | | | | |
| 5 | | | | | | | | | | | | |
| 6 | | | | | | | | | | | | |
| 7 | | | | | | | | | | | | |
| 8 | | | | | | | | | | | | |
| 9 | | | | | | | | | | | | |
| 10 | | | | | | | | | | | | |
| 11 | | | | | | | | | | | | |
| 12 | | | | | | | | | | | | |
| 13 | | | | | | | | | | | | |
| 14 | 1 | | | | | | | | | | | |
| 15 | 0.557 | 0.831 | 1 | | | | | | | | | |
| 16 | 0.473 | 0.299 | 0.560 | 0.828 | 1 | | | | | | | |
| 17 | 0.430 | 0.211 | 0.478 | 0.298 | 0.564 | 0.826 | 1 | | | | | |
| 18 | 0.398 | 0.172 | 0.433 | 0.210 | 0.482 | 0.297 | 0.566 | 0.824 | 1 | | | |
| 19 | 0.374 | 0.150 | 0.403 | 0.171 | 0.437 | 0.210 | 0.486 | 0.296 | 0.568 | 0.823 | 1 | |
| 20 | 0.354 | 0.134 | 0.379 | 0.149 | 0.407 | 0.171 | 0.441 | 0.209 | 0.488 | 0.296 | 0.572 | 1 |

| $x/\Delta$ | $\tilde{u}^2_{14\,max}$ | $u^2_{1,15\,max}$ | $\tilde{u}^2_{15\,max}$ | $u^2_{1,16\,max}$ | $\tilde{u}^2_{16\,max}$ | $u^2_{1,17\,max}$ | $\tilde{u}^2_{17\,max}$ | $u^2_{1,18\,max}$ | $\tilde{u}^2_{18\,max}$ | $u^2_{1,19\,max}$ | $\tilde{u}^2_{19\,max}$ | $\tilde{u}^2_{20\,max}$ |
|---|---|---|---|---|---|---|---|---|---|---|---|---|
| 0 | | | | | | | | | | | | |
| 1 | | | | | | | | | | | | |
| 2 | | | | | | | | | | | | |
| 3 | | | | | | | | | | | | |
| 4 | | | | | | | | | | | | |
| 5 | | | | | | | | | | | | |
| 6 | | | | | | | | | | | | |
| 7 | | | | | | | | | | | | |
| 8 | | | | | | | | | | | | |
| 9 | | | | | | | | | | | | |
| 10 | | | | | | | | | | | | |
| 11 | | | | | | | | | | | | |
| 12 | | | | | | | | | | | | |
| 13 | | | | | | | | | | | | |
| 14 | 1 | | | | | | | | | | | |
| 15 | 0.311 | 0.689 | 1 | | | | | | | | | |
| 16 | 0.224 | 0.0895 | 0.314 | 0.686 | 1 | | | | | | | |
| 17 | 0.185 | 0.0445 | 0.229 | 0.0890 | 0.318 | 0.682 | 1 | | | | | |
| 18 | 0.158 | 0.0297 | 0.188 | 0.0442 | 0.232 | 0.0885 | 0.321 | 0.679 | 1 | | | |
| 19 | 0.140 | 0.0244 | 0.163 | 0.0293 | 0.192 | 0.0442 | 0.236 | 0.0877 | 0.324 | 0.676 | 1 | |
| 20 | 0.126 | 0.0179 | 0.144 | 0.0222 | 0.166 | 0.0293 | 0.195 | 0.0437 | 0.239 | 0.0877 | 0.326 | 1 |

TABLE 2
Numerical Calculation of Eq. (4-16)

| x/Δ | $C^{\frac{1}{2}}_{D0}$ | $C^{\frac{1}{2}}_{D1}$ | $C^{\frac{1}{2}}_{D2}$ | $C^{\frac{1}{2}}_{D3}$ | $C^{\frac{1}{2}}_{D4}$ | $C^{\frac{1}{2}}_{D5}$ | $C^{\frac{1}{2}}_{D6}$ | $C^{\frac{1}{2}}_{D7}$ | $C^{\frac{1}{2}}_{D8}$ | $C^{\frac{1}{2}}_{D9}$ | $C^{\frac{1}{2}}_{D10}$ | $C^{\frac{1}{2}}_{D11}$ | $C^{\frac{1}{2}}_{D12}$ | $C^{\frac{1}{2}}_{D13}$ | $C^{\frac{1}{2}}_{D14}$ | $C^{\frac{1}{2}}_{D15}$ | $C^{\frac{1}{2}}_{D16}$ | $C^{\frac{1}{2}}_{D17}$ | $C^{\frac{1}{2}}_{D18}$ | $C^{\frac{1}{2}}_{D19}$ | $C^{\frac{1}{2}}_{D20}$ |
|---|---|---|---|---|---|---|---|---|---|---|---|---|---|---|---|---|---|---|---|---|---|
| 0 | 1.04 | | | | | | | | | | | | | | | | | | | | |
| 1 | 1.04 | 1.04 | | | | | | | | | | | | | | | | | | | |
| 2 | 1.04 | 1.22 | 1.04 | | | | | | | | | | | | | | | | | | |
| 3 | 1.04 | 1.29 | 1.31 | 1.04 | | | | | | | | | | | | | | | | | |
| 4 | 1.04 | 1.33 | 1.44 | 1.37 | 1.04 | | | | | | | | | | | | | | | | |
| 5 | 1.04 | 1.35 | 1.50 | 1.54 | 1.41 | 1.04 | | | | | | | | | | | | | | | |
| 6 | 1.04 | 1.36 | 1.54 | 1.63 | 1.61 | 1.46 | 1.04 | | | | | | | | | | | | | | |
| 7 | 1.04 | 1.37 | 1.56 | 1.68 | 1.73 | 1.67 | 1.48 | 1.04 | | | | | | | | | | | | | |
| 8 | 1.04 | 1.37 | 1.58 | 1.72 | 1.79 | 1.80 | 1.72 | 1.51 | 1.04 | | | | | | | | | | | | |
| 9 | 1.04 | 1.37 | 1.59 | 1.74 | 1.83 | 1.87 | 1.86 | 1.76 | 1.53 | 1.04 | | | | | | | | | | | |
| 10 | 1.04 | 1.39 | 1.61 | 1.77 | 1.88 | 1.94 | 1.95 | 1.92 | 1.80 | 1.54 | 1.04 | | | | | | | | | | |
| 11 | 1.04 | 1.38 | 1.62 | 1.79 | 1.90 | 1.98 | 2.01 | 2.02 | 1.97 | 1.83 | 1.56 | 1.04 | | | | | | | | | |
| 12 | 1.04 | 1.40 | 1.62 | 1.80 | 1.93 | 2.02 | 2.07 | 2.09 | 2.07 | 2.01 | 1.86 | 1.58 | 1.04 | | | | | | | | |
| 13 | 1.04 | 1.39 | 1.64 | 1.81 | 1.95 | 2.05 | 2.11 | 2.15 | 2.15 | 2.11 | 2.04 | 1.88 | 1.59 | 1.04 | | | | | | | |
| 14 | 1.04 | 1.40 | 1.64 | 1.83 | 1.98 | 2.06 | 2.16 | 2.20 | 2.22 | 2.21 | 2.16 | 2.08 | 1.90 | 1.60 | 1.04 | | | | | | |
| 15 | 1.04 | 1.40 | 1.65 | 1.83 | 1.99 | 2.09 | 2.18 | 2.24 | 2.27 | 2.28 | 2.26 | 2.20 | 2.10 | 1.93 | 1.61 | 1.04 | | | | | |
| 16 | 1.04 | 1.40 | 1.65 | 1.84 | 1.99 | 2.12 | 2.18 | 2.26 | 2.31 | 2.33 | 2.33 | 2.30 | 2.24 | 2.13 | 1.94 | 1.62 | 1.04 | | | | |
| 17 | 1.04 | 1.40 | 1.66 | 1.85 | 2.00 | 2.12 | 2.23 | 2.30 | 2.35 | 2.39 | 2.40 | 2.39 | 2.35 | 2.27 | 2.16 | 1.96 | 1.63 | 1.04 | | | |
| 18 | 1.04 | 1.40 | 1.64 | 1.84 | 2.00 | 2.13 | 2.23 | 2.32 | 2.37 | 2.42 | 2.45 | 2.45 | 2.43 | 2.38 | 2.30 | 2.18 | 1.98 | 1.64 | 1.04 | | |
| 19 | 1.04 | 1.40 | 1.64 | 1.84 | 2.01 | 2.13 | 2.25 | 2.33 | 2.42 | 2.45 | 2.49 | 2.55 | 2.50 | 2.47 | 2.42 | 2.33 | 2.19 | 1.99 | 1.64 | 1.04 | |
| 20 | 1.04 | 1.38 | 1.62 | 1.83 | 2.00 | 2.14 | 2.25 | 2.35 | 2.41 | 2.48 | 2.52 | 2.53 | 2.57 | 2.54 | 2.51 | 2.45 | 2.35 | 2.22 | 2.00 | 1.65 | 1.04 |

TABLE 3
Numerical Calculation of Eq. (4-18) $b_0 = 0.135 \cdot (x/d)^{\frac{1}{2}}$ (in)

| x/Δ | $b_0$(x10) | $b_1$ | $b_2$ | $b_3$ | $b_4$ | $b_5$ | $b_6$ | $b_7$ | $b_8$ | $b_9$ | $b_{10}$ | $b_{11}$ | $b_{12}$ | $b_{13}$ | $b_{14}$ | $b_{15}$ | $b_{16}$ | $b_{17}$ | $b_{18}$ | $b_{19}$ | $b_{20}$ |
|---|---|---|---|---|---|---|---|---|---|---|---|---|---|---|---|---|---|---|---|---|---|
| 0 | 0 | | | | | | | | | | | | | | | | | | | | |
| 1 | 3.12 | 0 | | | | | | | | | | | | | | | | | | | |
| 2 | 4.40 | 3.79 | 0 | | | | | | | | | | | | | | | | | | |
| 3 | 5.40 | 5.65 | 4.08 | 0 | | | | | | | | | | | | | | | | | |
| 4 | 6.23 | 7.15 | 6.32 | 4.27 | 0 | | | | | | | | | | | | | | | | |
| 5 | 6.98 | 8.40 | 8.10 | 6.75 | 4.41 | 0 | | | | | | | | | | | | | | | |
| 6 | 7.64 | 9.47 | 9.56 | 8.28 | 7.08 | 4.54 | 0 | | | | | | | | | | | | | | |
| 7 | 8.25 | 10.42 | 10.90 | 10.45 | 9.32 | 7.35 | 4.62 | 0 | | | | | | | | | | | | | |
| 8 | 8.83 | 11.30 | 12.05 | 11.95 | 11.10 | 9.70 | 7.55 | 4.70 | 0 | | | | | | | | | | | | |
| 9 | 9.36 | 12.10 | 13.05 | 13.25 | 12.75 | 11.60 | 10.03 | 7.73 | 4.75 | 0 | | | | | | | | | | | |
| 10 | 9.87 | 12.95 | 14.22 | 14.55 | 14.30 | 13.50 | 12.15 | 10.35 | 7.90 | 4.80 | 0 | | | | | | | | | | |
| 11 | 10.33 | 13.55 | 15.10 | 15.75 | 15.65 | 15.10 | 14.00 | 12.60 | 10.62 | 8.05 | 4.87 | 0 | | | | | | | | | |
| 12 | 10.80 | 14.40 | 16.00 | 16.85 | 17.05 | 16.65 | 15.80 | 14.60 | 12.90 | 10.85 | 8.18 | 4.92 | 0 | | | | | | | | |
| 13 | 11.23 | 15.00 | 16.90 | 17.80 | 18.25 | 17.70 | 17.40 | 16.40 | 15.00 | 13.15 | 11.00 | 8.27 | 4.94 | 0 | | | | | | | |
| 14 | 11.65 | 15.75 | 17.65 | 18.80 | 19.50 | 19.35 | 18.95 | 18.15 | 16.95 | 15.40 | 13.45 | 11.40 | 8.36 | 4.99 | 0 | | | | | | |
| 15 | 12.07 | 16.25 | 18.50 | 19.75 | 20.50 | 20.55 | 20.40 | 19.47 | 18.70 | 17.40 | 15.75 | 13.70 | 11.35 | 8.47 | 5.02 | 0 | | | | | |
| 16 | 12.47 | 16.90 | 19.15 | 20.70 | 21.40 | 21.85 | 21.50 | 21.10 | 20.40 | 19.02 | 17.80 | 16.05 | 13.90 | 11.50 | 8.54 | 5.03 | 0 | | | | |
| 17 | 12.85 | 17.45 | 20.00 | 21.50 | 22.50 | 22.90 | 22.95 | 22.70 | 22.00 | 21.10 | 19.80 | 18.20 | 16.40 | 14.15 | 11.65 | 8.62 | 5.08 | 0 | | | |
| 18 | 13.22 | 18.00 | 20.40 | 22.20 | 23.20 | 23.90 | 24.10 | 23.90 | 23.40 | 22.60 | 21.60 | 20.20 | 18.55 | 16.60 | 14.30 | 11.75 | 8.69 | 5.10 | 0 | | |
| 19 | 13.57 | 21.60 | 21.00 | 22.90 | 24.30 | 24.80 | 25.20 | 25.20 | 25.00 | 24.10 | 23.30 | 22.55 | 20.60 | 18.85 | 16.95 | 14.50 | 11.85 | 8.76 | 5.11 | 0 | |
| 20 | 13.95 | 22.00 | 24.20 | 23.50 | 24.95 | 25.80 | 25.90 | 26.40 | 26.00 | 25.60 | 24.90 | 23.70 | 22.65 | 20.90 | 19.13 | 17.10 | 14.65 | 11.95 | 8.80 | 5.14 | 0 |

FIGURES

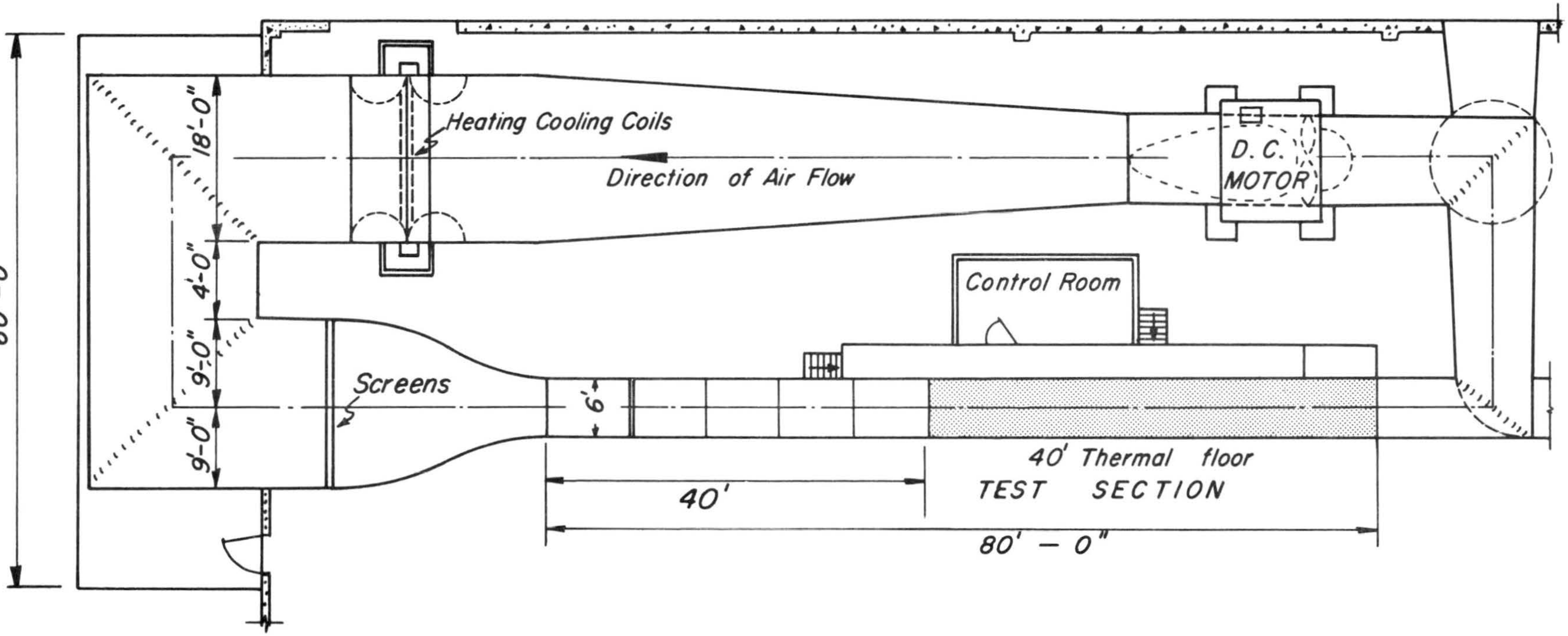


PLAN VIEW

Fig. 1 Wind tunnel

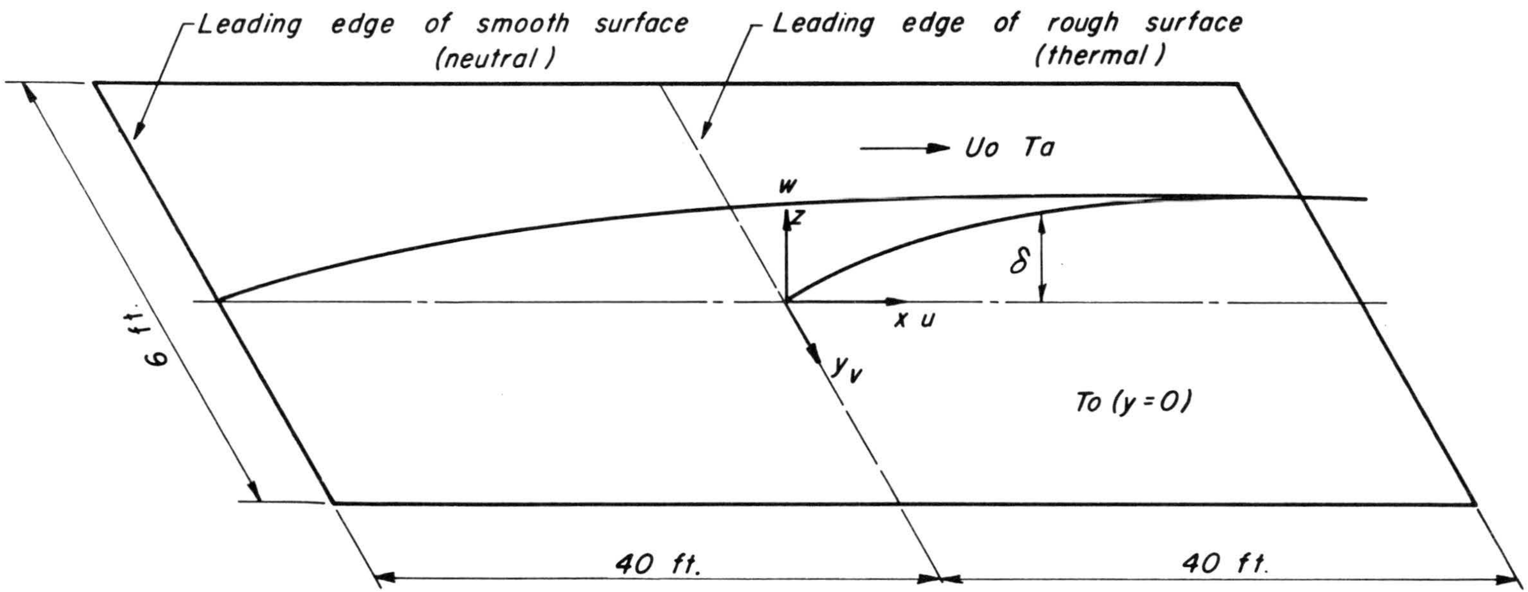


Fig. 2 Definition sketch

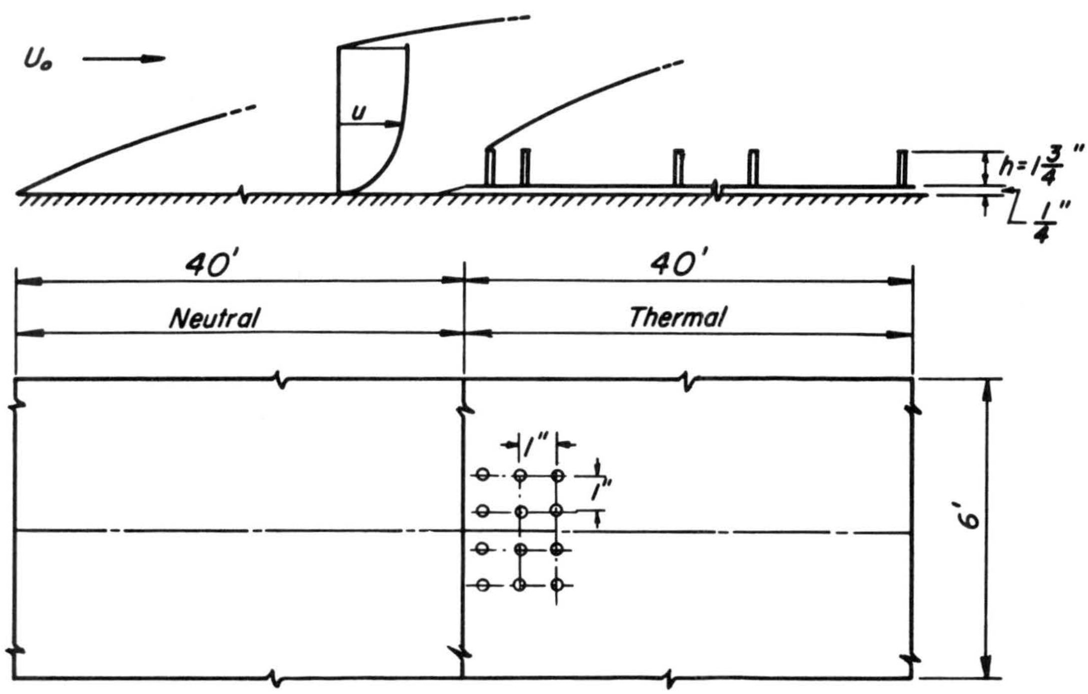


*Fig. 3 Schematic experimental model in wind tunnel*

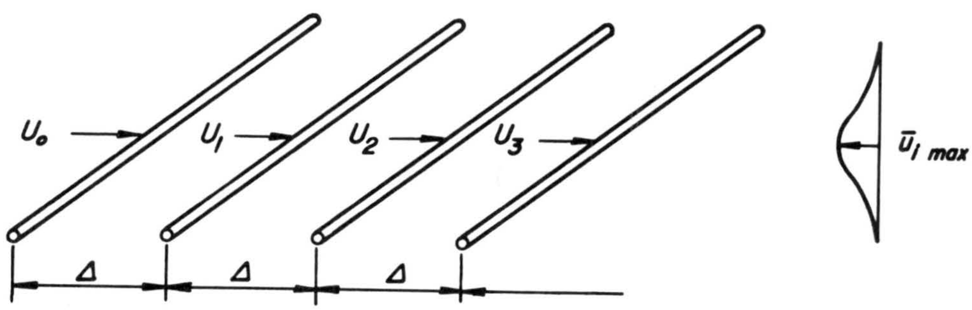


*Fig. 4 Schematic model of the aligned cylinders*

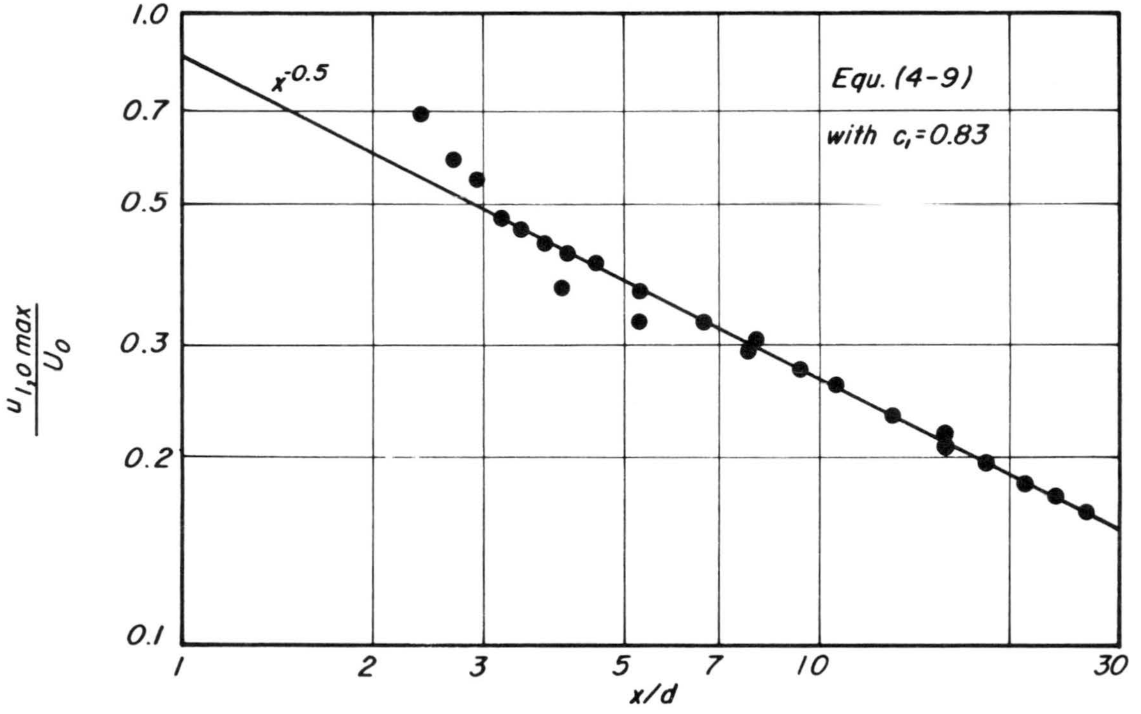


Fig. 5 Maximum velocity defect $u_{1,0\,max}$ of two-dimensional wake

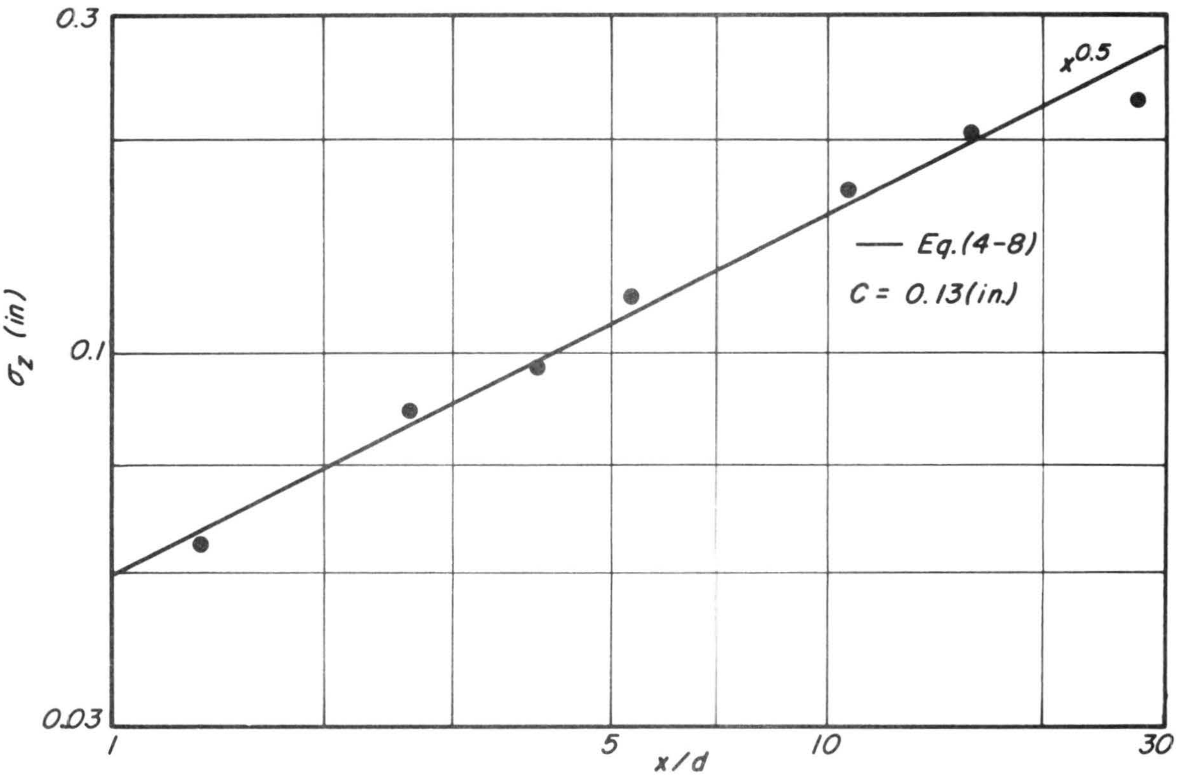


Fig. 6 Standard deviation of two - dimensional wake

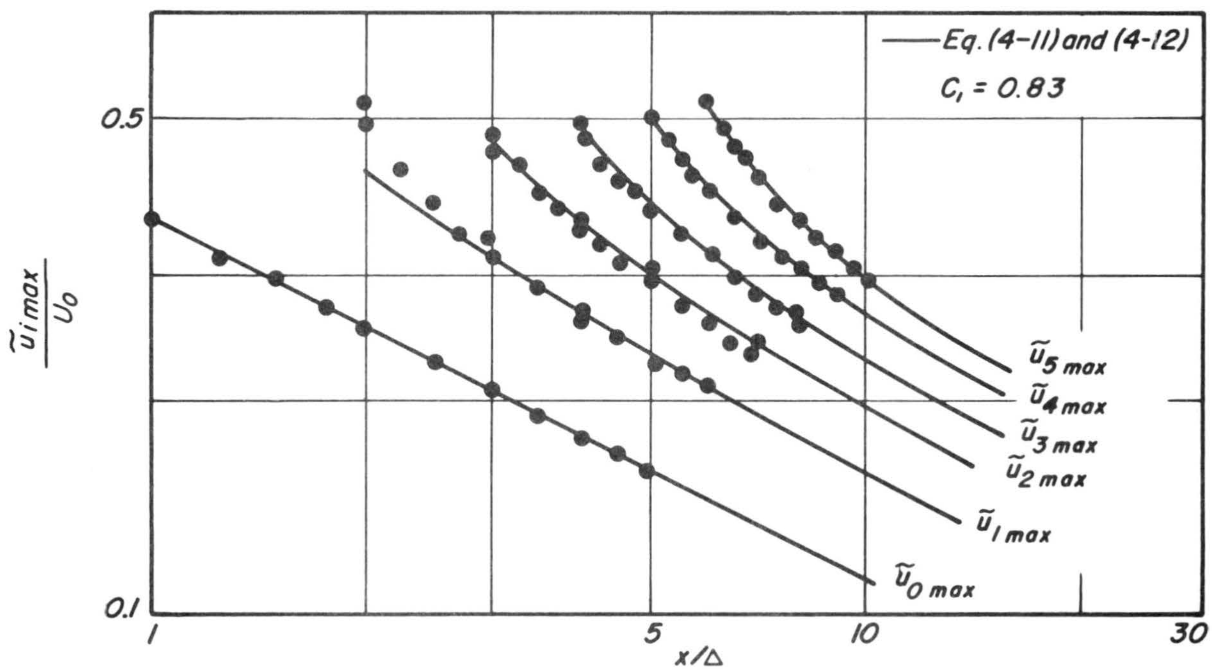


Fig. 7 Maximum velocity defect of combination of wakes

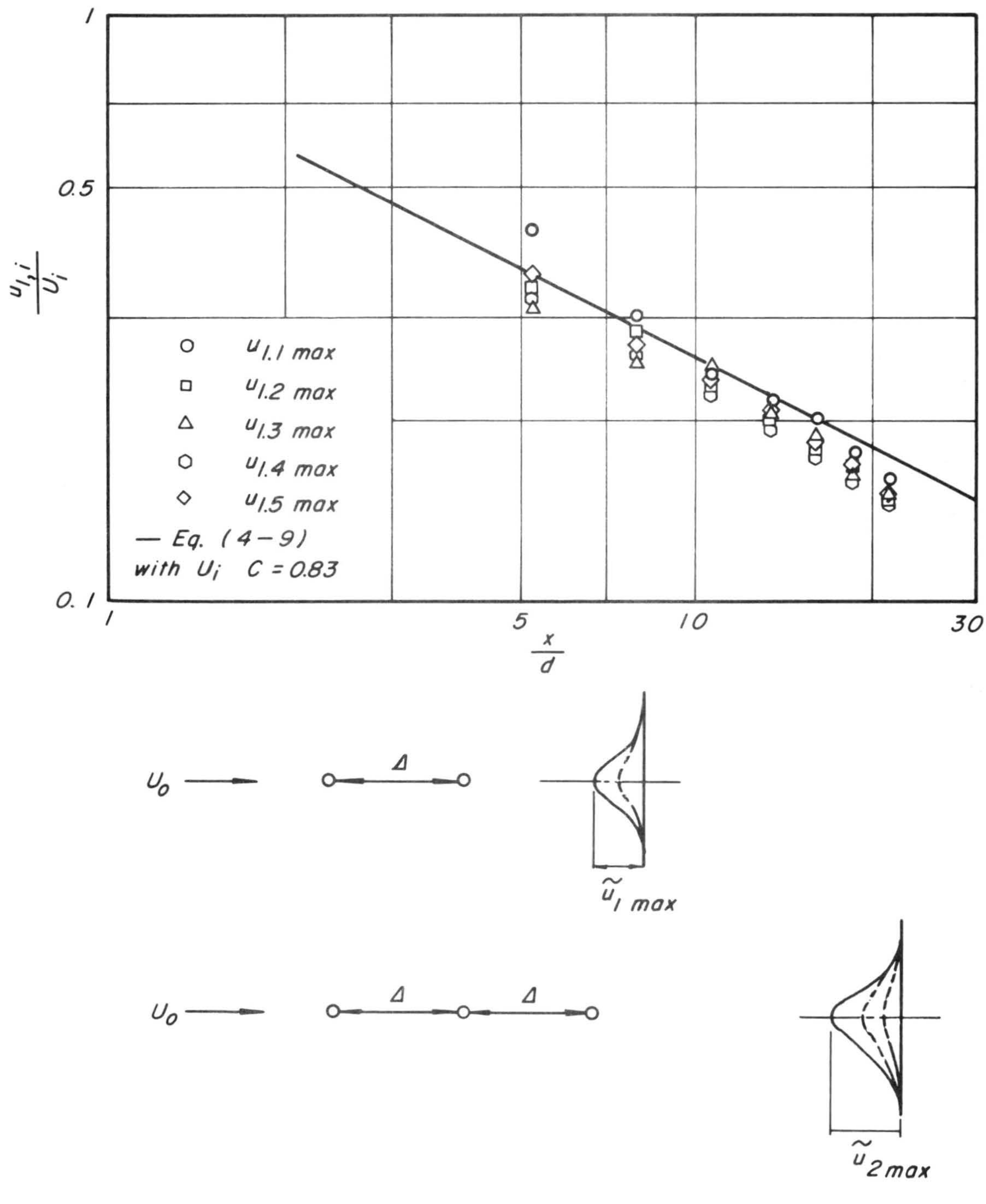


*Fig. 8 Maximum velocity defect of each wake in combination of wakes*

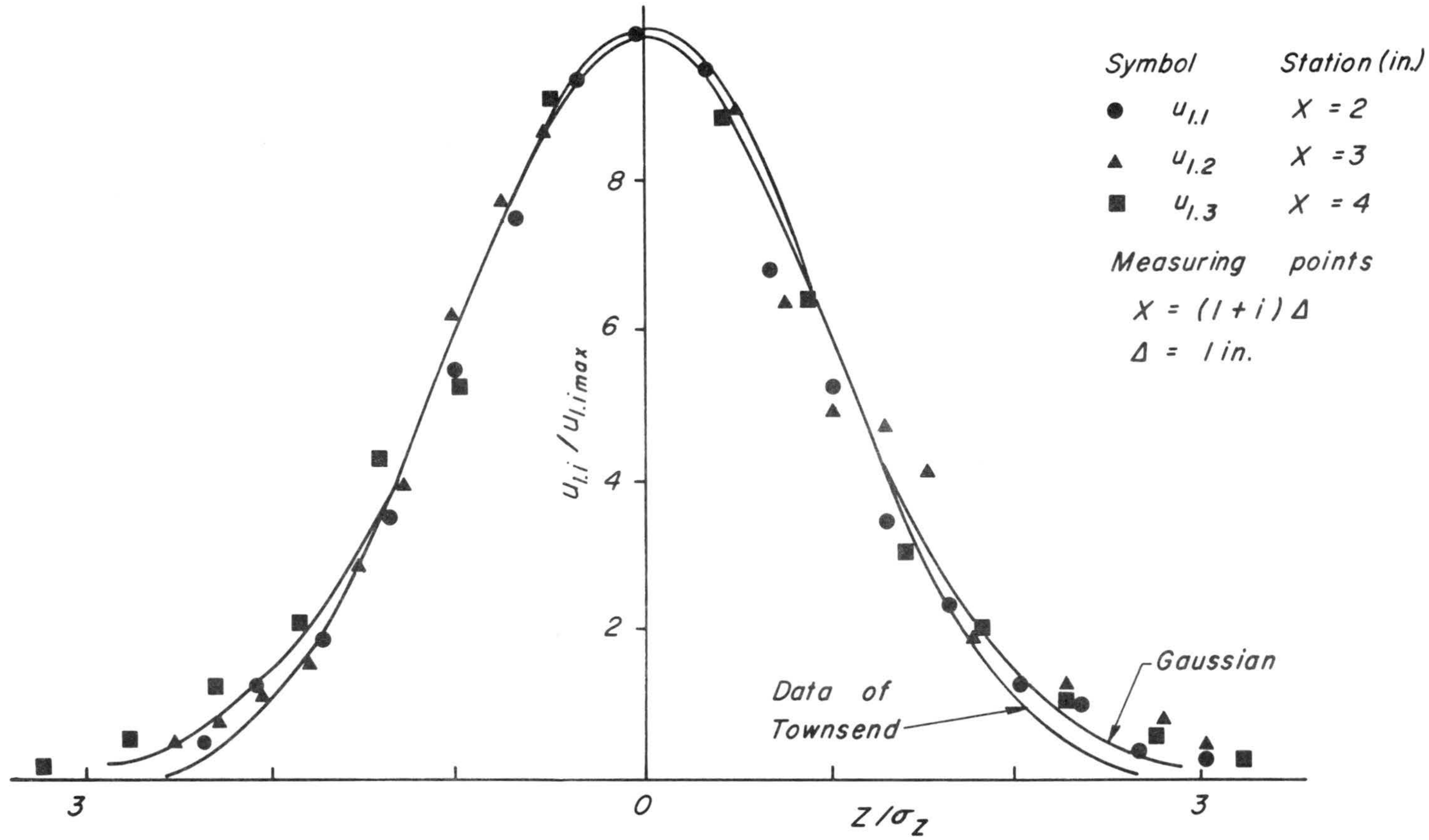


Fig. 9A Velocity profiles of $u_{1.i}$

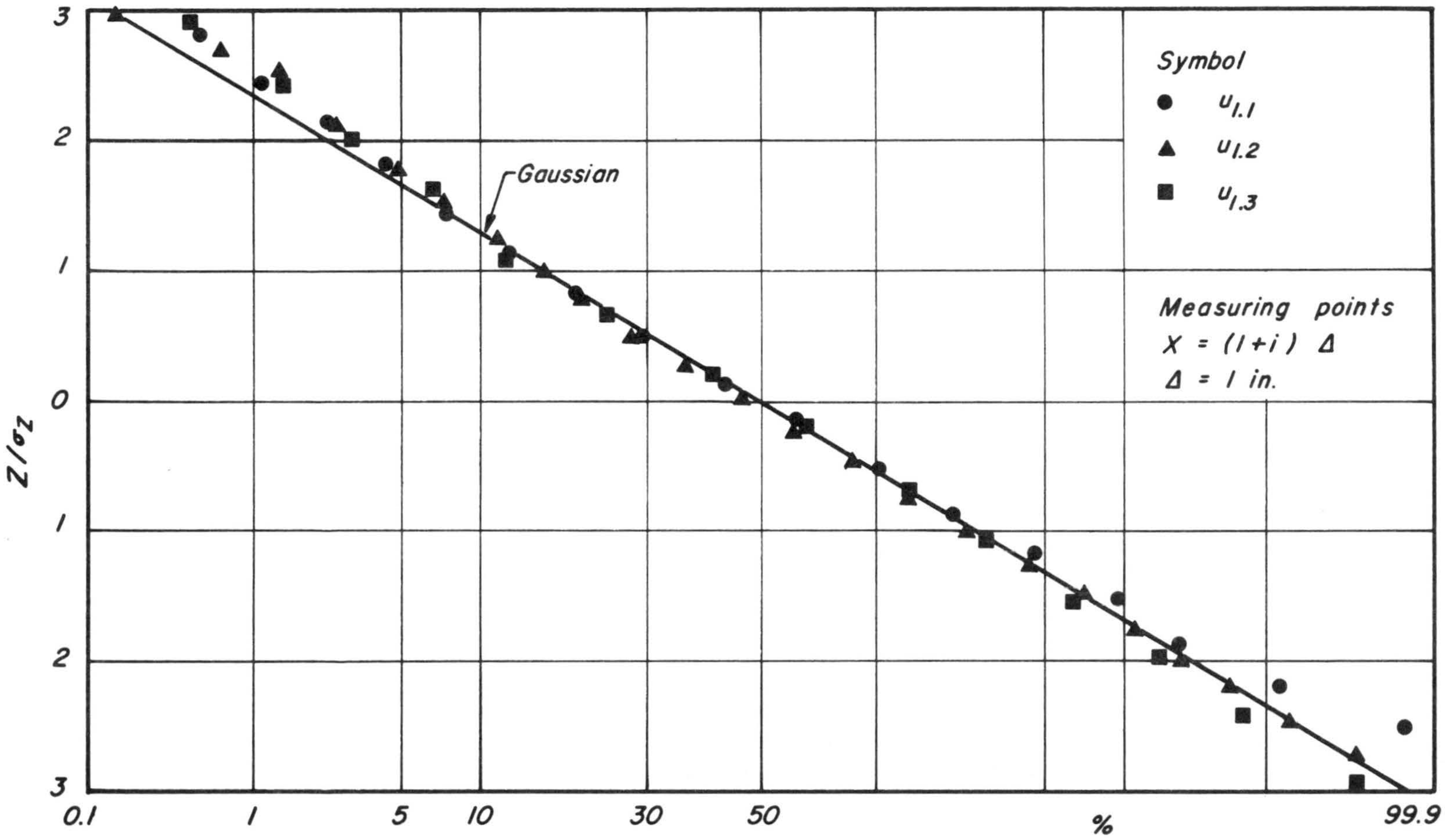


Fig. 9 B $u_{1.i}$ in Gaussian scale

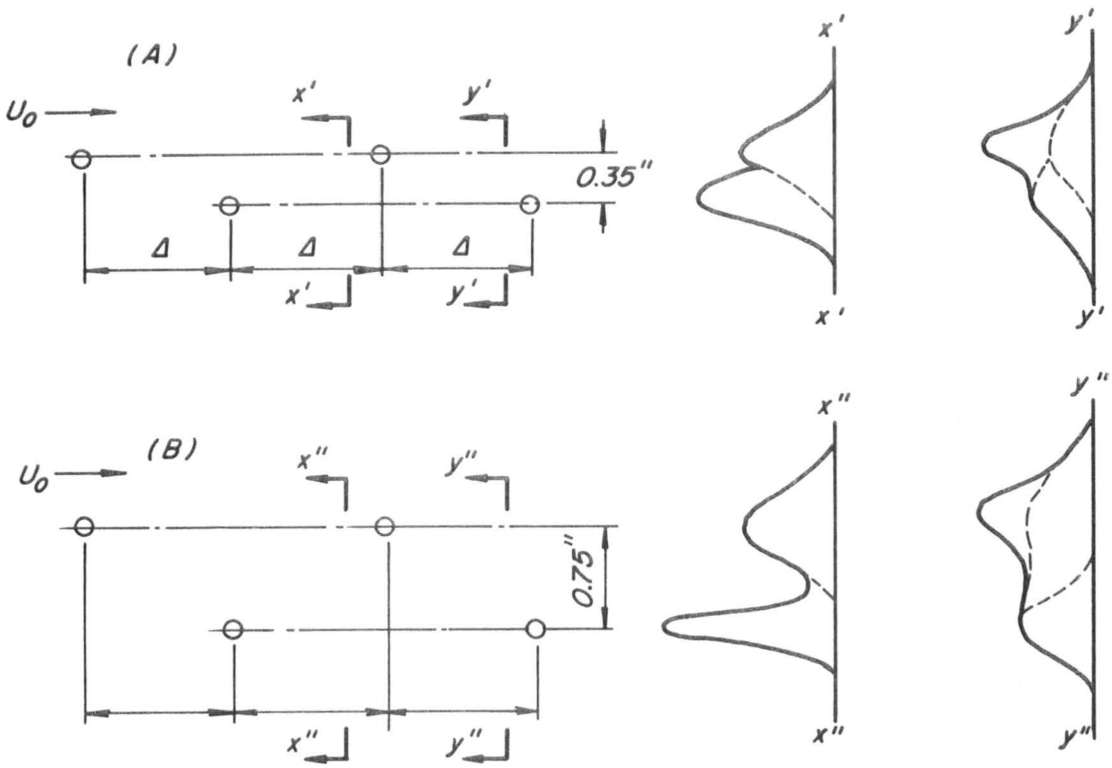


Fig. 10 Schematic model of irregularly alined cylinders

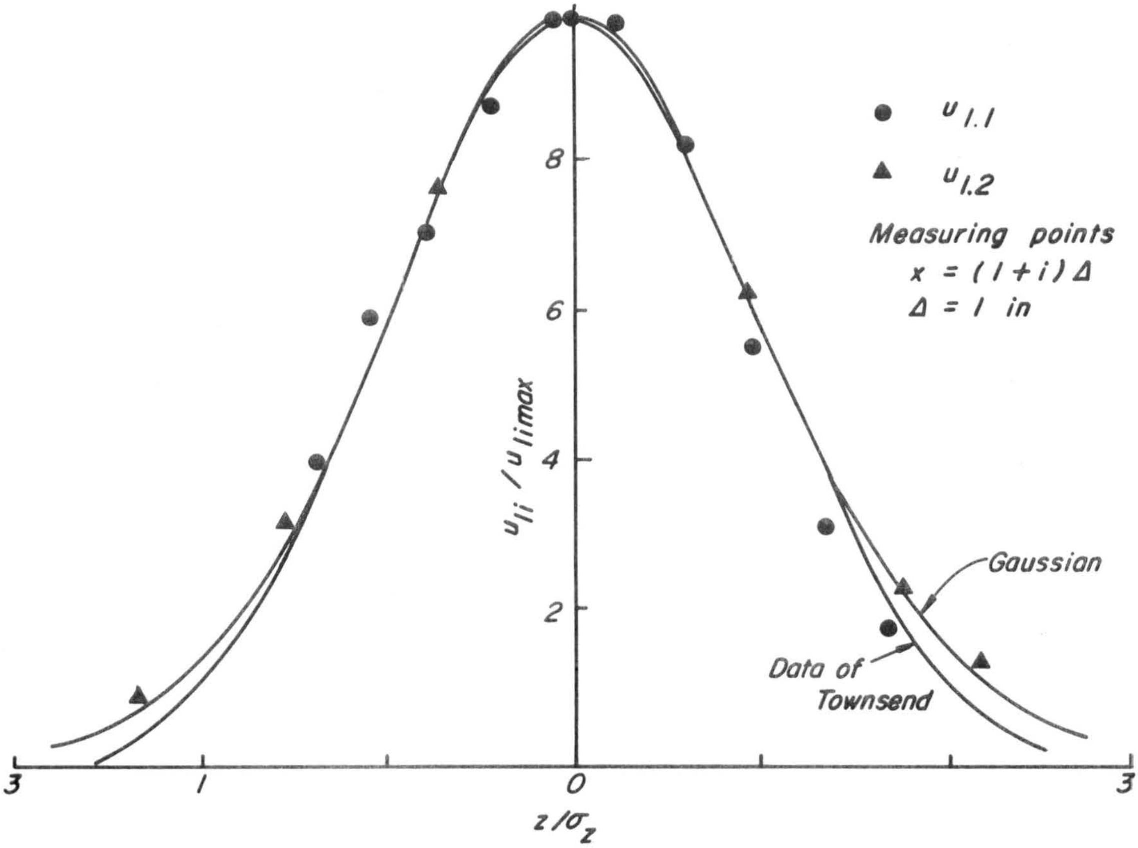


Fig. 11 Velocity profiles $u_{1,i}$ of Fig. 10 (A)

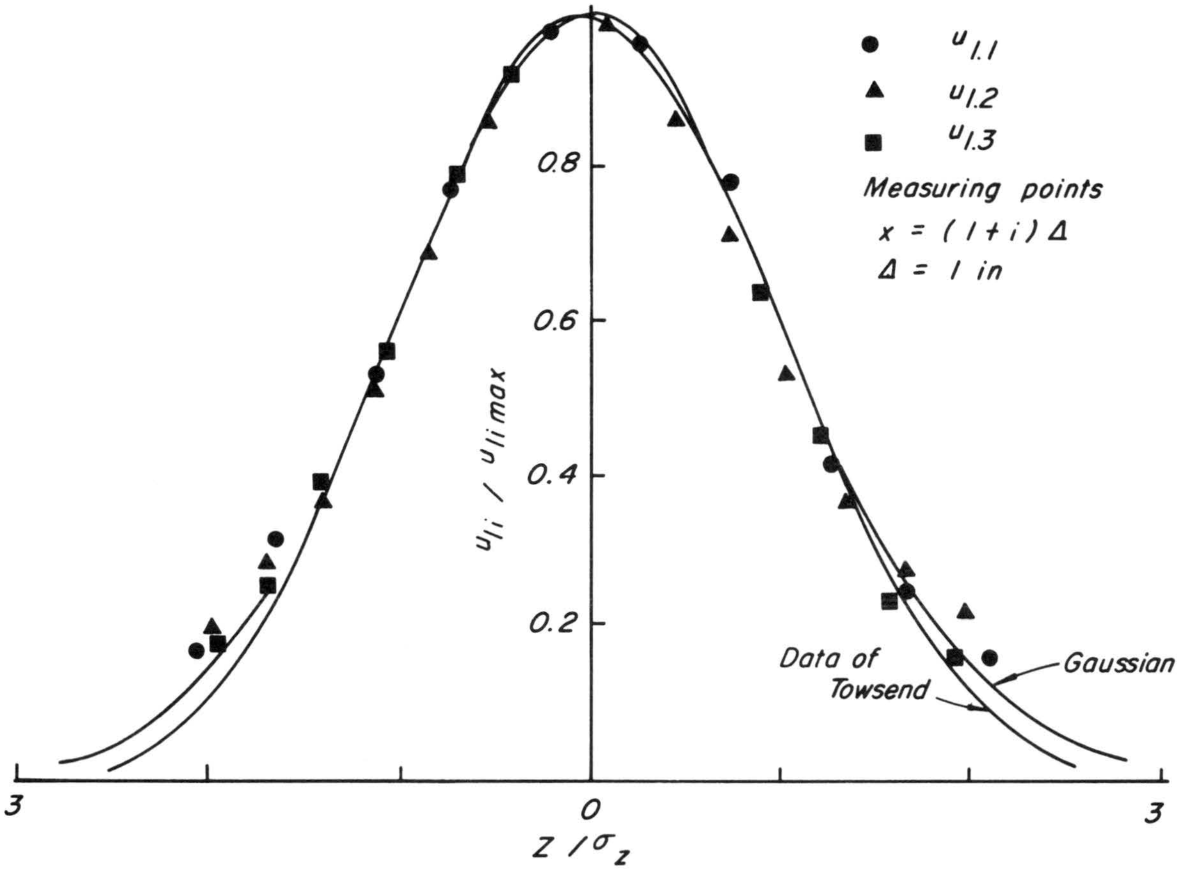


Fig. 12 Velocity profile of $u_{1i}$ of Fig. 10 (B)

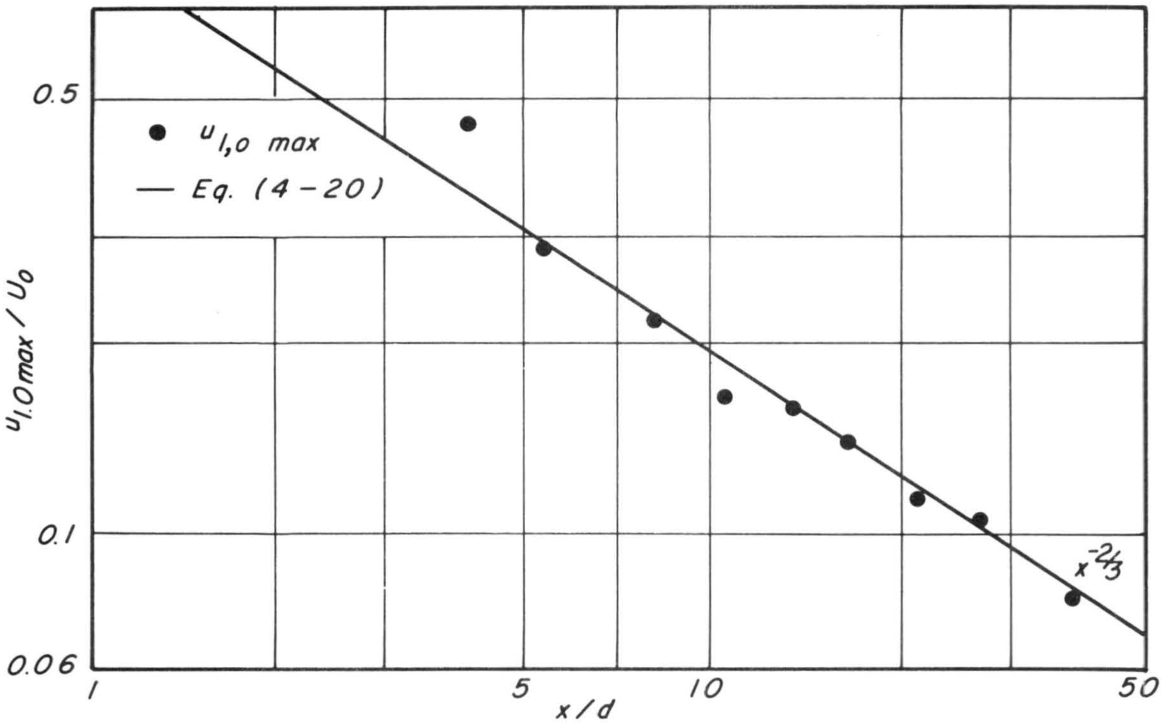


Fig. 13 $u_{1.0}$ max of 3-D wake generated by the end of semi-infinite cylinder

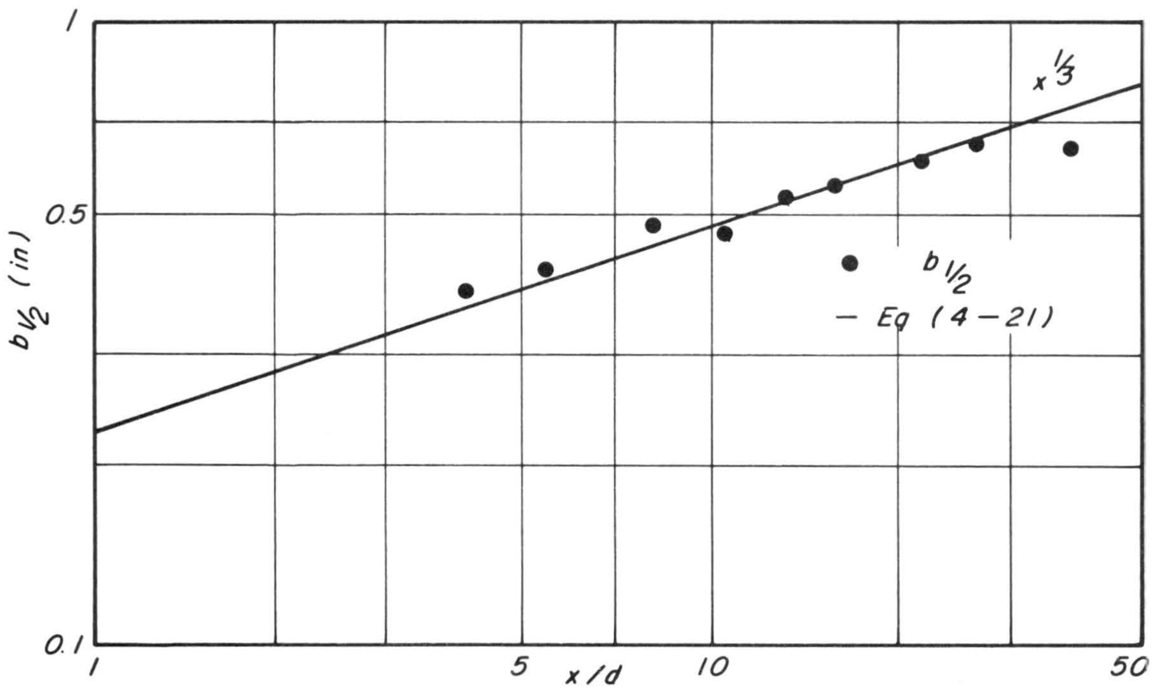


Fig. 14 Half width of 3-D wake in Fig. 13

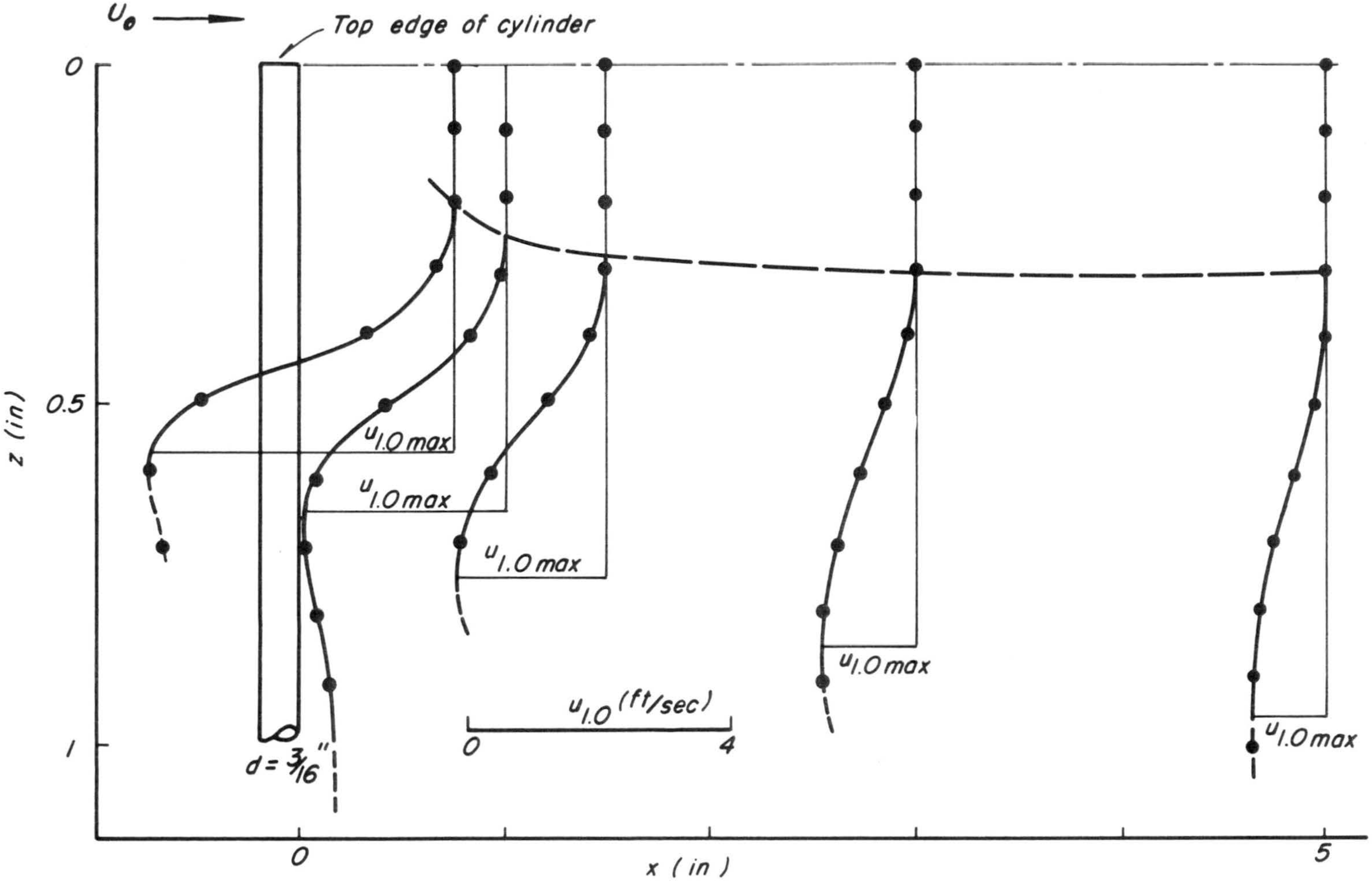


Fig. 15 Velocity profiles behind one semi-infinite cylinder

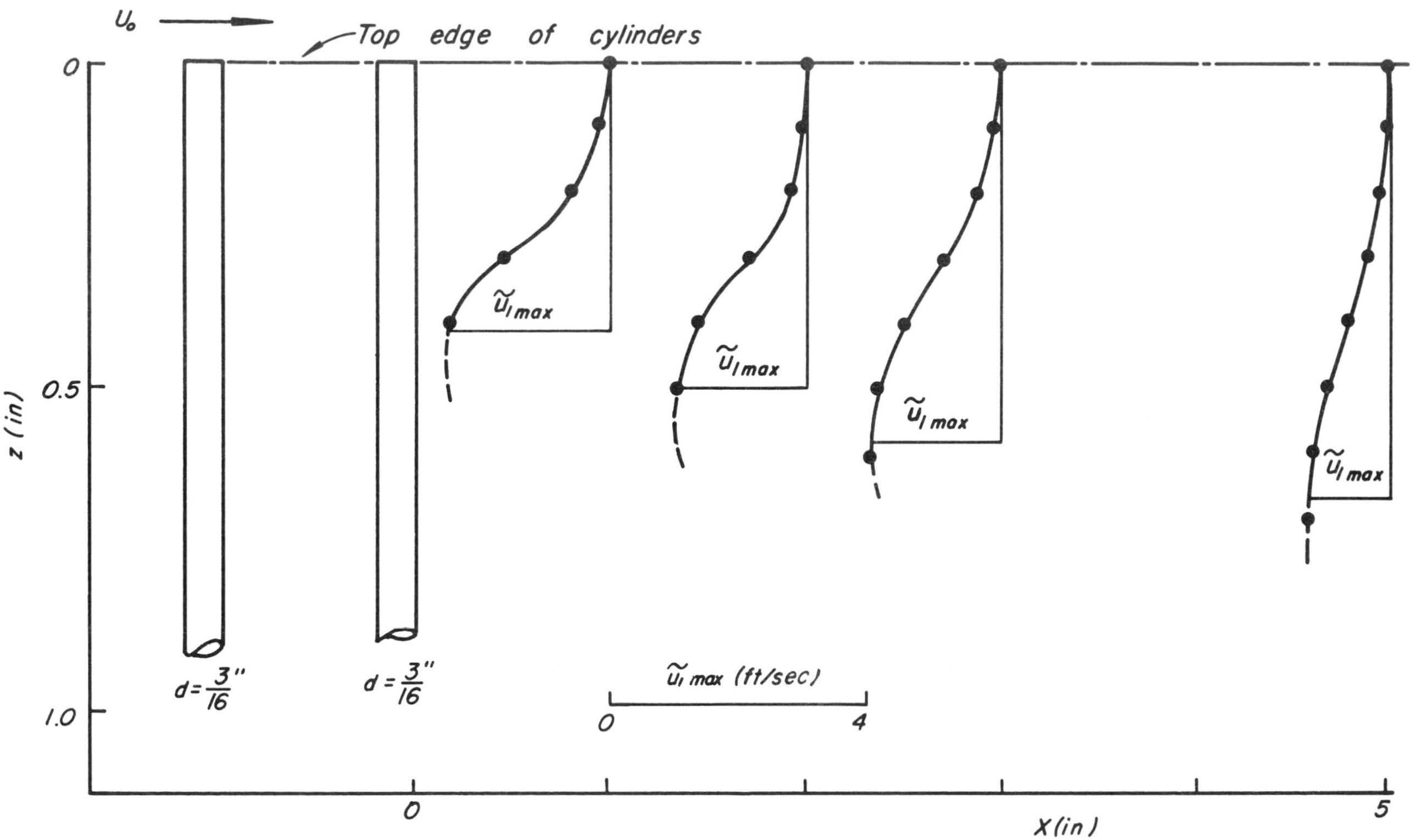


Fig. 16 Velocity profiles behind two semi-infinite cylinders

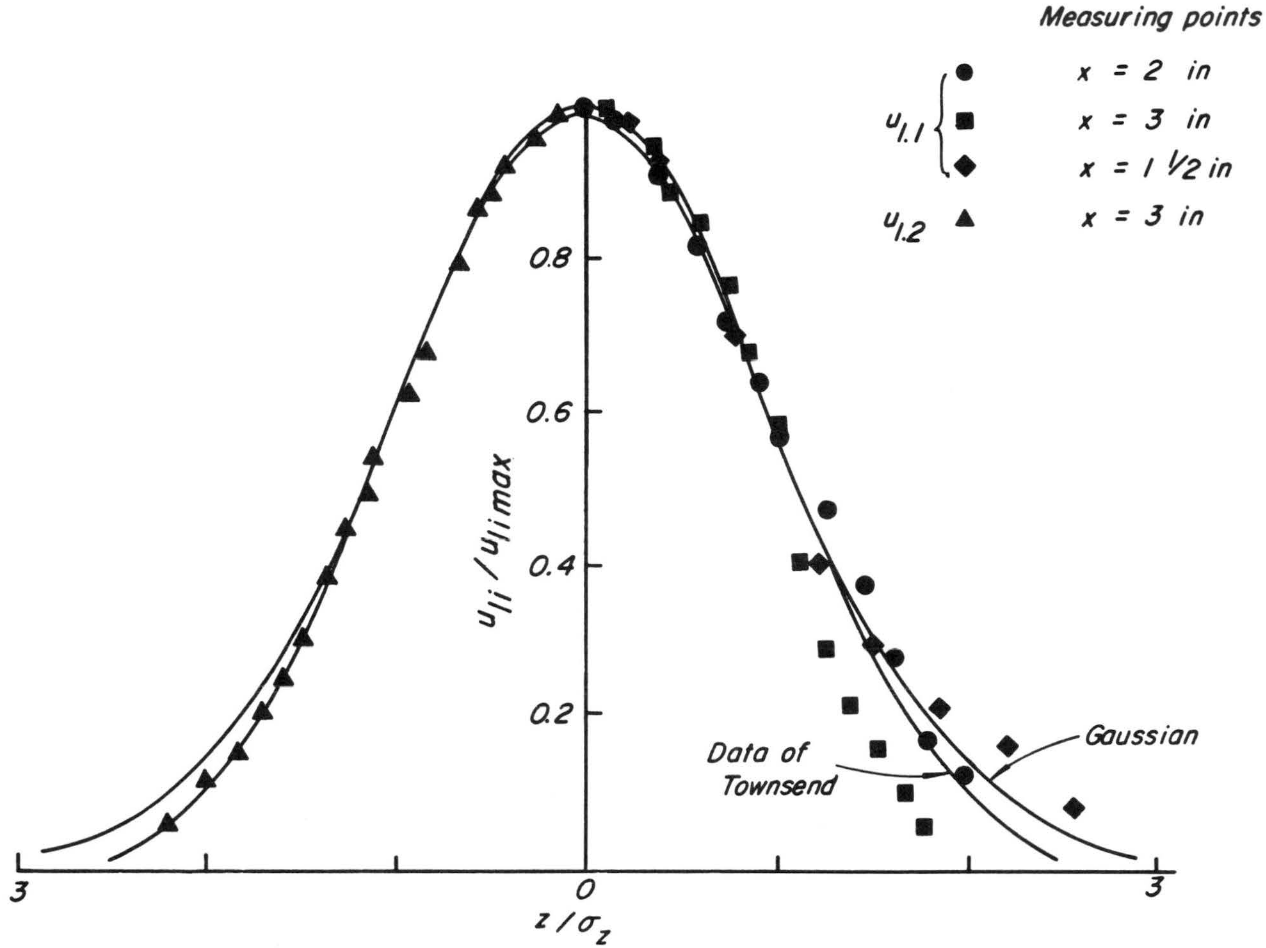


Fig. 17 Velocity profile of $u_{l.i}$ (3–D)

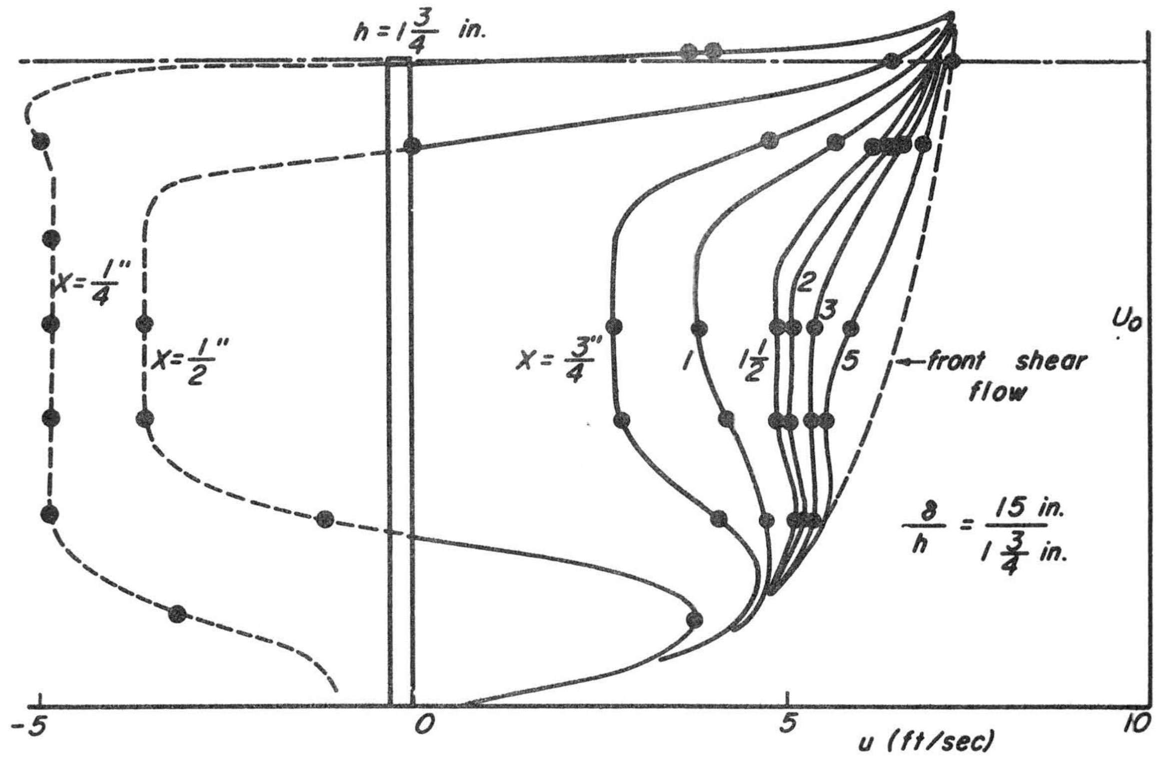


*Fig. 18 Velocity profile behind single roughness element in the turbulent shear flow*

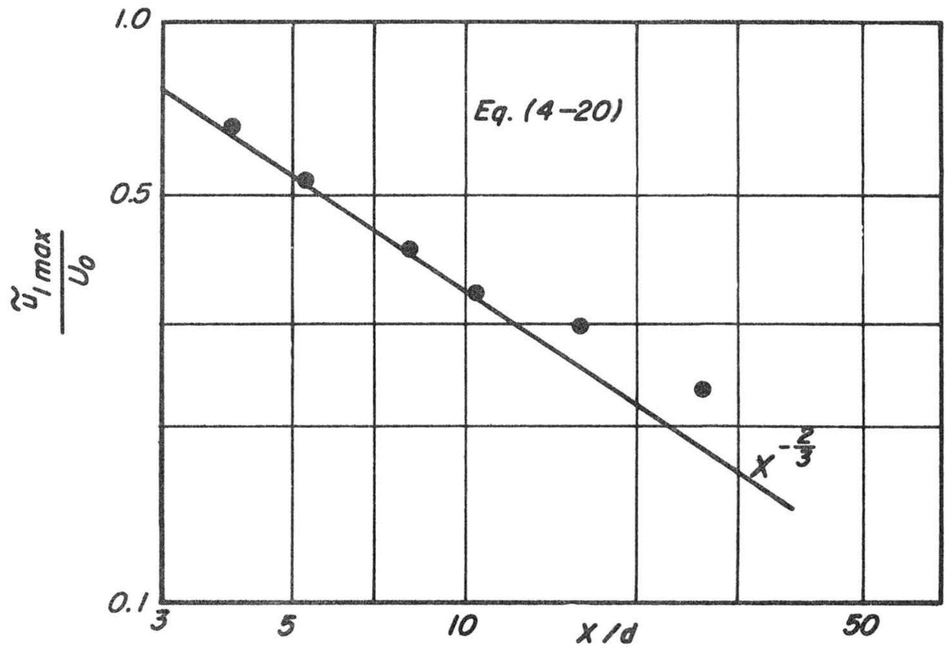


*Fig. 19 $u_{1,omax}$ of 3-D wake in Fig. 18*

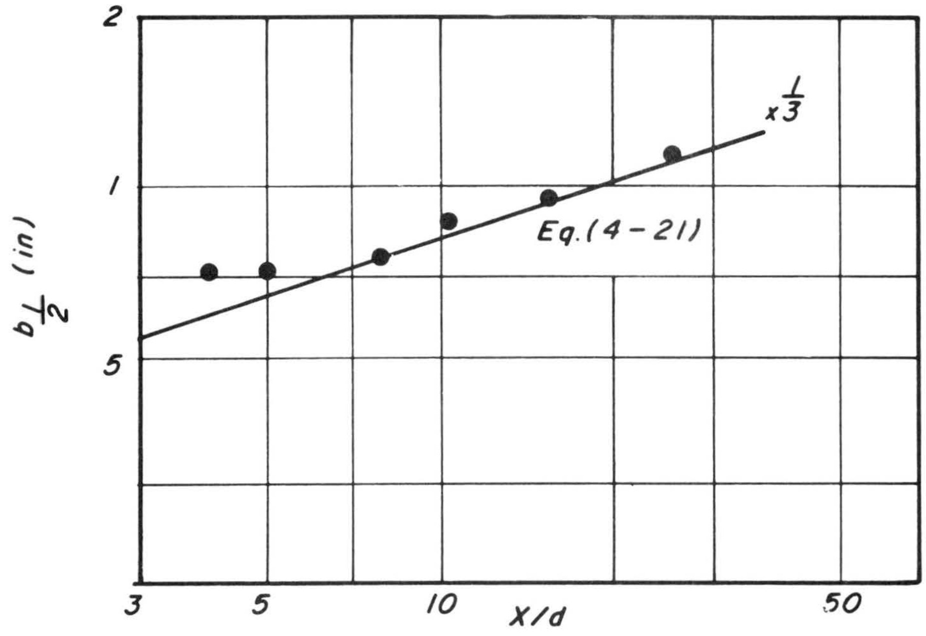


Fig. 20 Half width of 3−D wake in Fig. 18

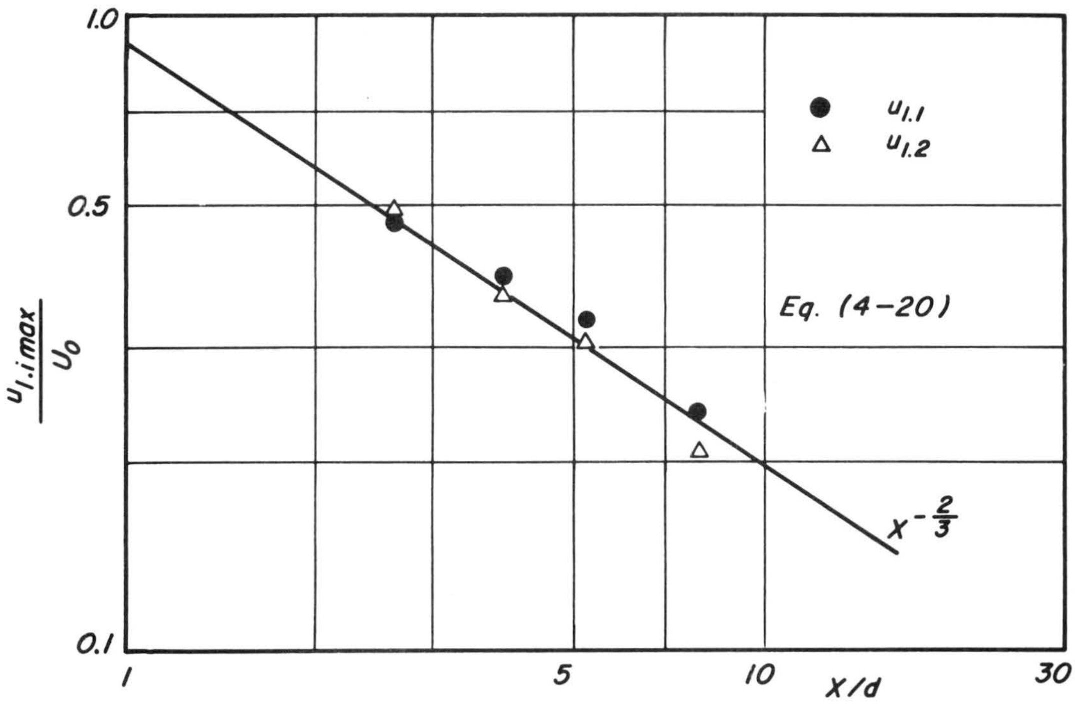


Fig. 21 $u_{1.i\,max}$ of 3−D wakes generated by each roughness element in the turbulent shear flow

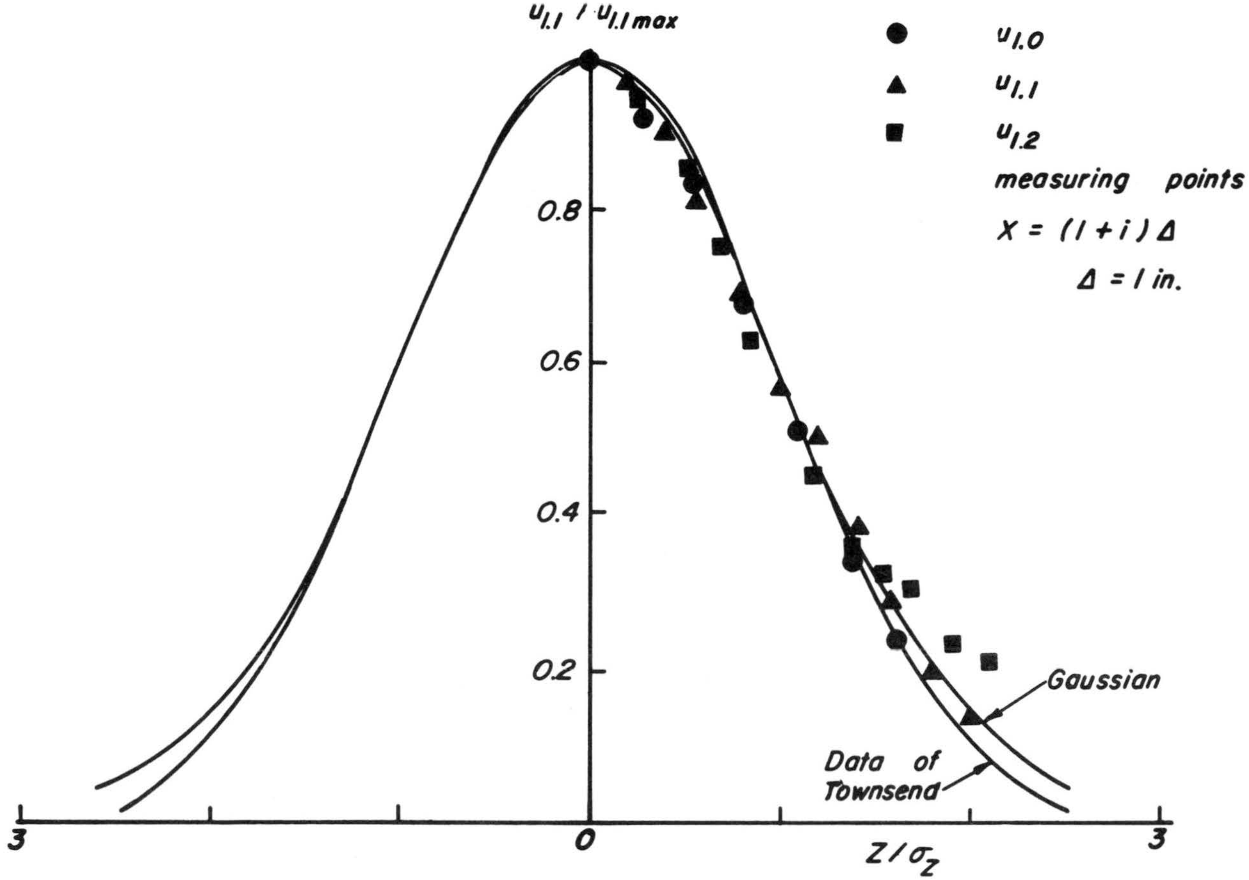


*Fig. 22 Velocity profile of $u_{1.i}$ (3–D) in Fig. 21*

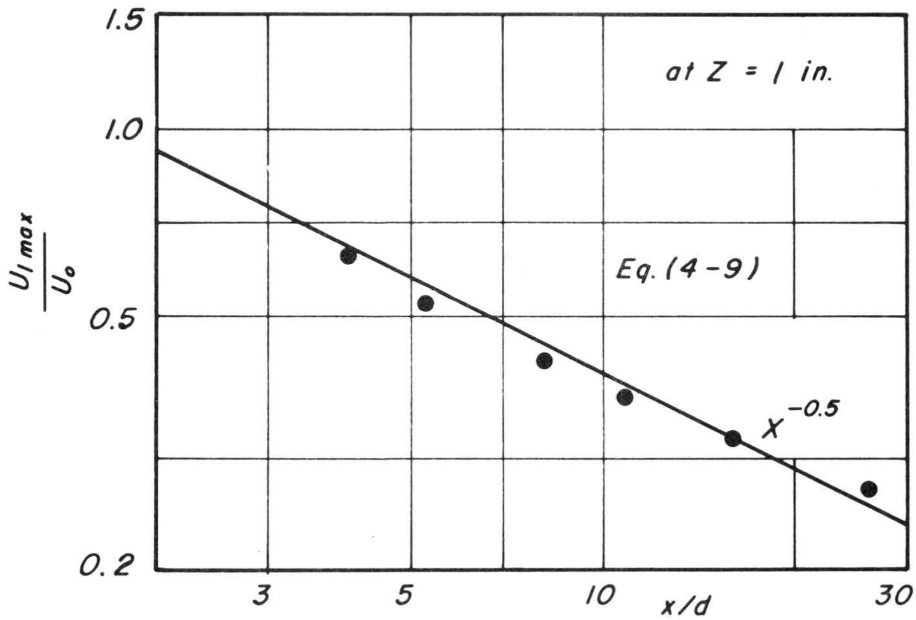


*Fig. 23 Maximum velocity of 2-D wake generated by single roughness element in the turbulent shear flow.*

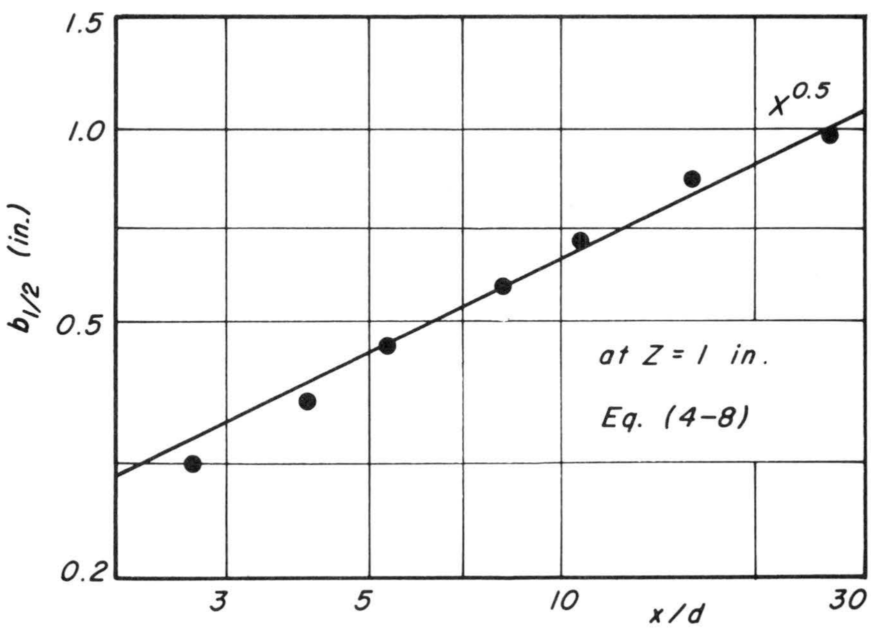


*Fig. 24 Half width of 2-D wake in Fig. 23*

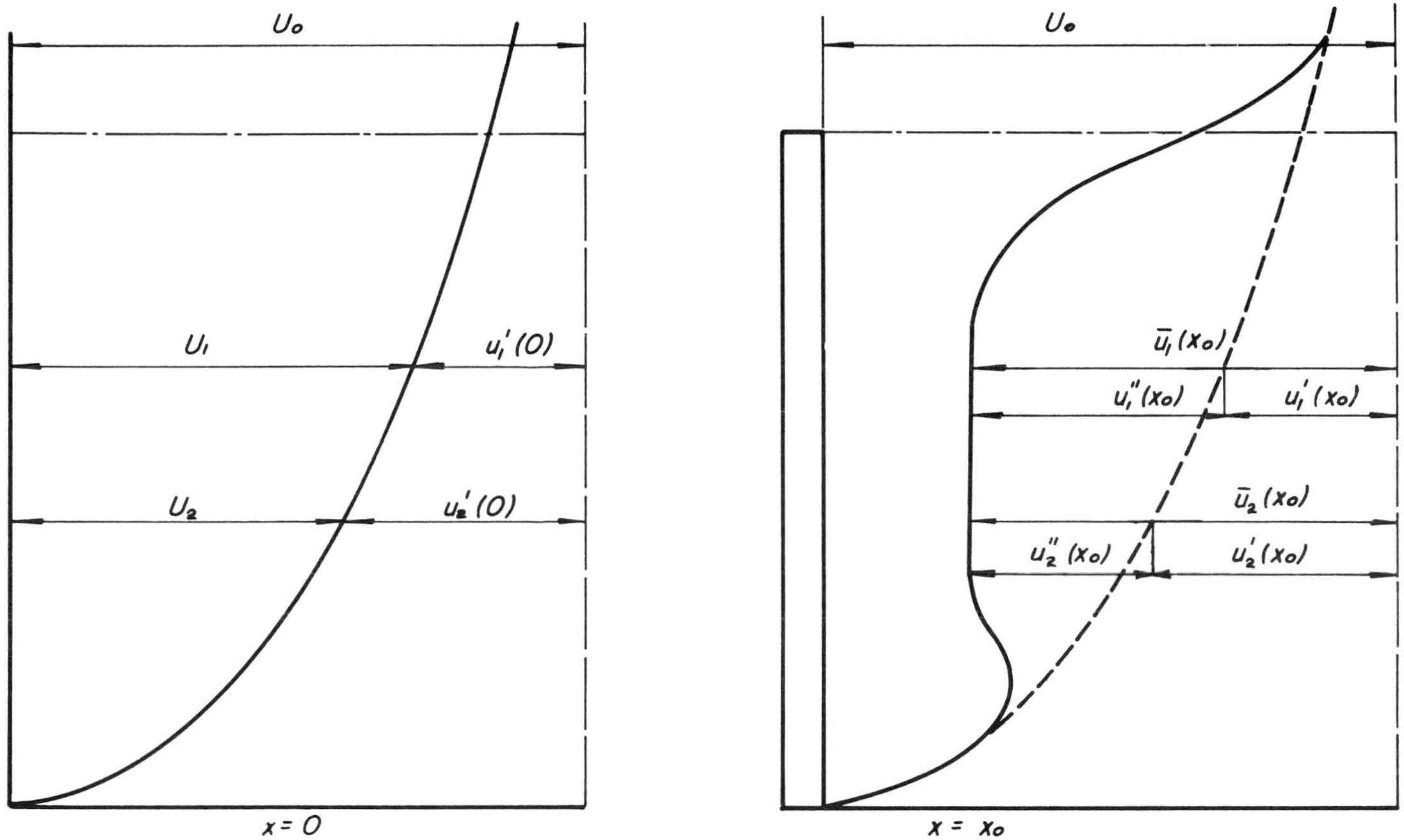


*Fig. 25 Schematic wake flow behind the roughness element in the turbulent shear flow*

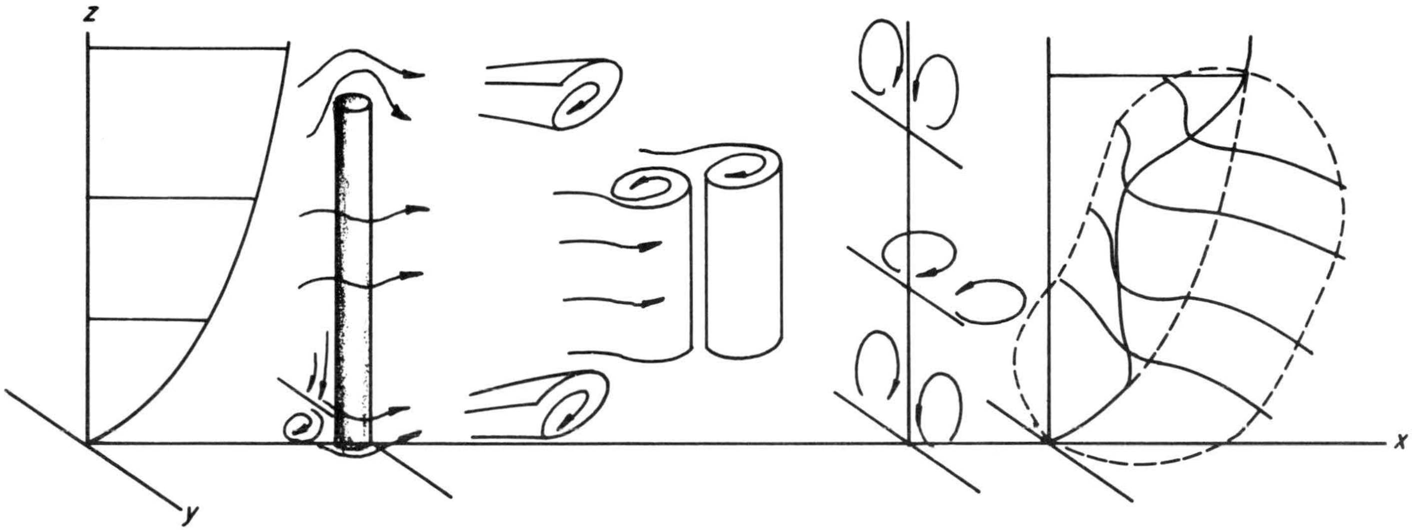


*Fig. 26 Schematic flow diagram behind the roughness element*

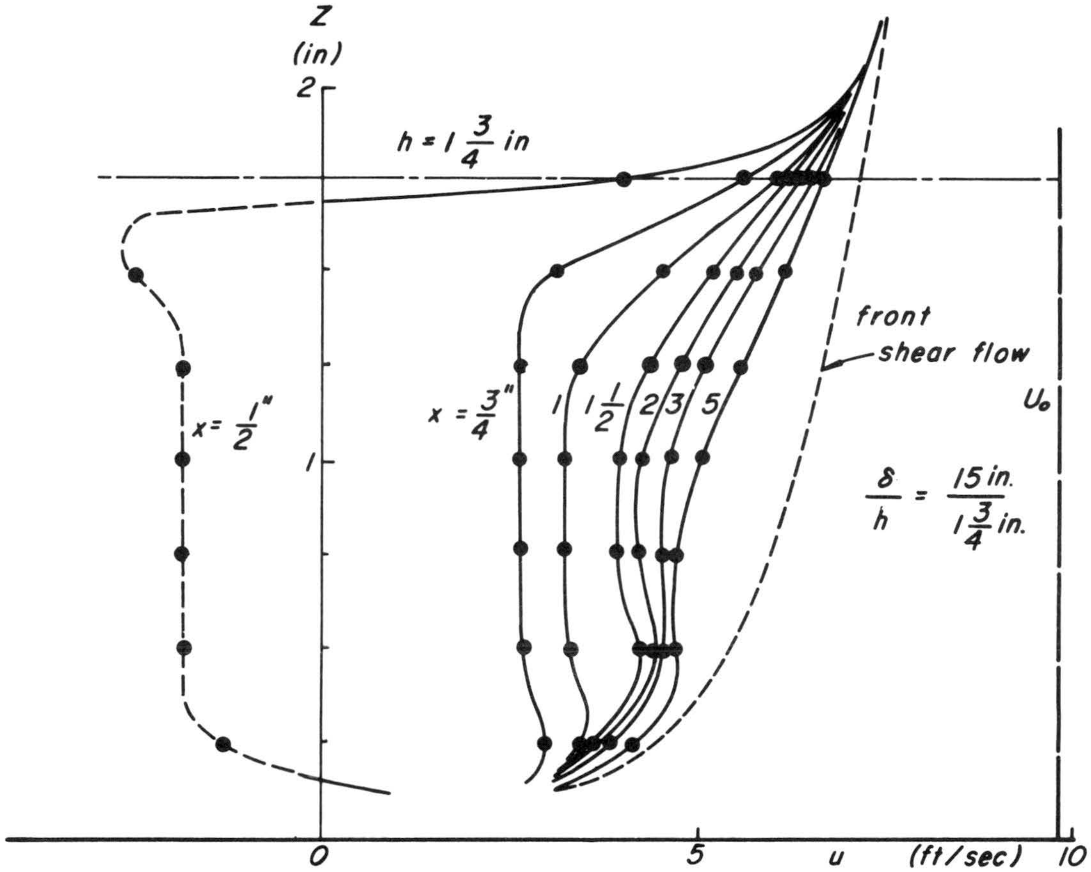


*Fig. 27 Combined wakes--flow behind 5 elements (aligned x-direction) in the turbulent shear flow*

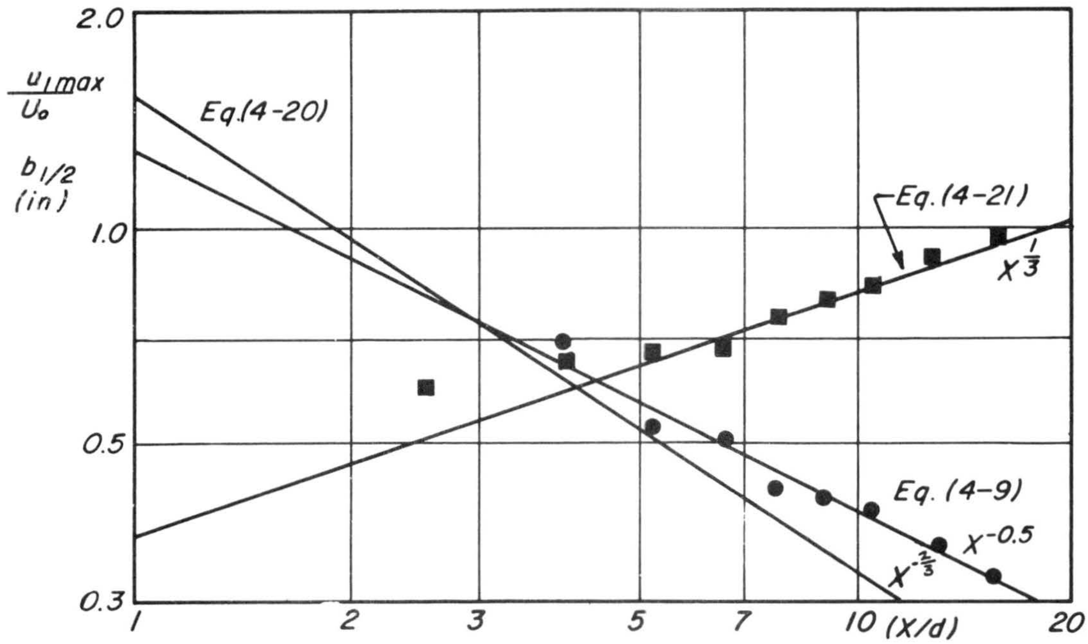


Fig. 28 $u_{1.0max}$ and half width of 3-D wake in Fig. 29

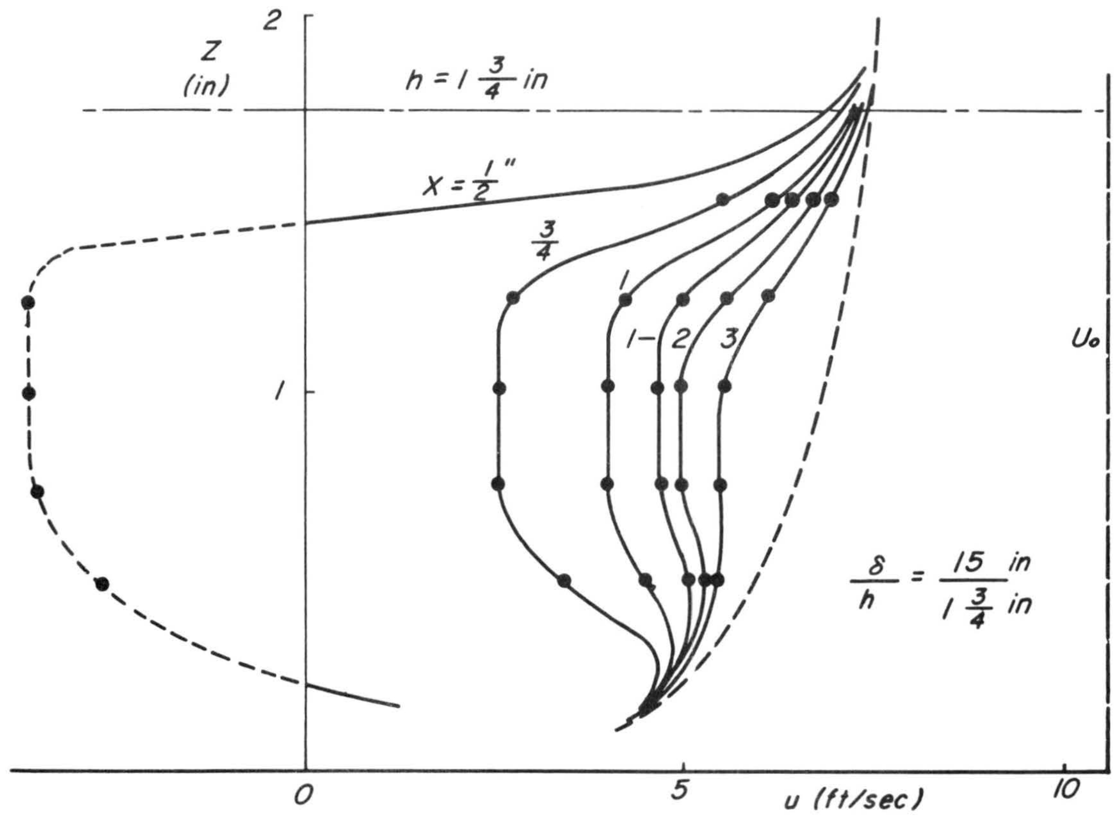


Fig. 29 Combined flow behind a single row (y-direction) of roughness elements in the turbulent shear flow

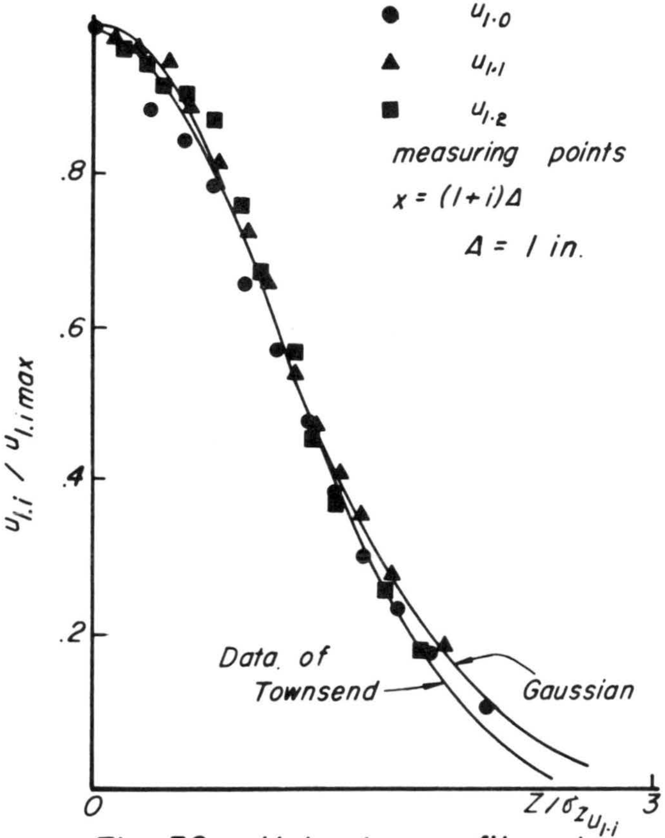


Fig. 30 Velocity profile $u_{1\cdot i}$ (3-D) of cylinder of a row (y-direction)

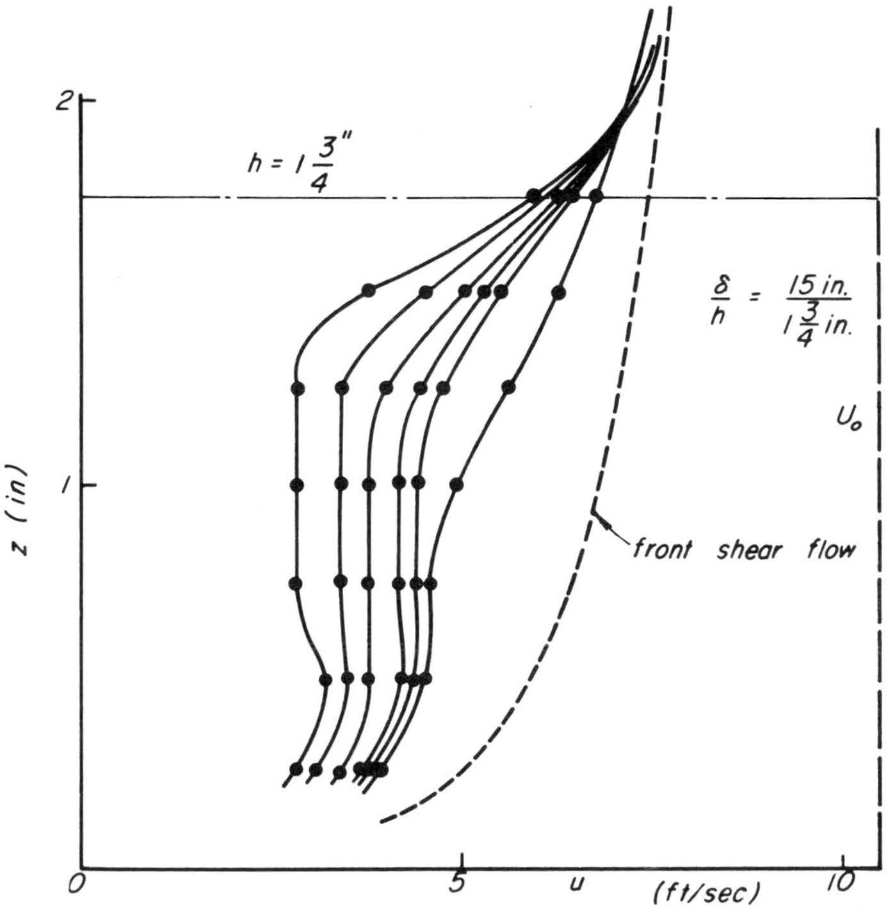


Fig. 31 Combined flow behind cylinder of (y-direction) in the turbulent shear flow

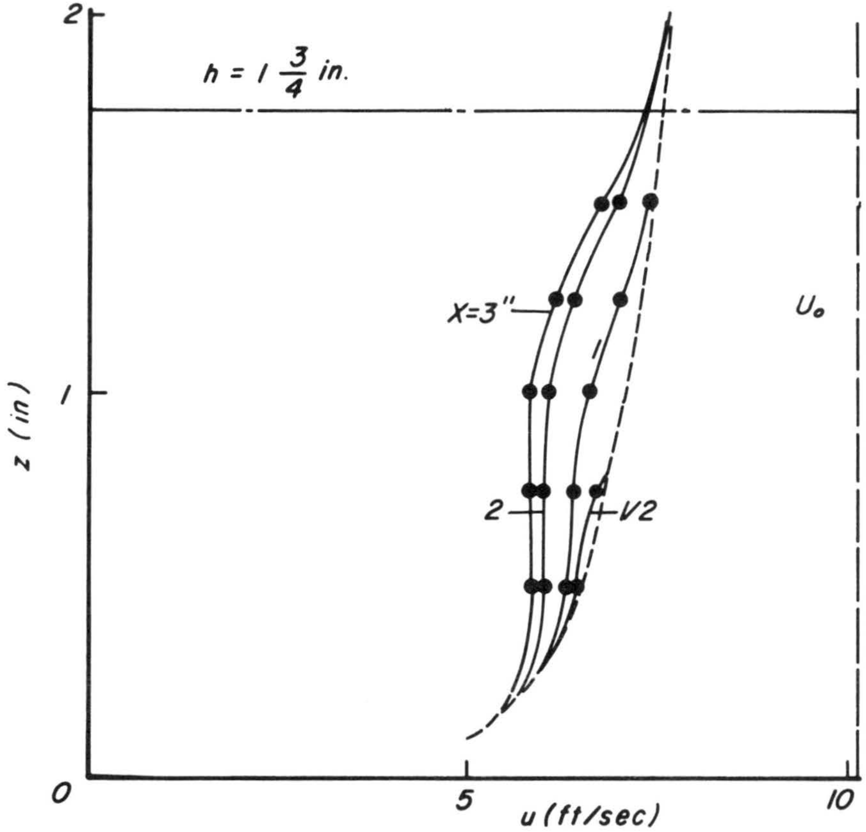


*Fig. 32 Combined flow behind cylinder of a row (y-direction) in the turbulent shear flow (measuring points are midway between cylinders.)*

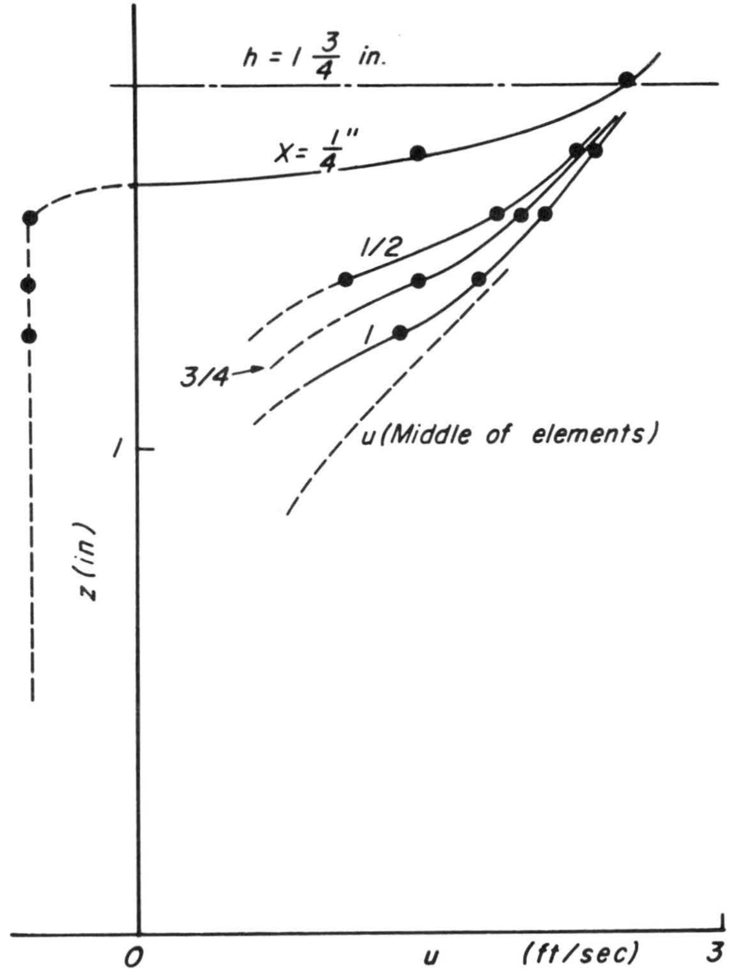


*Fig. 33 Combined wakes behind 188th cylinder in the rough surface*

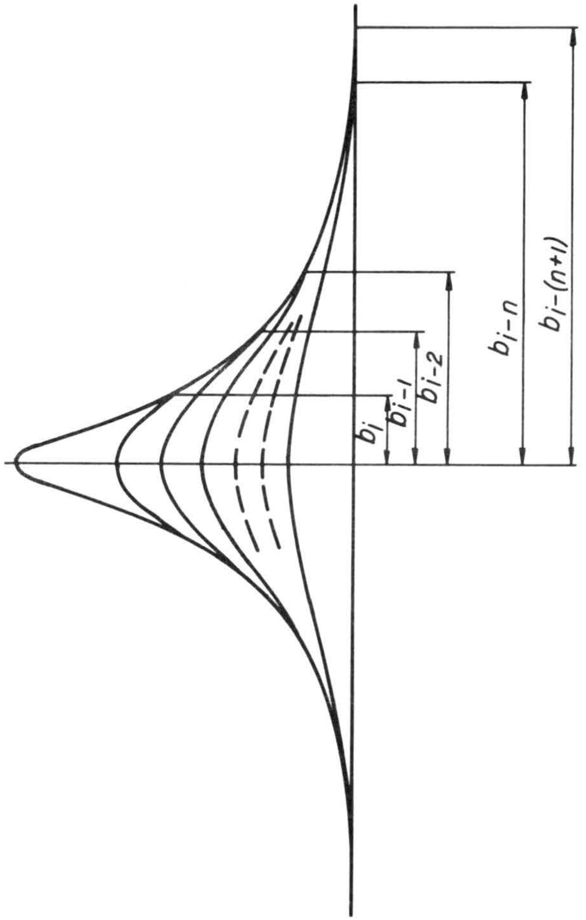


Fig. 34 Schematic diagram of combined wakes

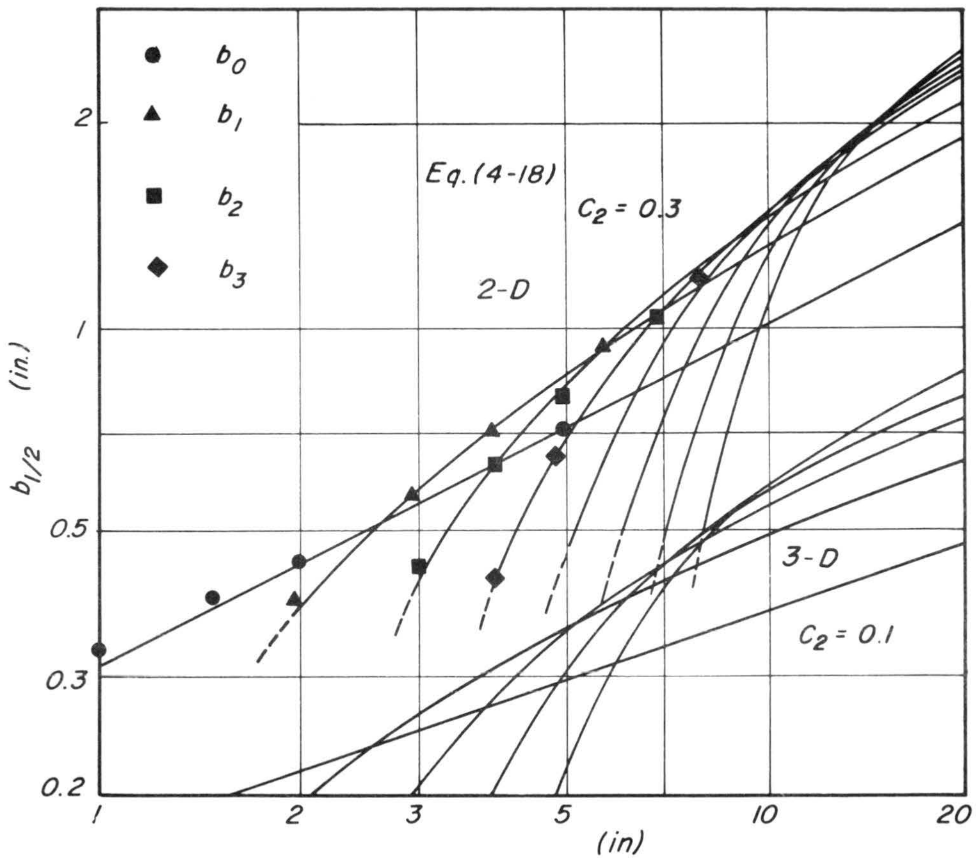


Fig. 35 Half width of combined wakes

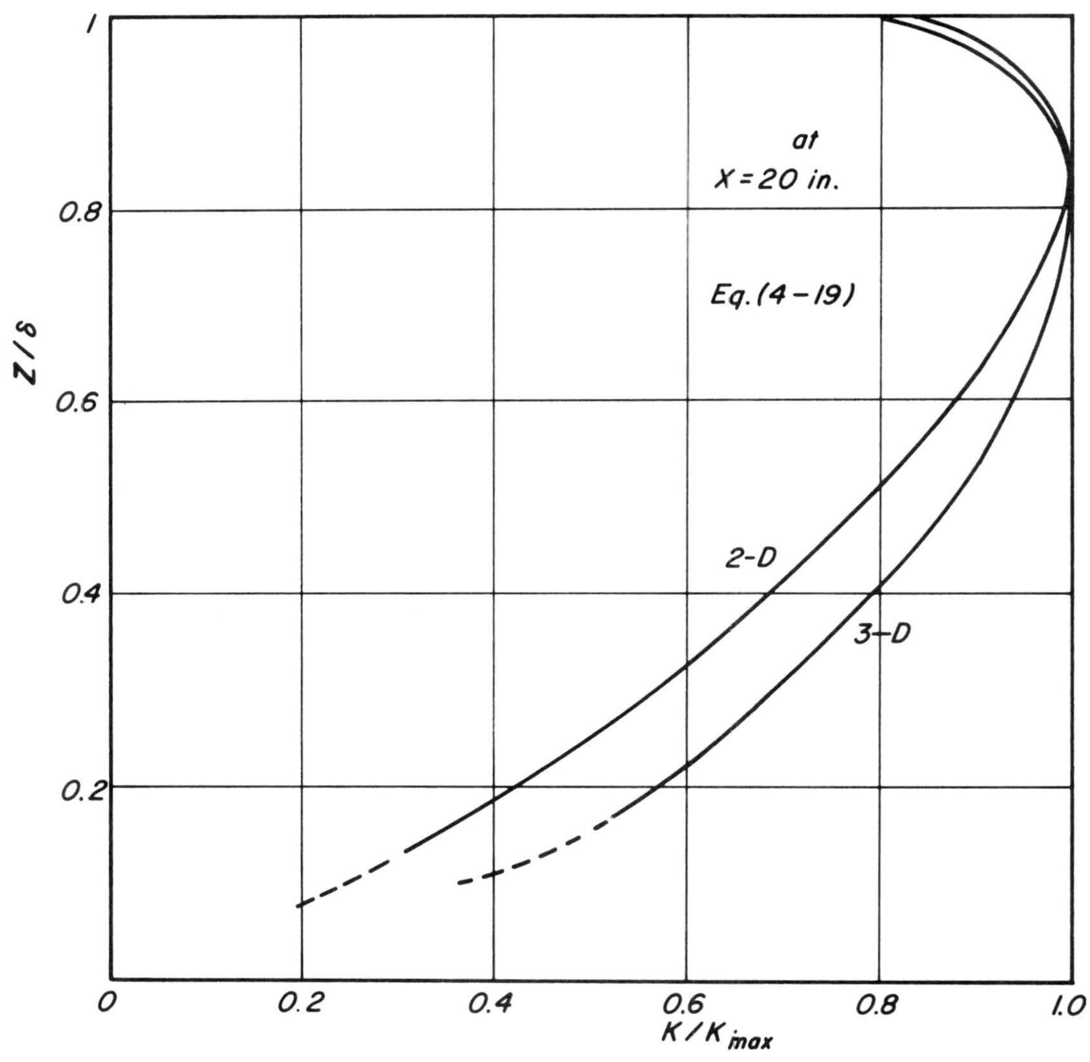


*Fig. 36 Coefficient of the turbulent diffusion of momentum*

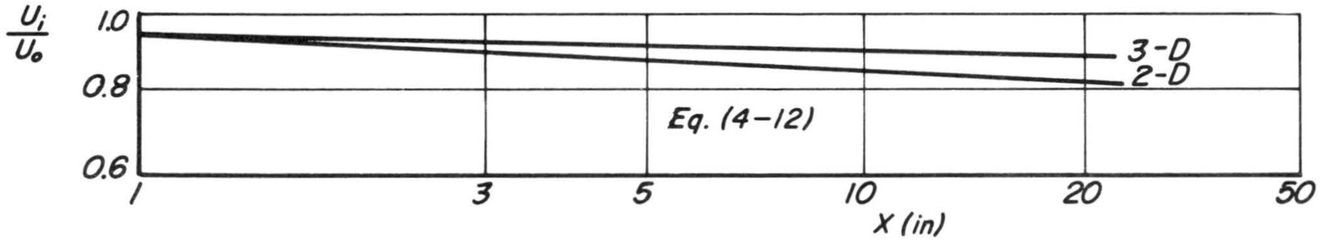


Fig. 37 Value of $U_i$

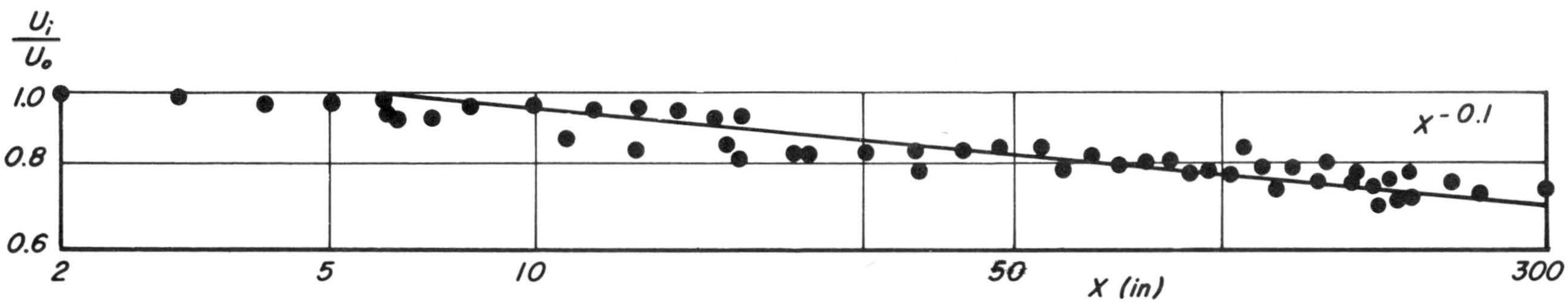


Fig. 38 Experimental data of $U_i$

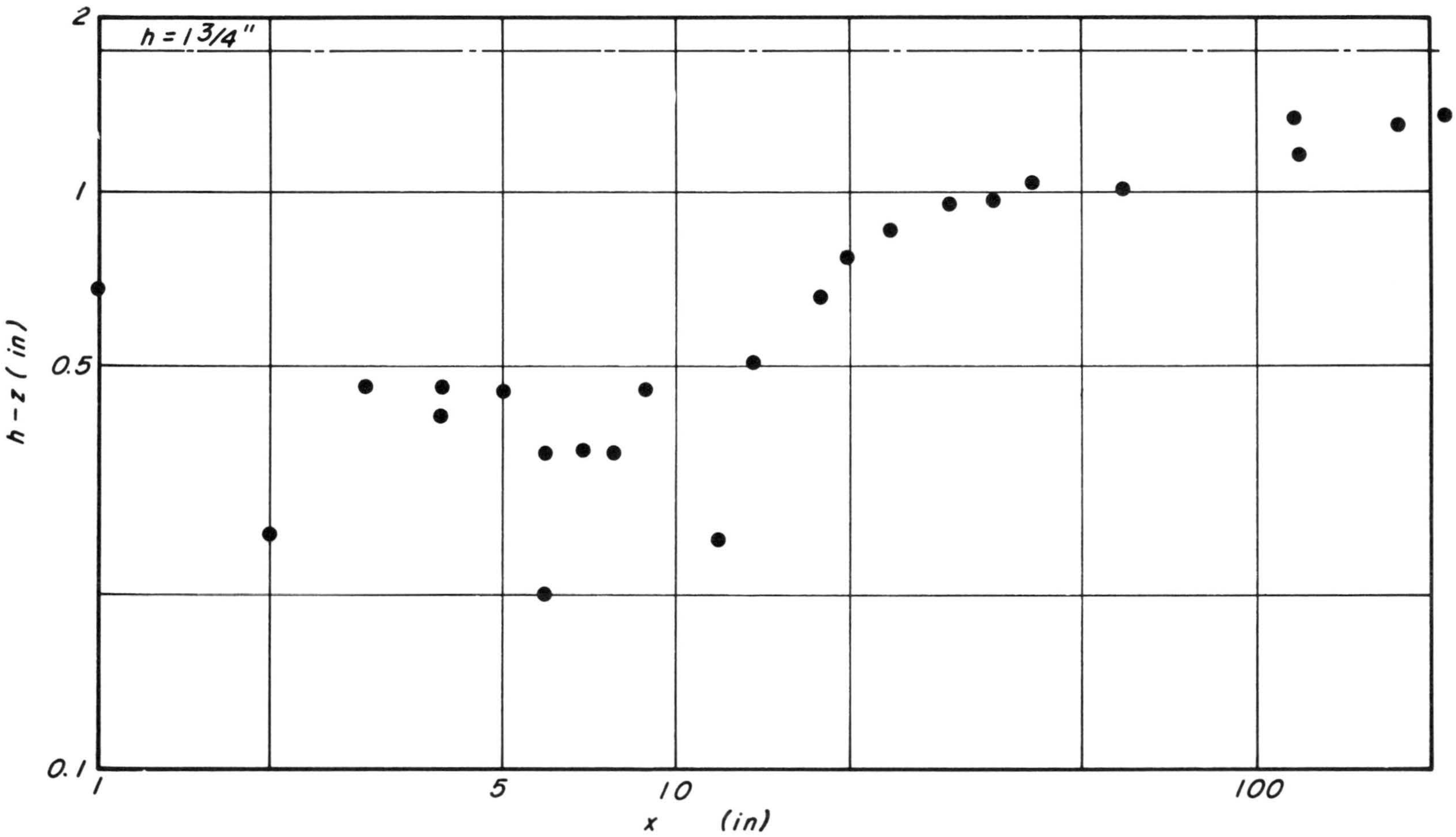


*Fig. 39 Height to the vertical uniform profile zone ( between the roughness) from top of cylinder*

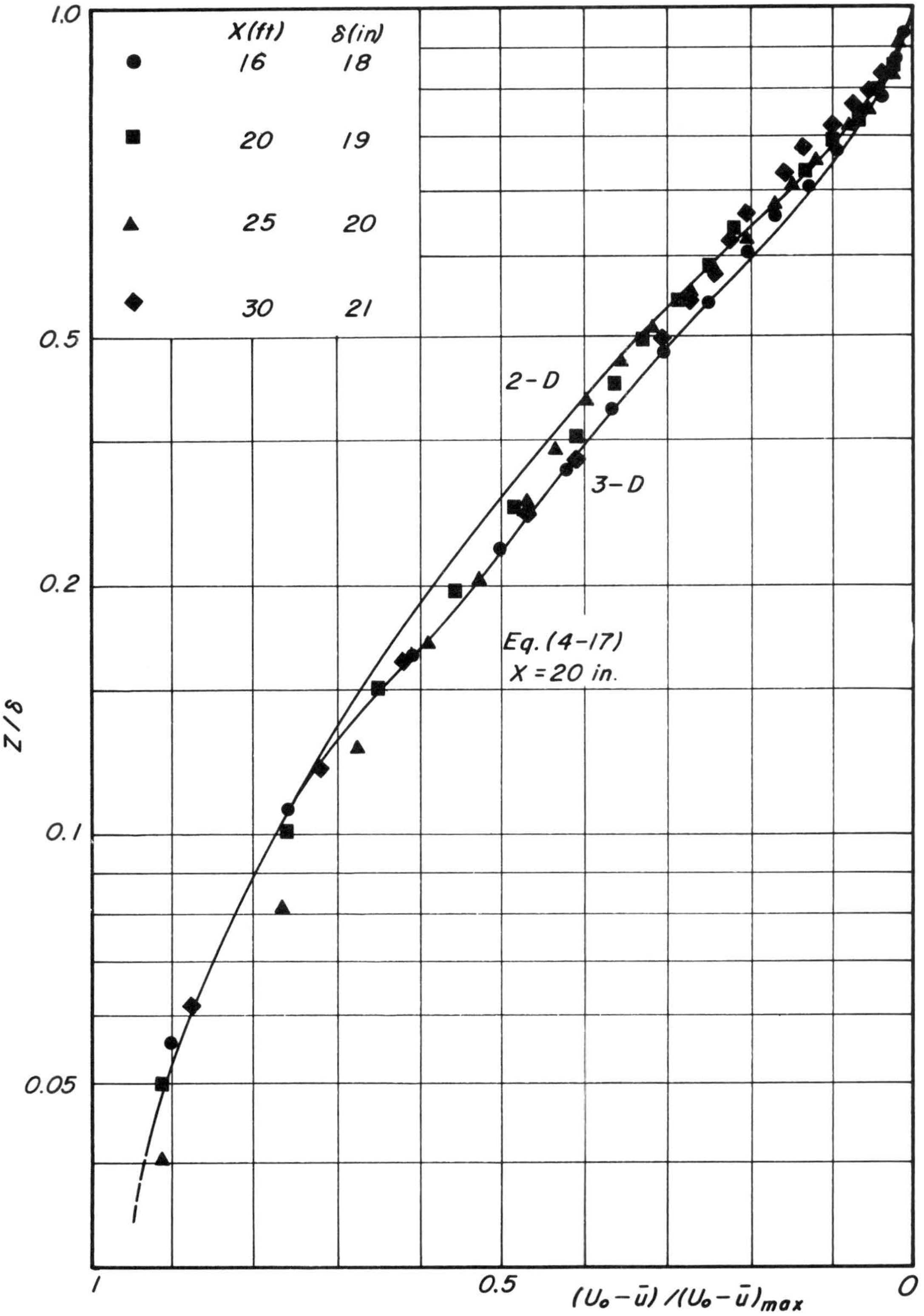


Fig. 40 Vertical velocity profile of the turbulent shear flow

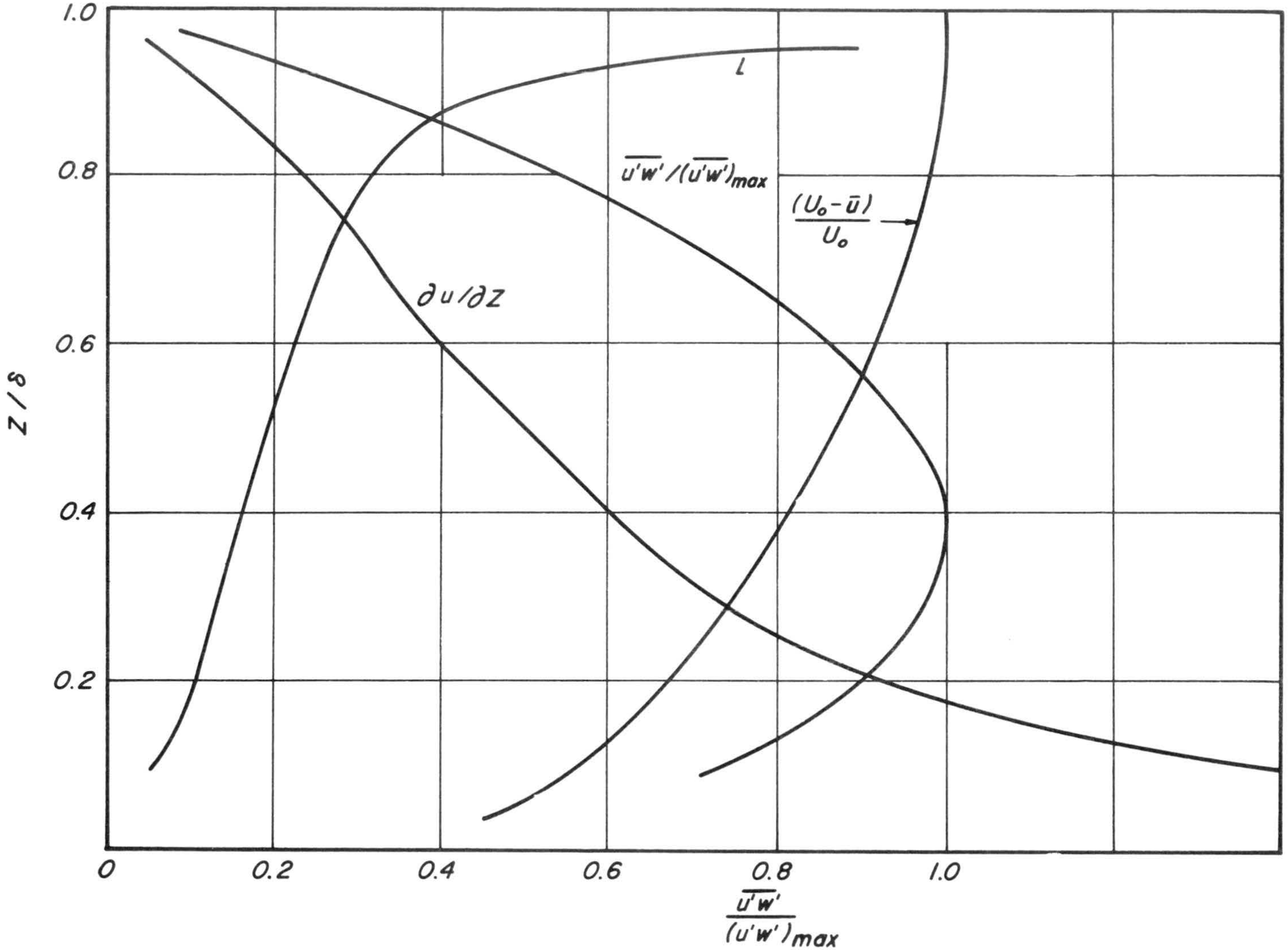


*Fig. 41 Analytical values of $\overline{u'w'}$ and $l$ of the turbulent shear flow (2-D wakes combination)*

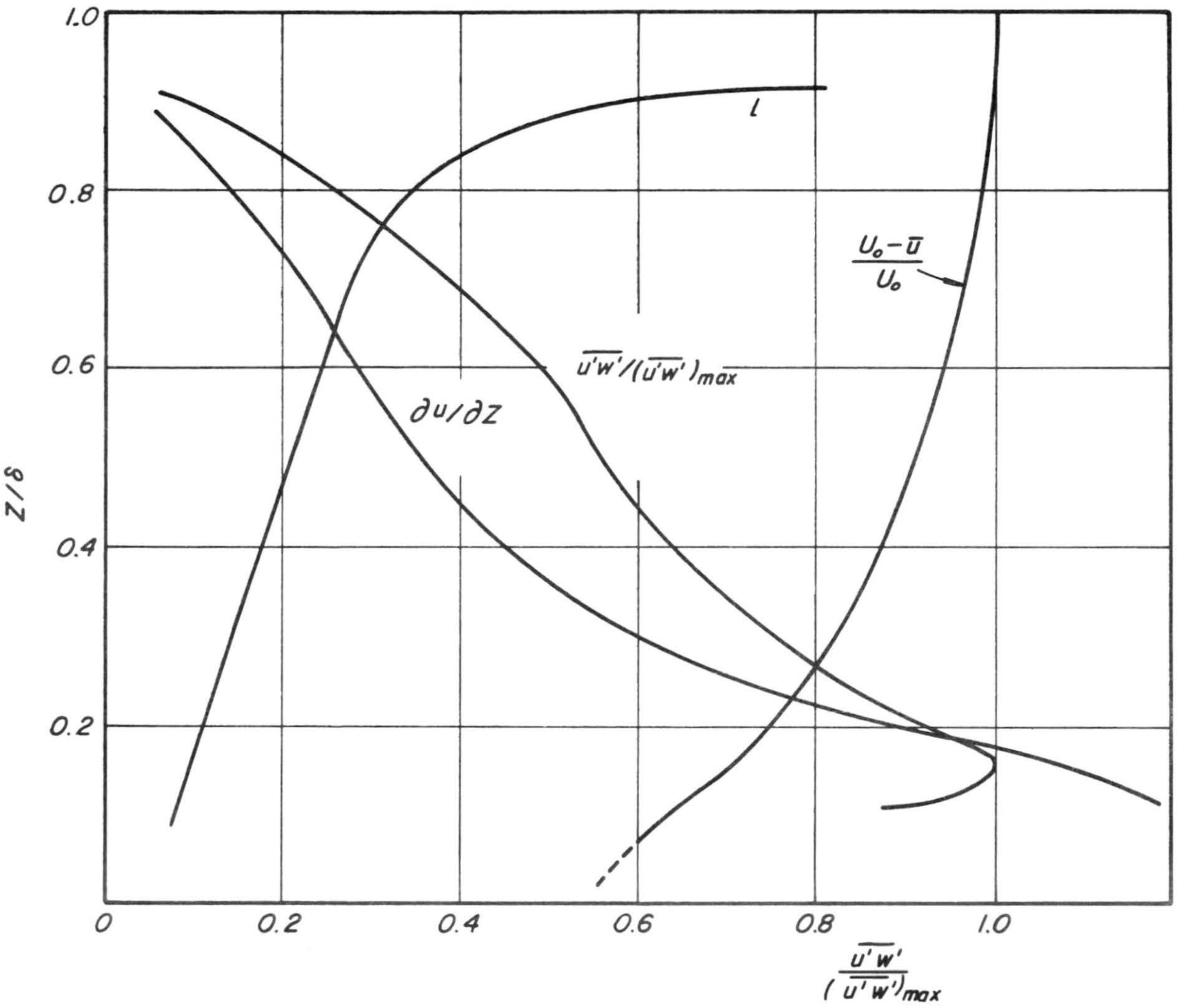


Fig. 42 Analytical values of $\overline{u'w'}$ and $l$ of turbulent shear flow (3-D wakes combination)

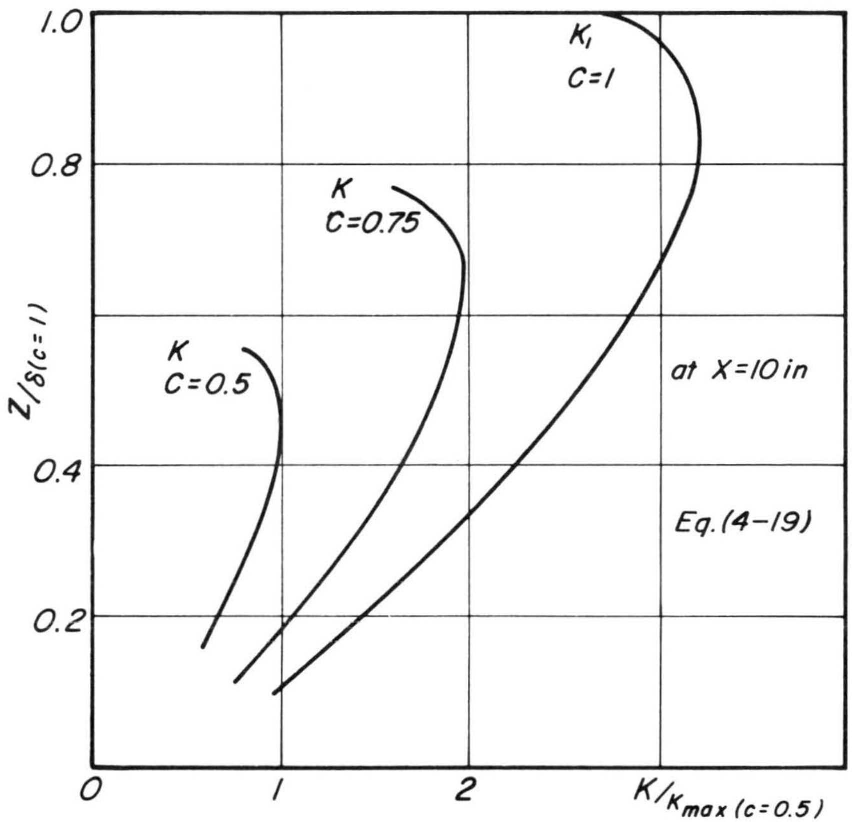


Fig. 43 Analytical K values of the turbulent shear flow by using different $C_l$ of 2-D wakes

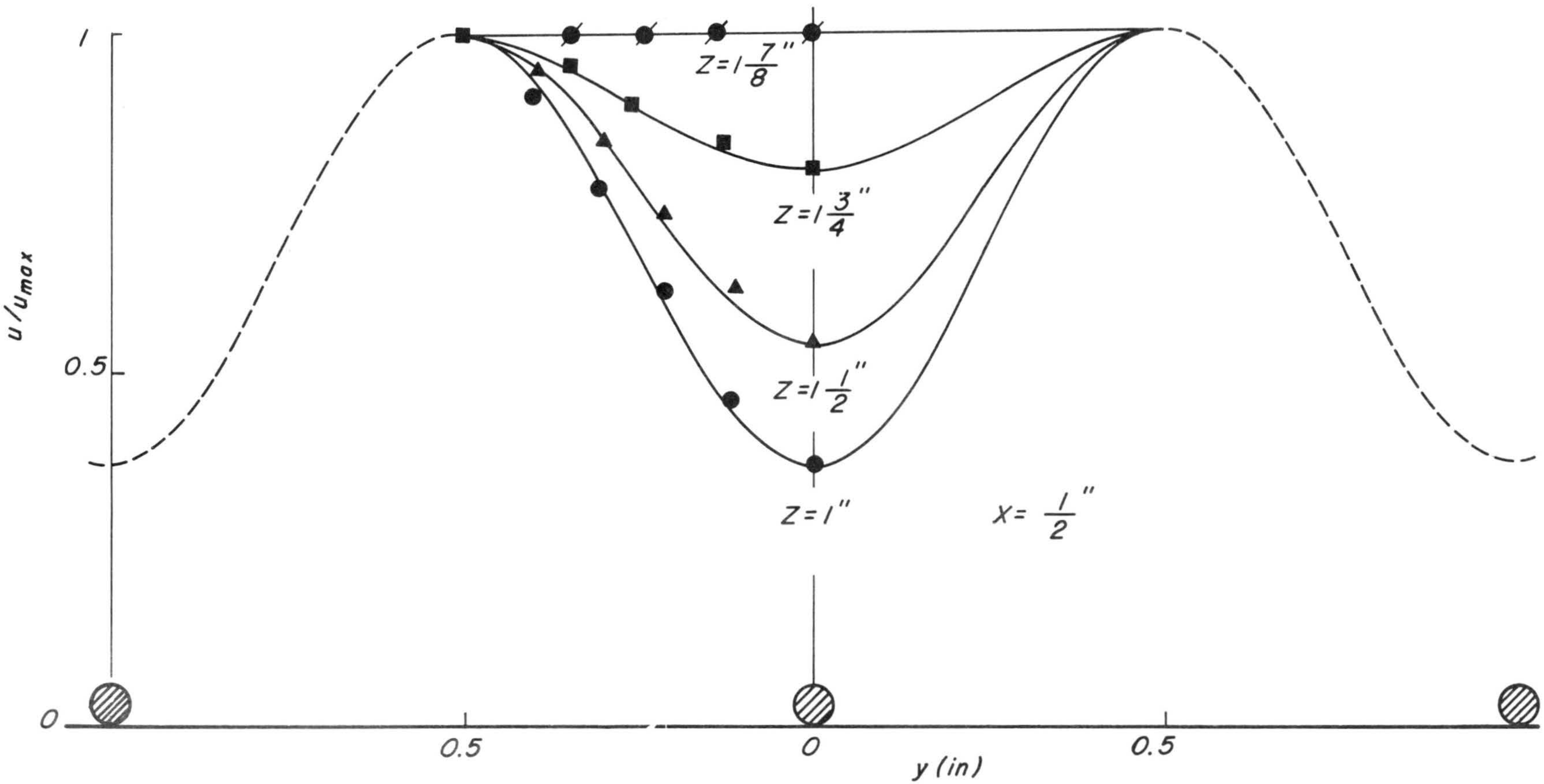


Fig. 44 Horizontal velocity profiles at X=4ft of the rough surface

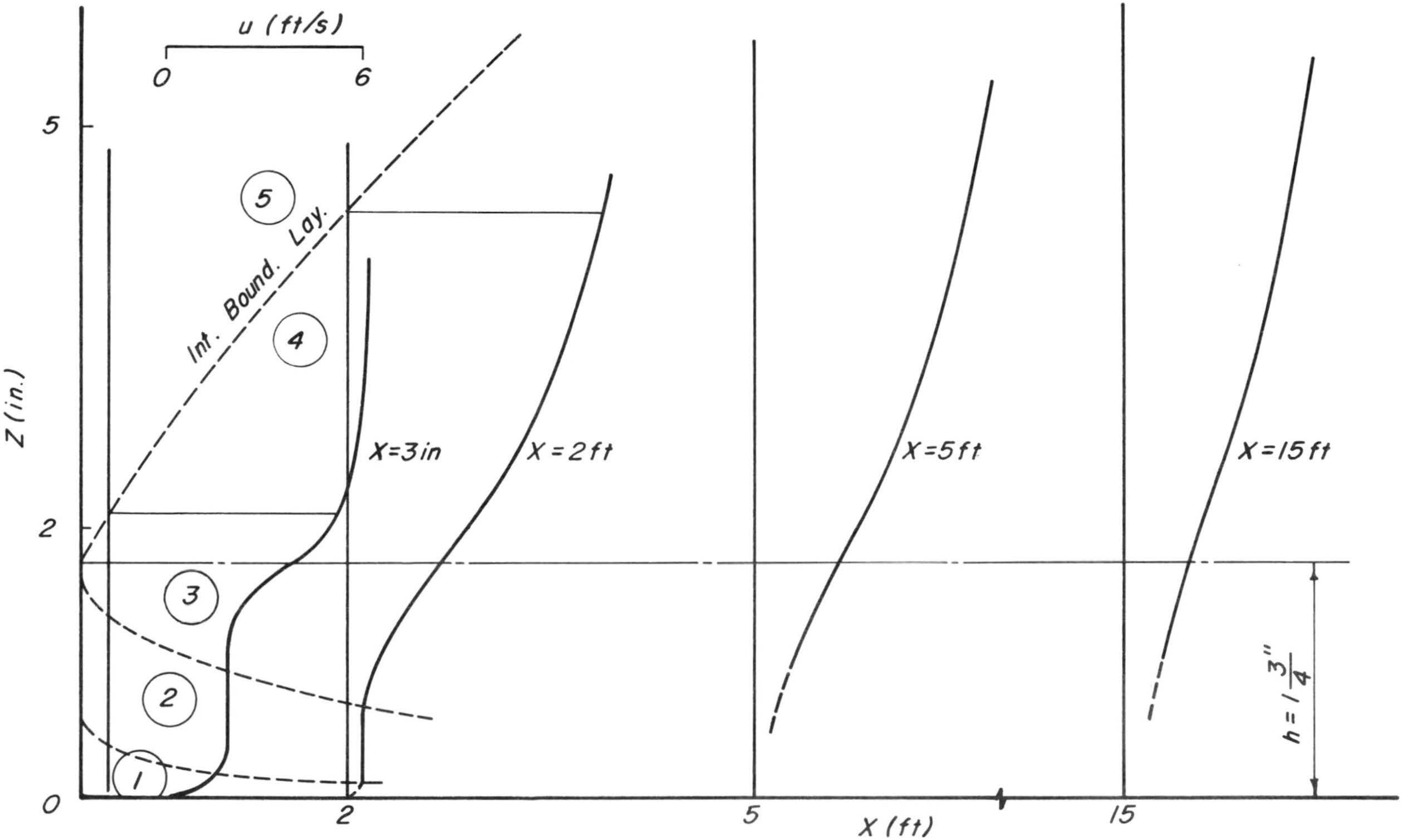


Fig. 45 Vertical velocity profiles in the rough surface in neutral condition

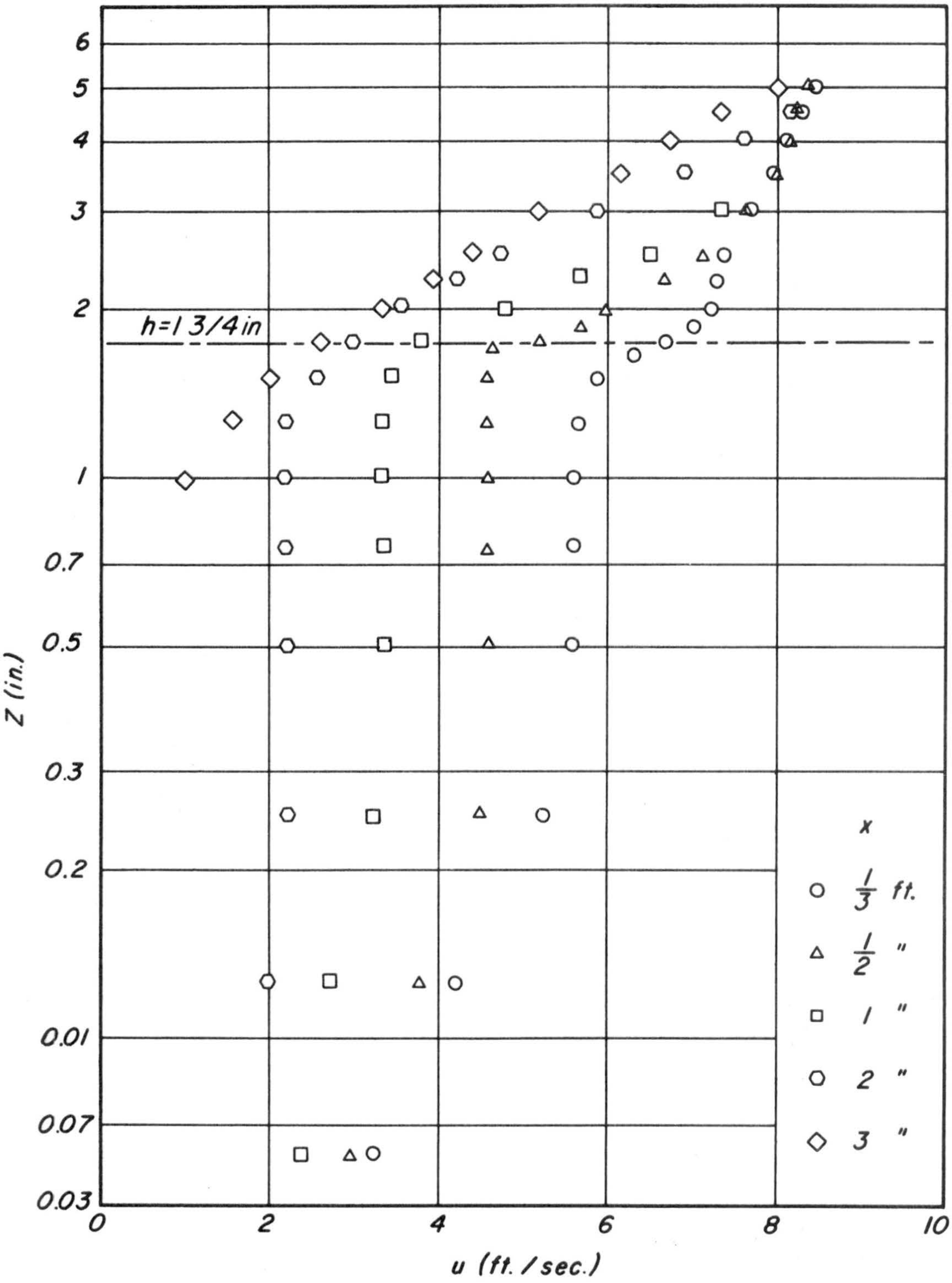


Fig. 46 Velocity data between cylinders of the rough surface

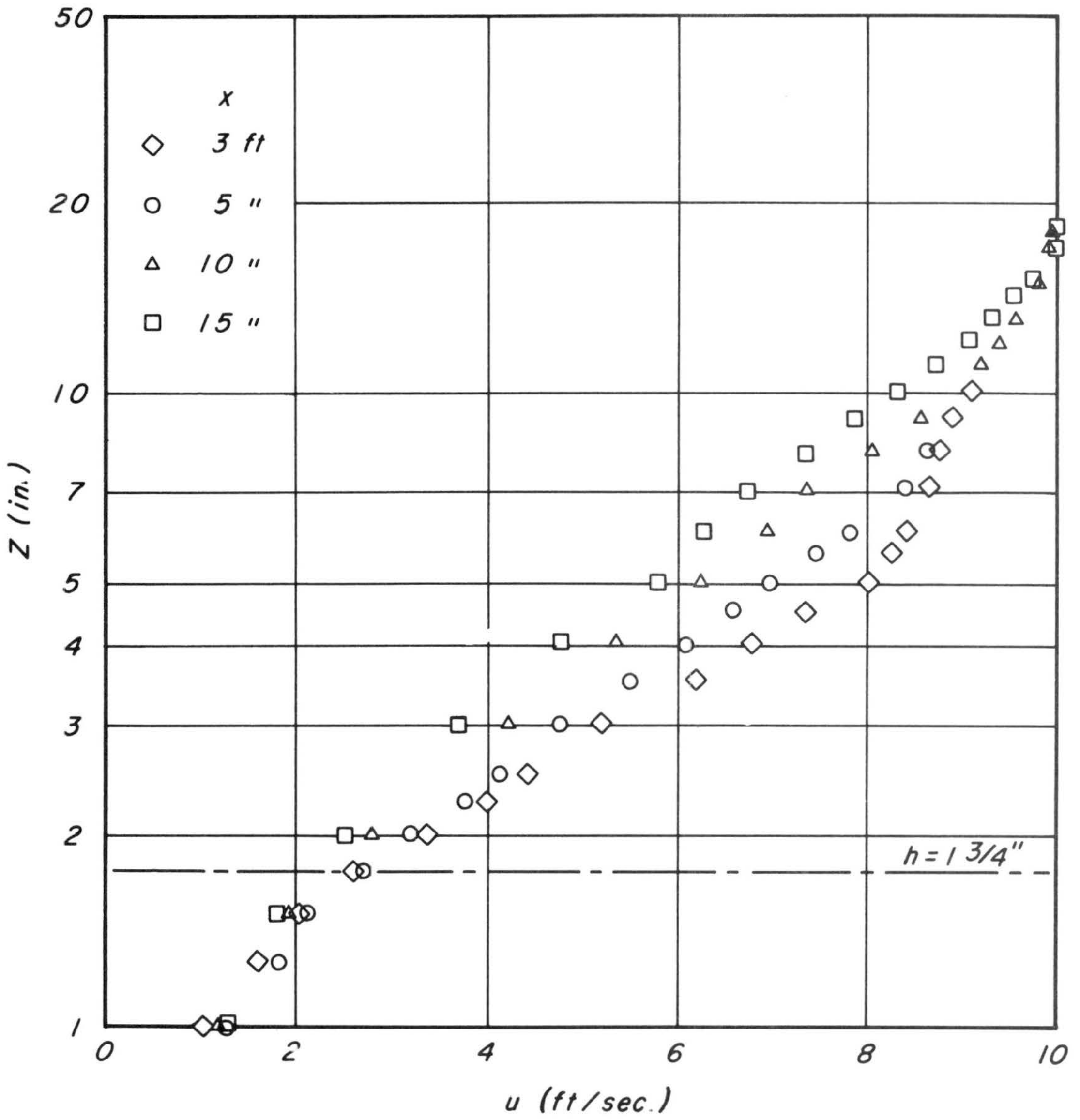


Fig. 47 Velocity data over the rough surface

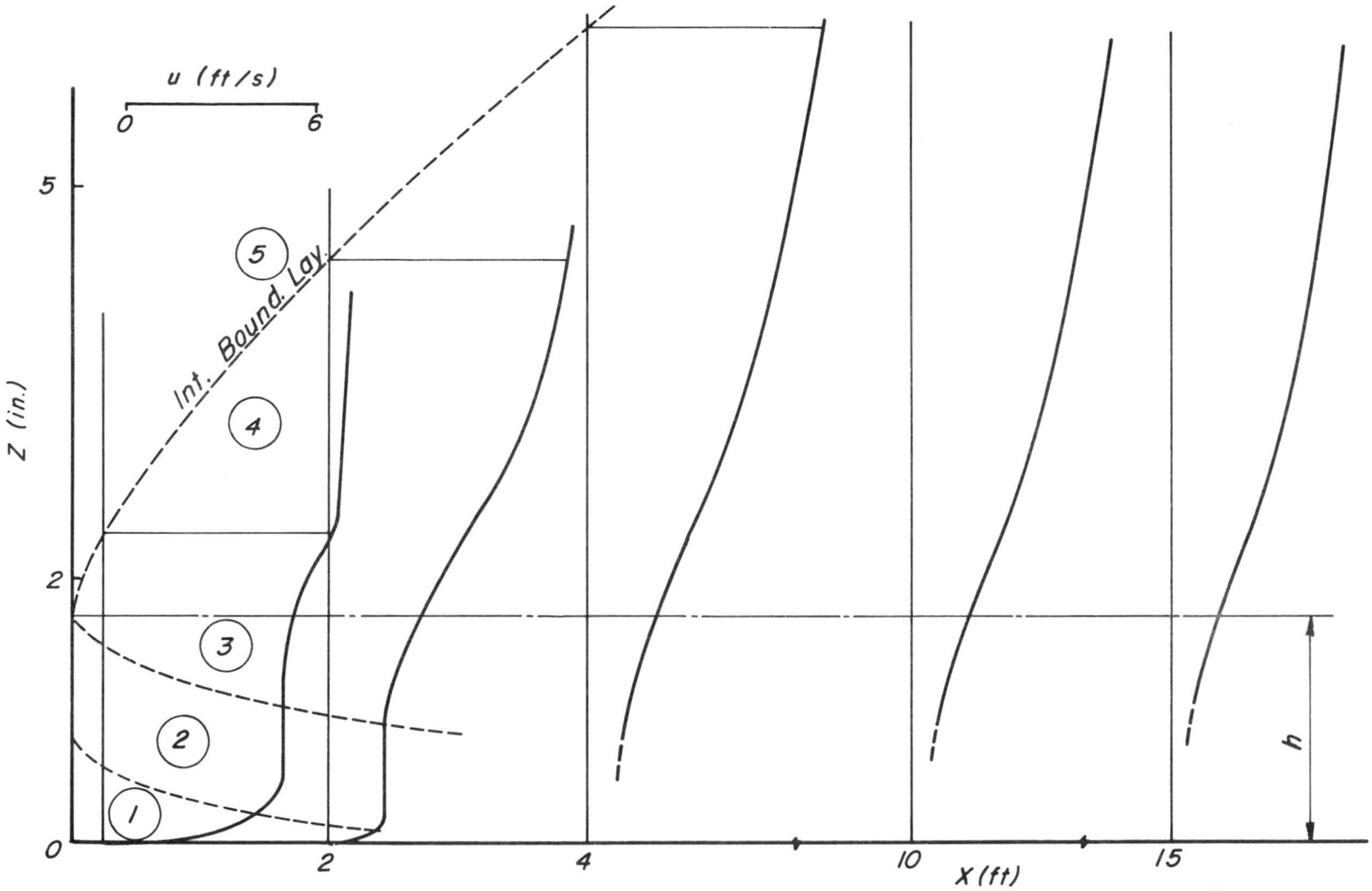


Fig. 48 Vertical velocity profiles in the rough surface in stable condition

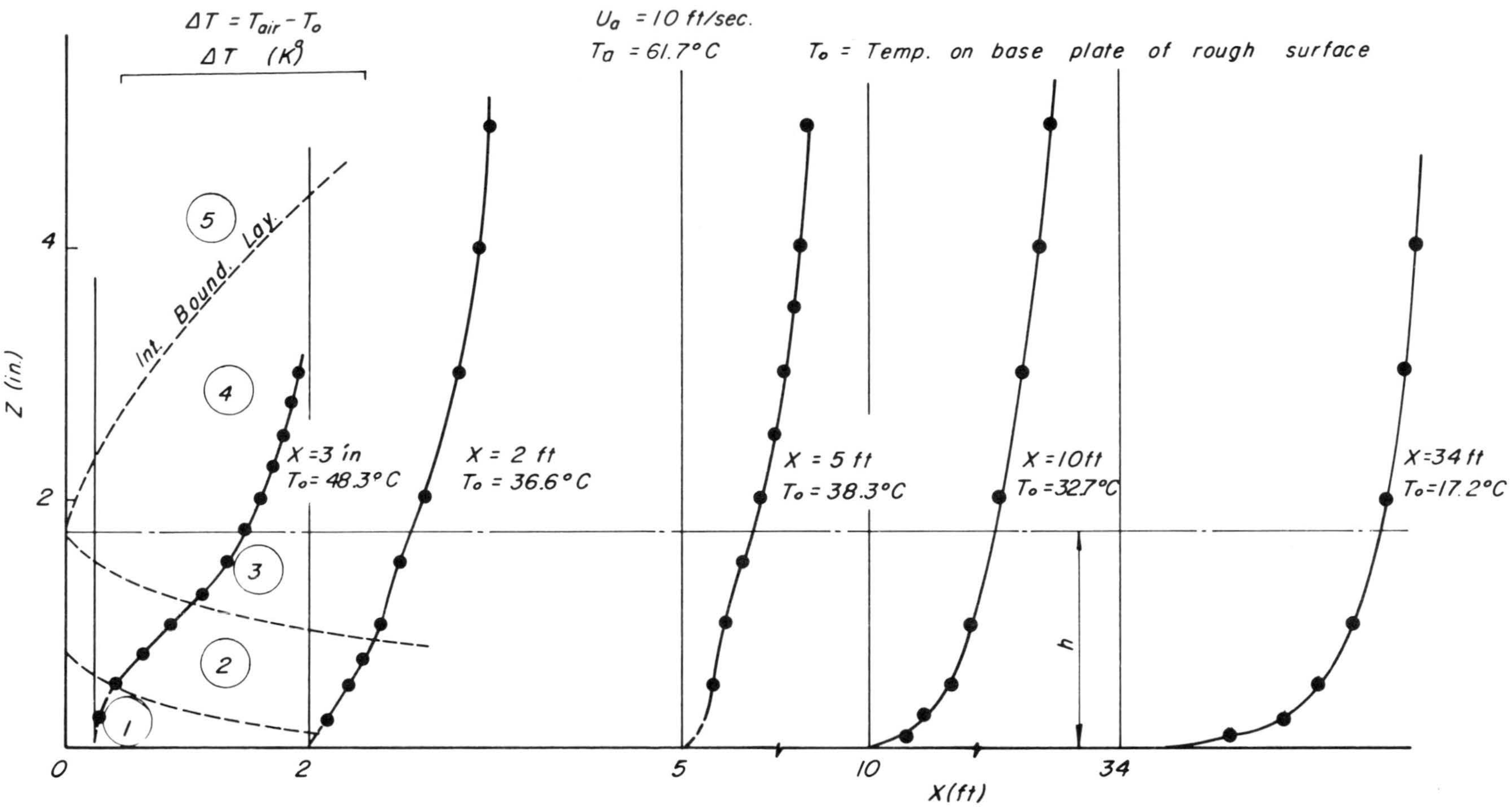


Fig. 49 Vertical temperature differences in the rough surface in stable case

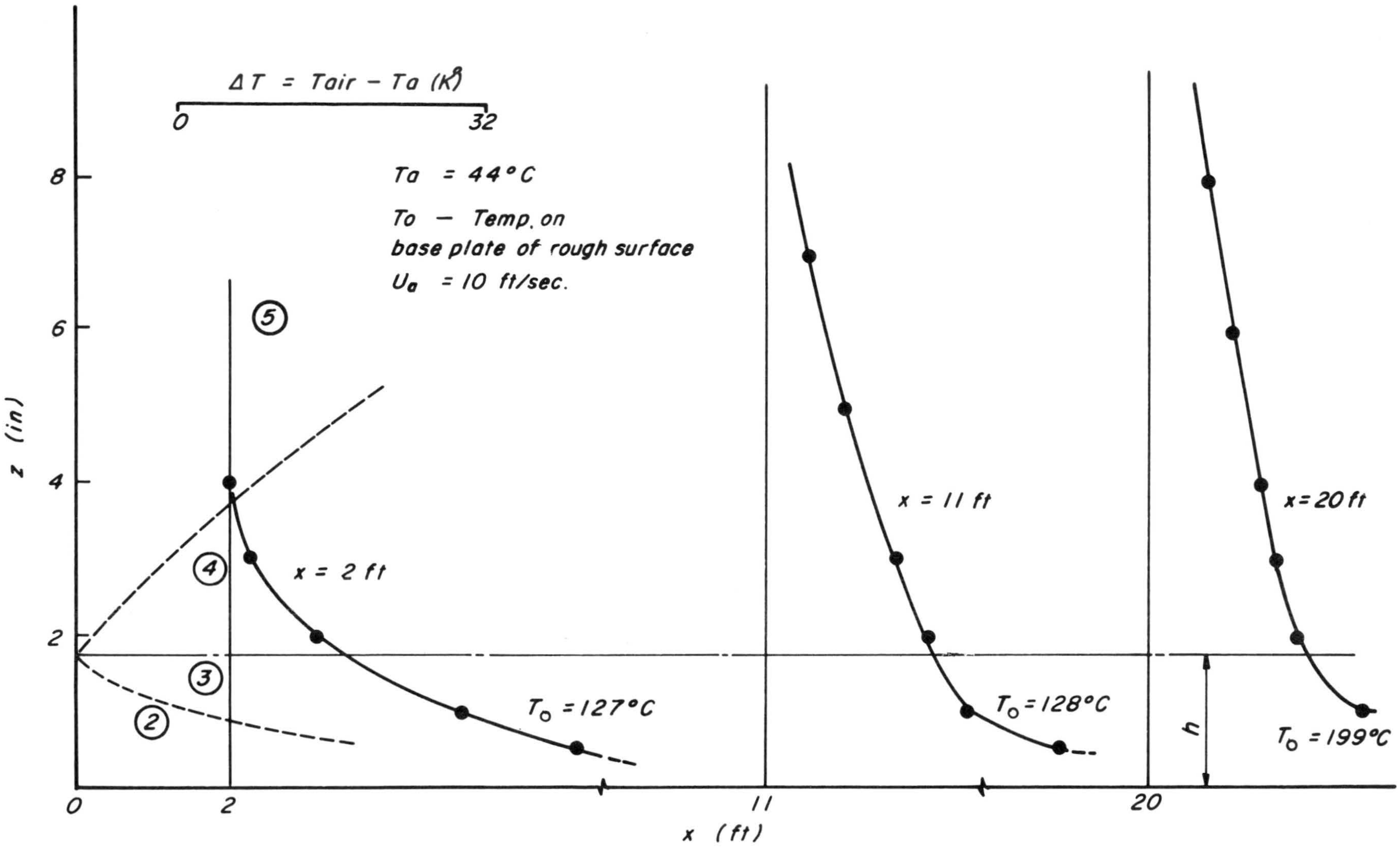


Fig. 50 Vertical temperature differences in the rough surface in unstable case

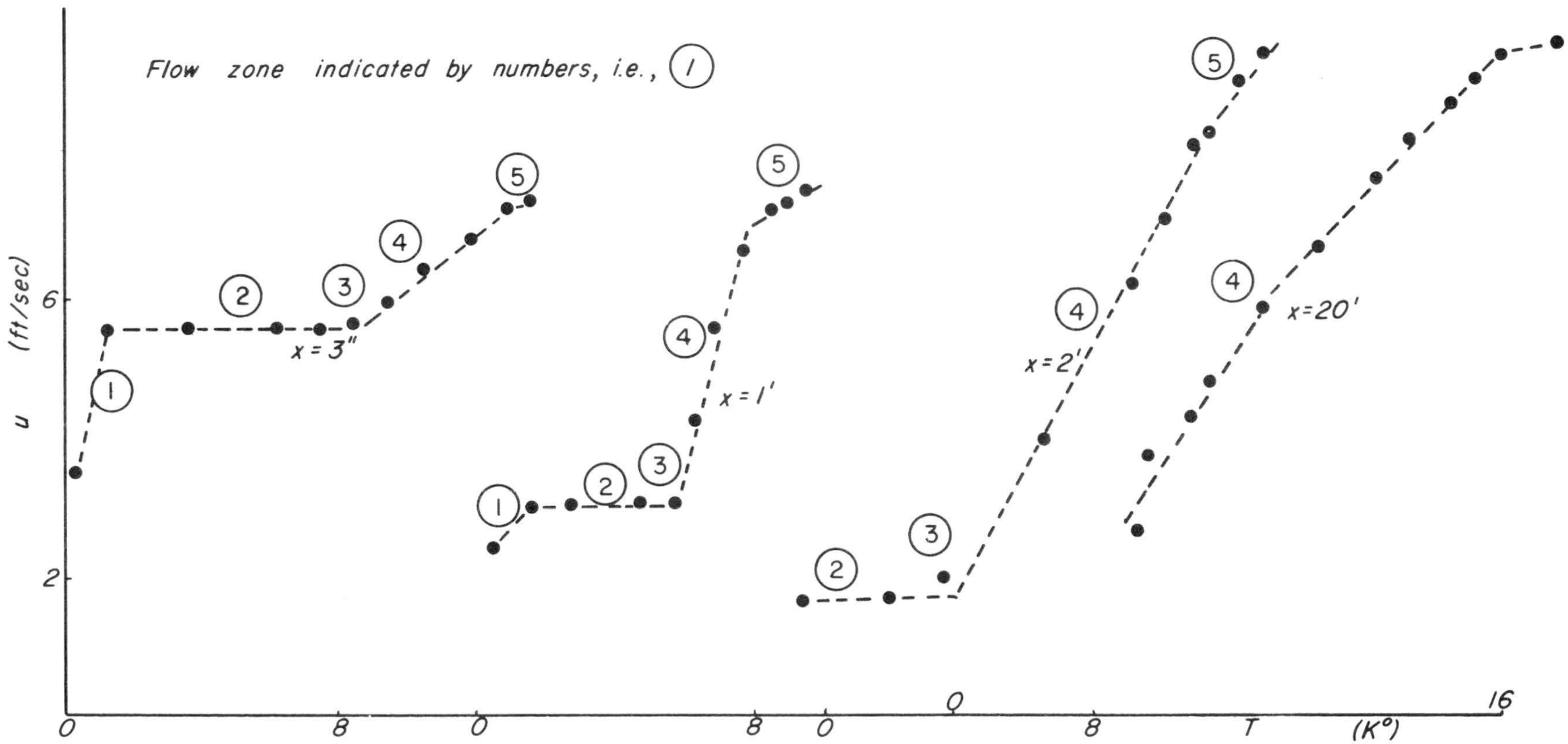


Fig. 51 Relation of u and T in stable case

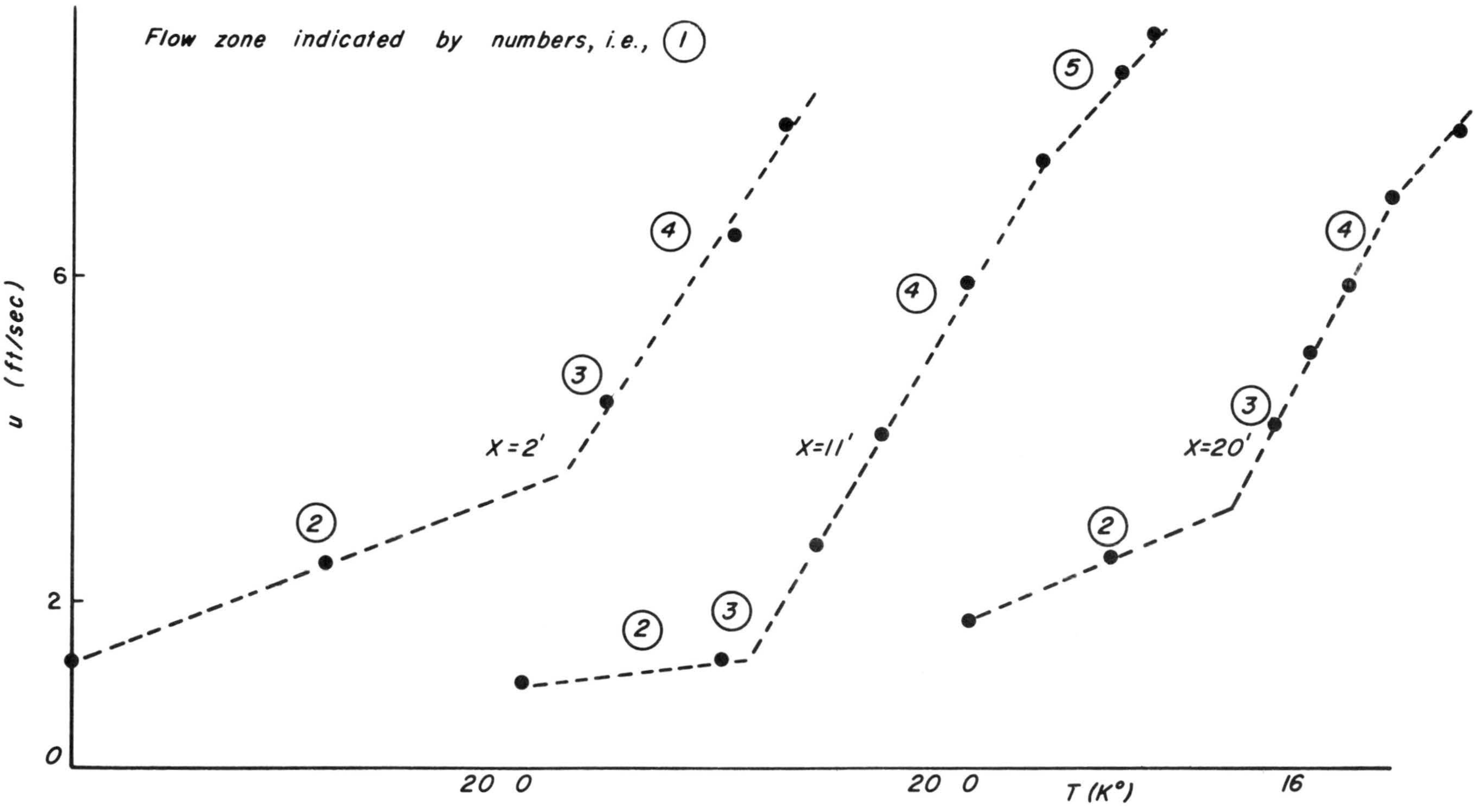


Fig. 52 Relation of u and T in unstable case

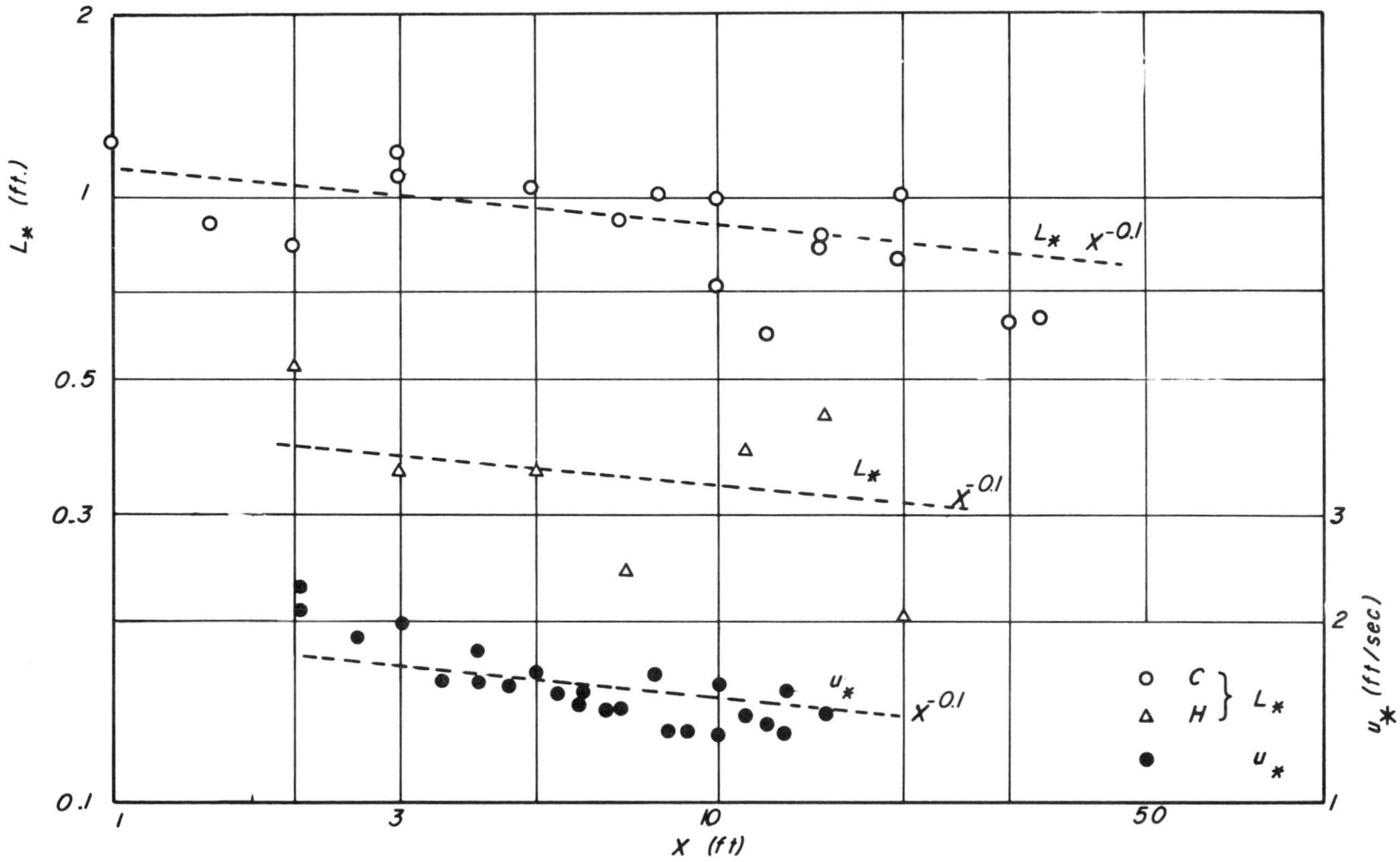


Fig. 53 Experimental data of $L_*$ $(\frac{K_H}{K_m}=1)$ in stable (C) and unstable (H) cases and $u_*$

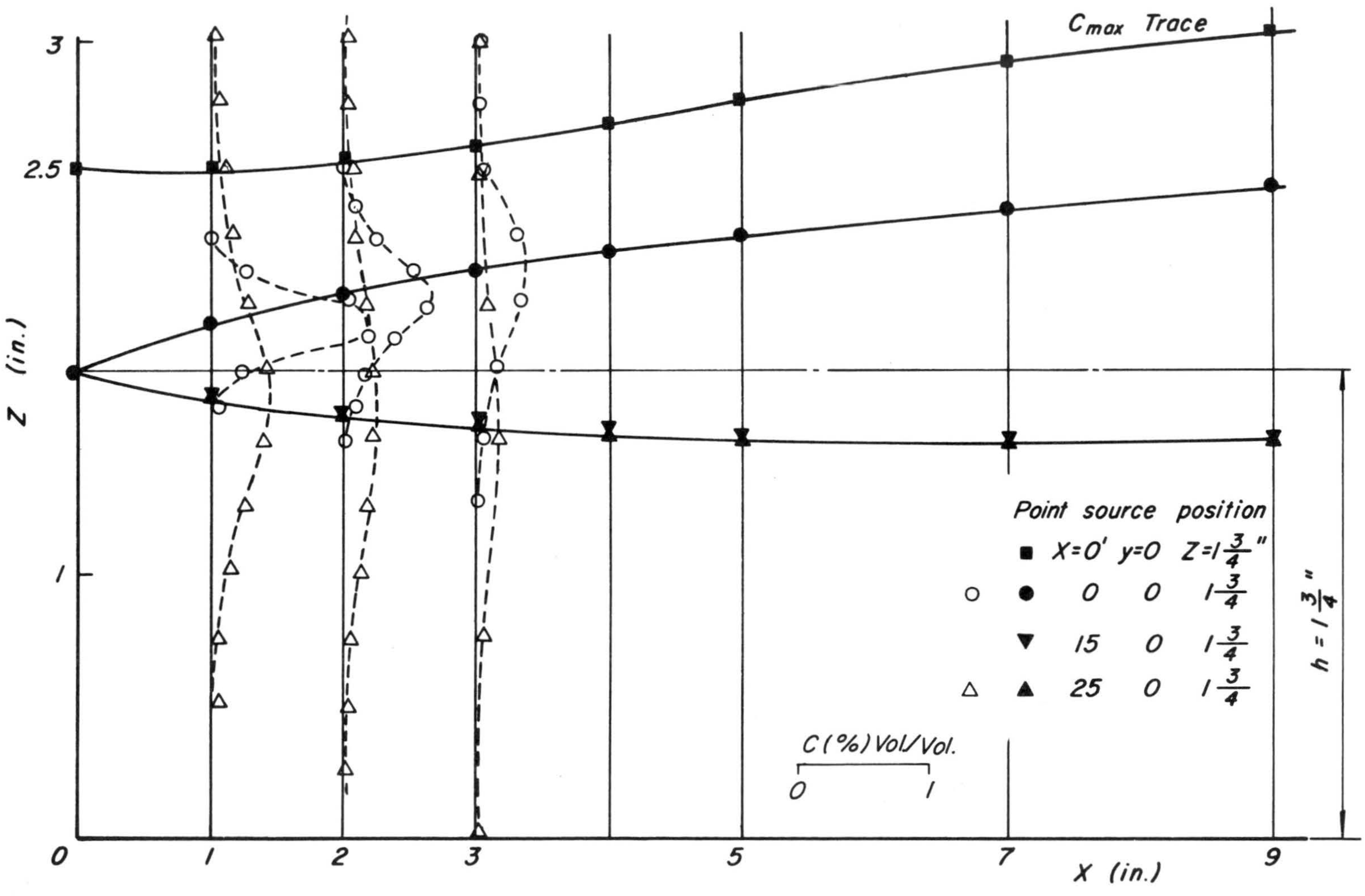


Fig. 54 Gas diffusion profiles and traces of the maximum concentration from point source in neutral case

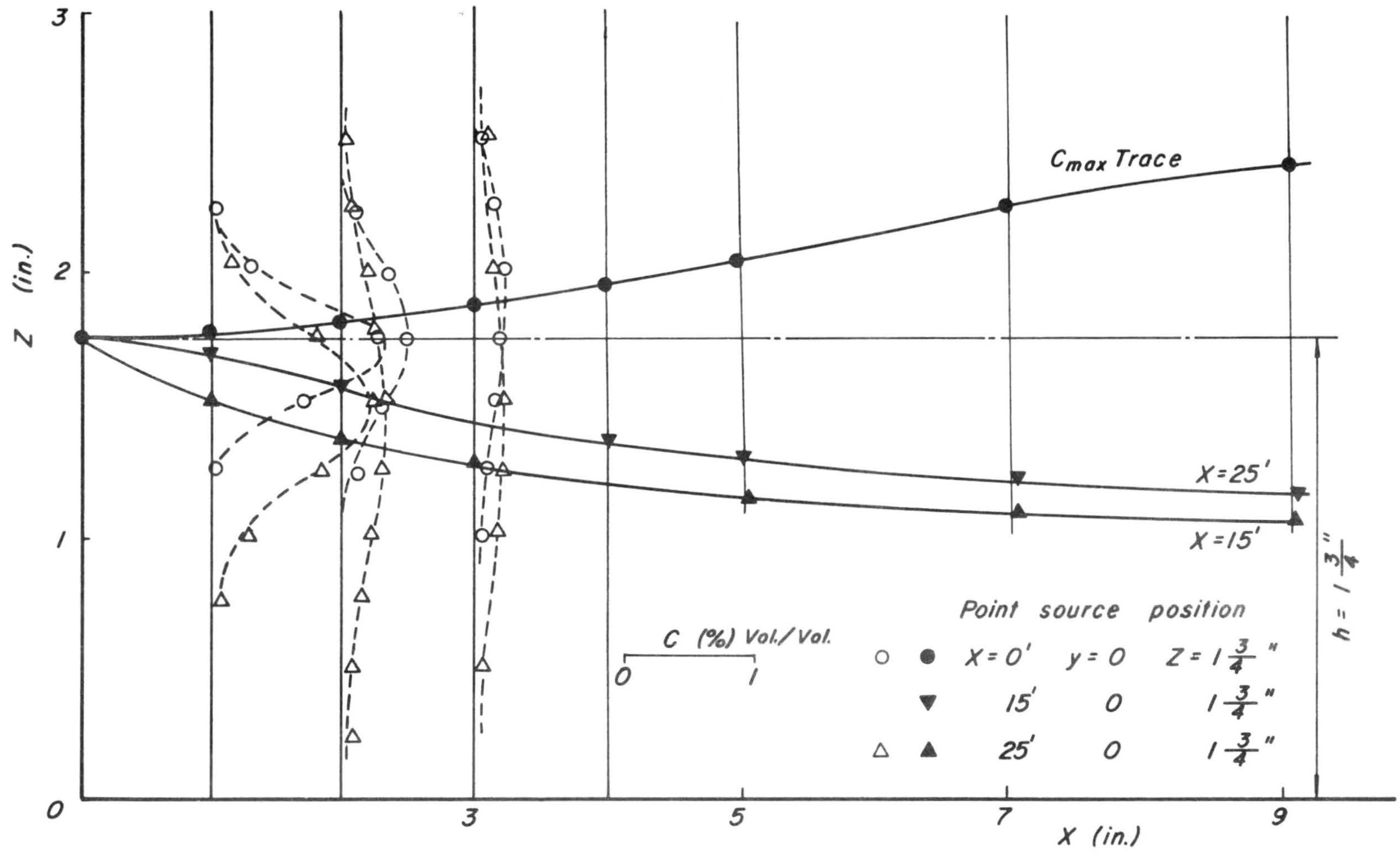


Fig. 55 Gas diffusion profiles and traces of the maximum concentration from point source in stable case

133

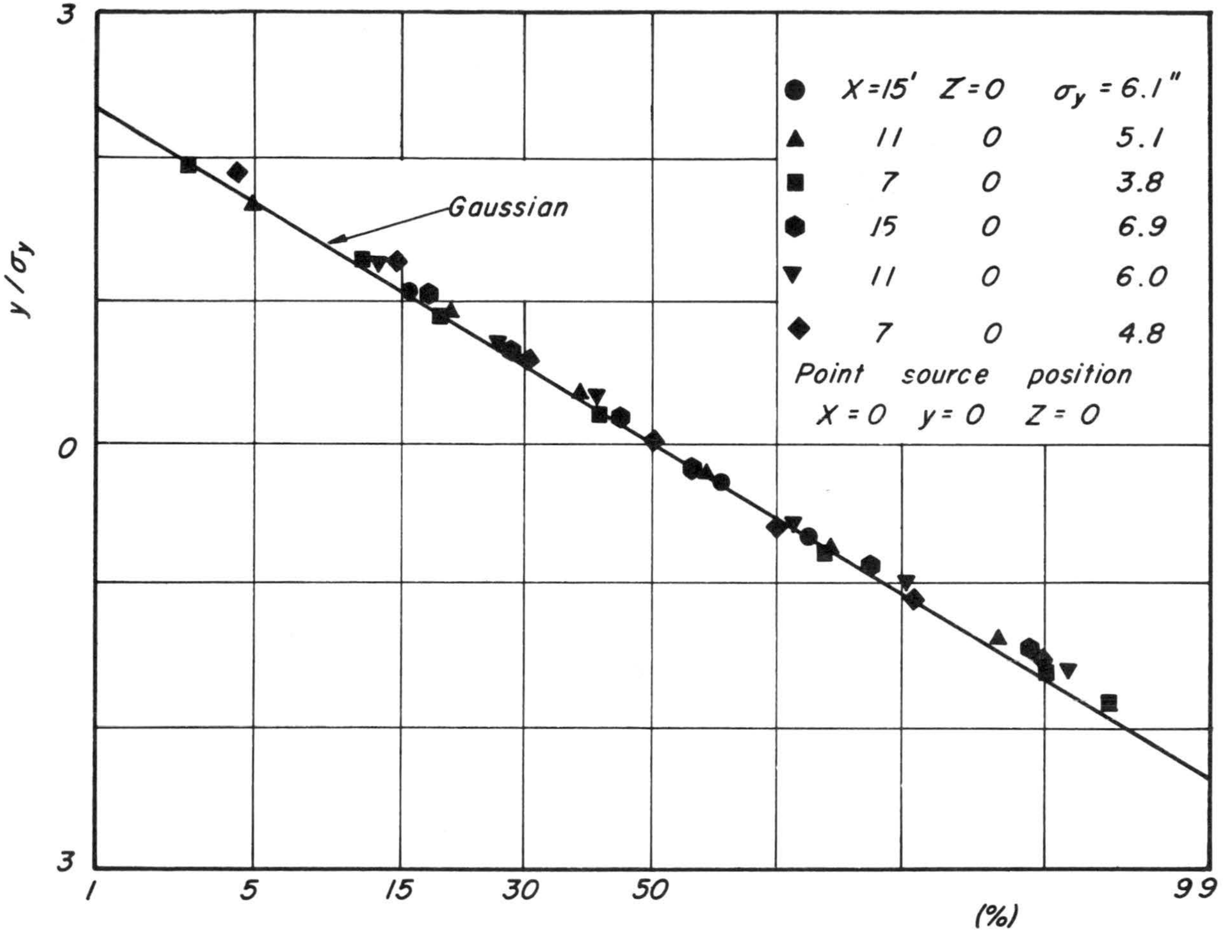


Fig. 56A Horizontal gas concentration profiles in Gaussian scale in stable (C) and unstable (H) cases

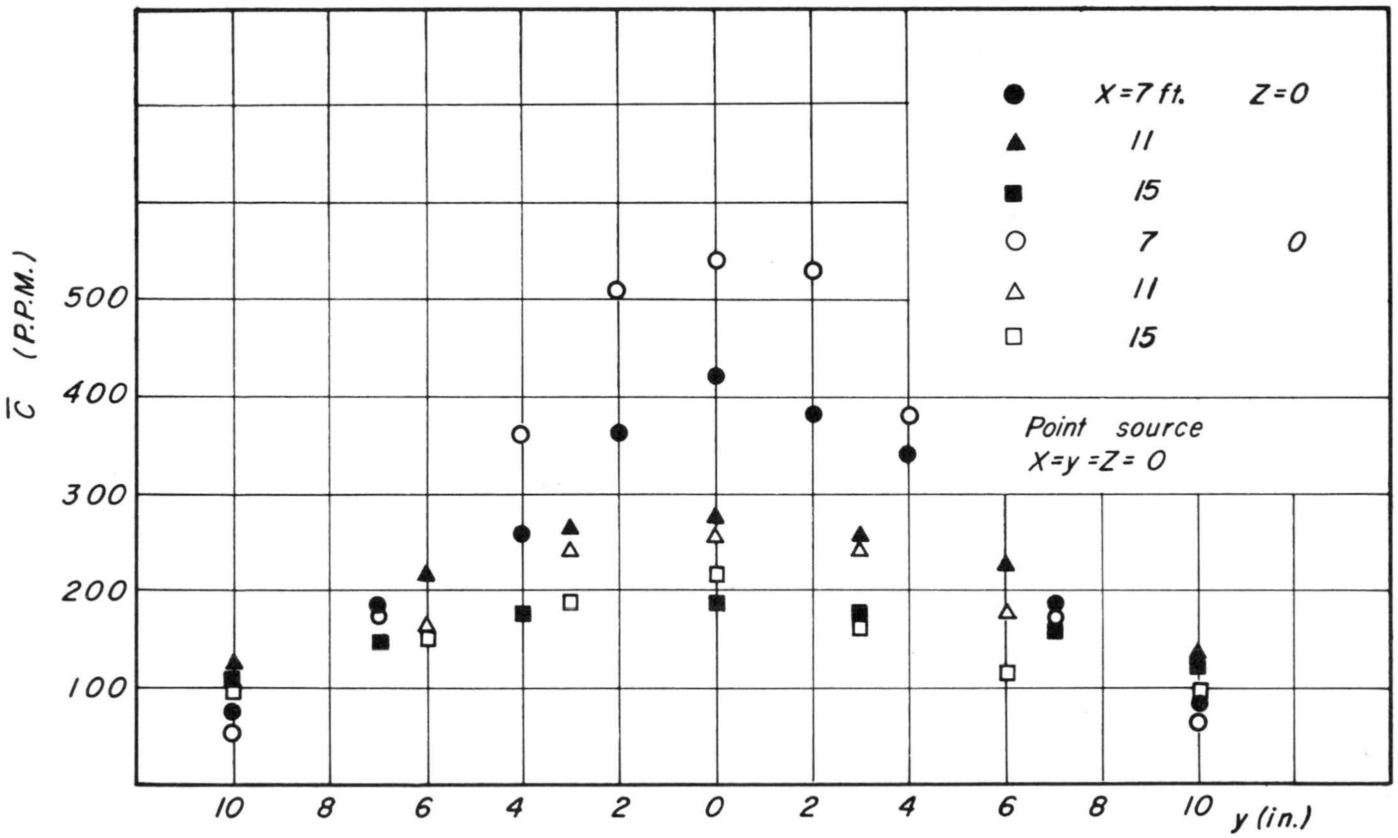


Fig. 56 B Horizontal gas concentration

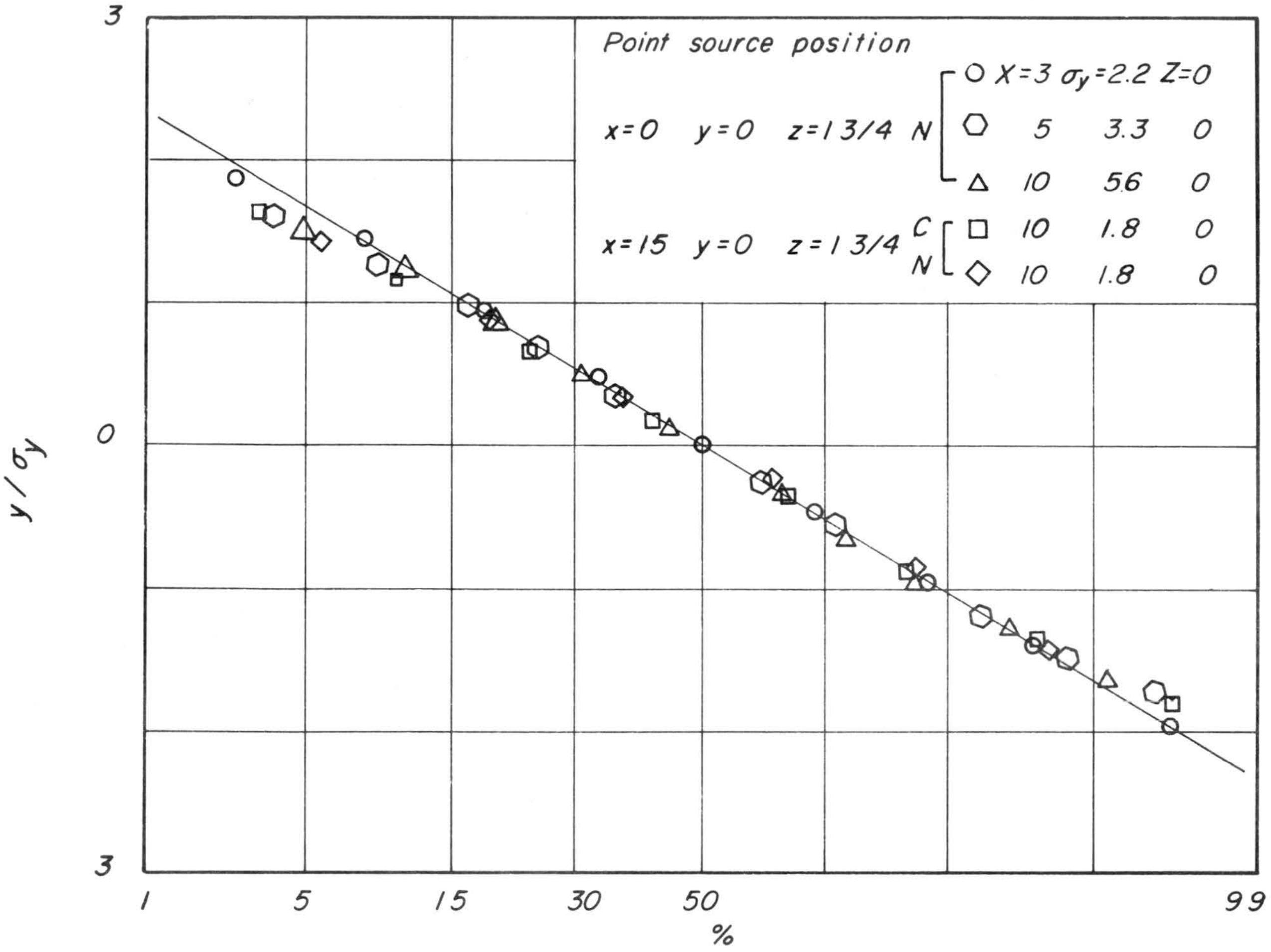


*Fig. 57 A Horizontal gas concentration profiles in Gaussian scale in neutral (N) and stable (C) cases*

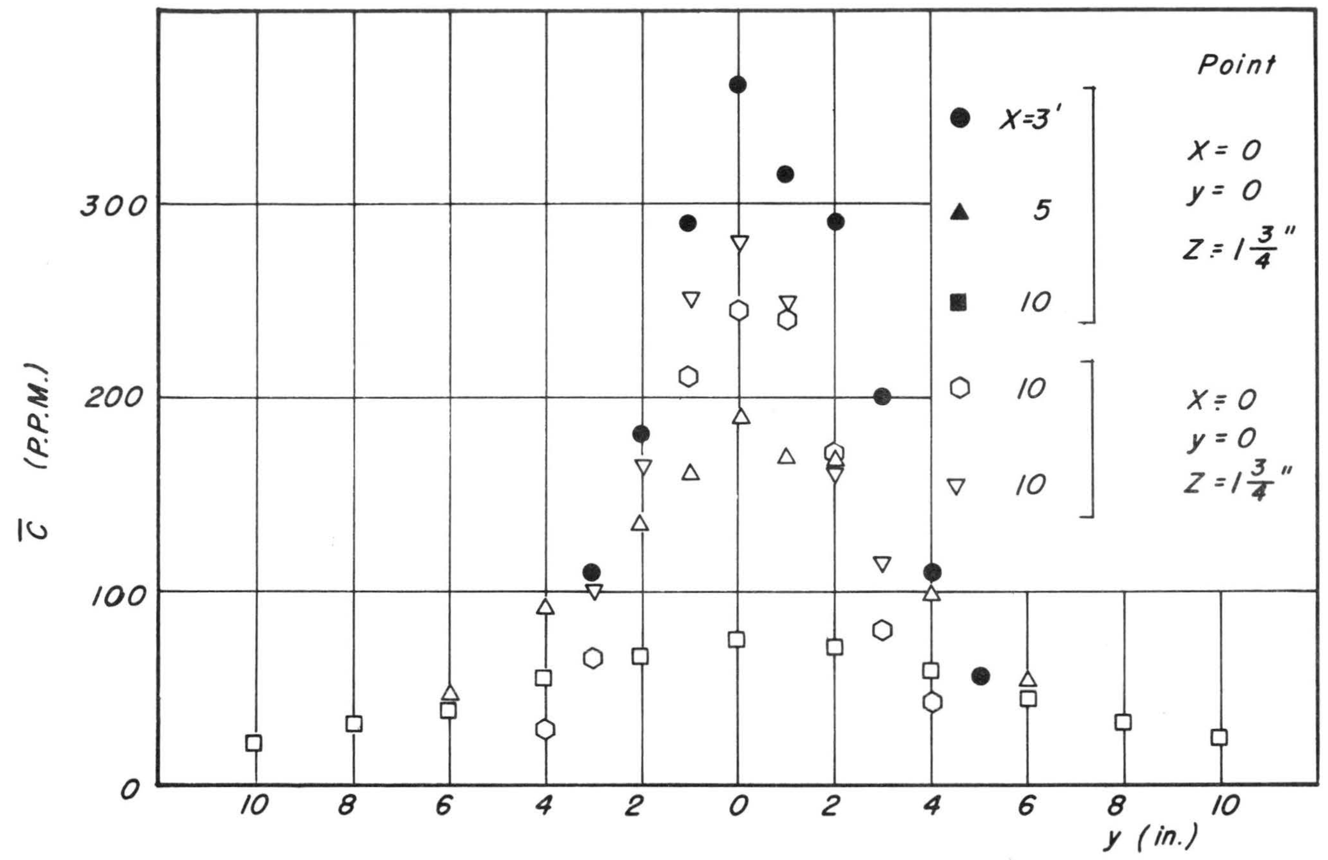


Fig. 57B Horizontal gas concentration

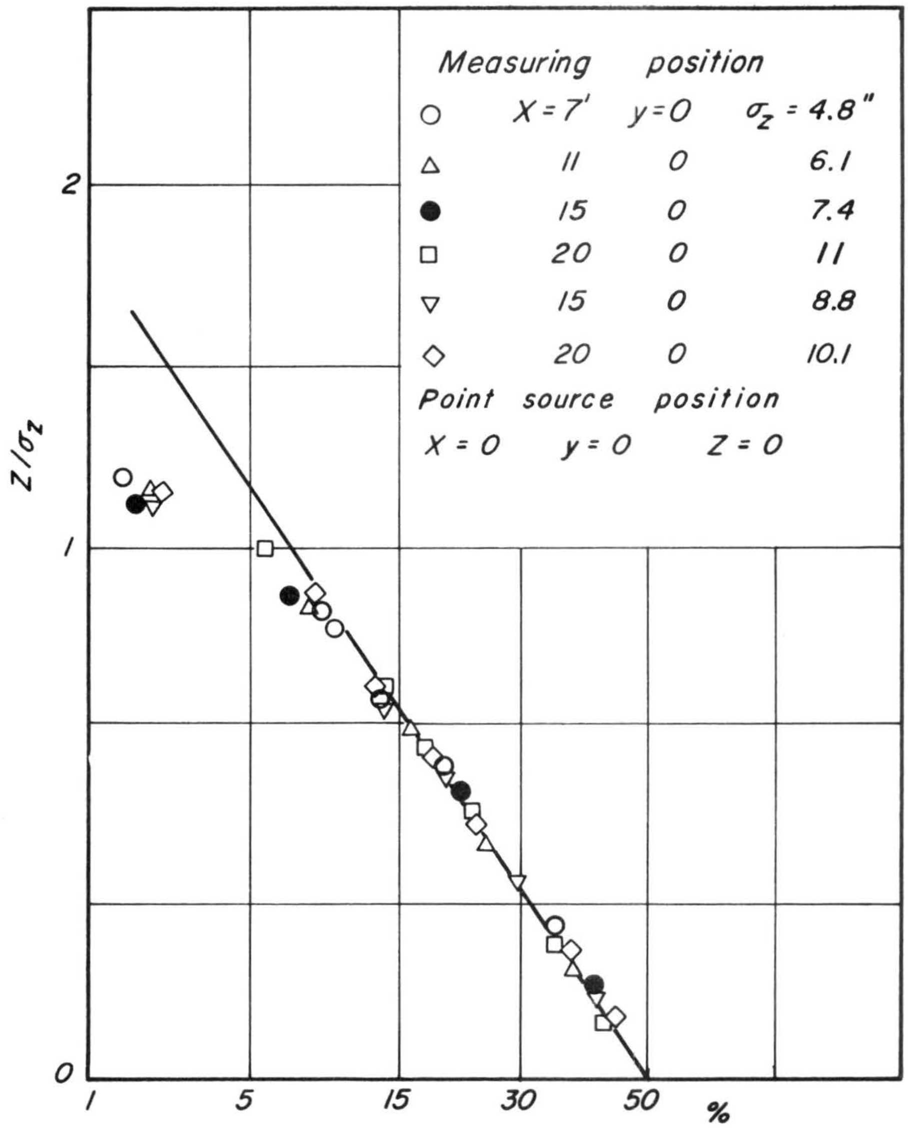


*Fig. 58A Vertical gas diffusion profiles Gaussian scale in neutral (N), stable (C) and unstable (H) cases*

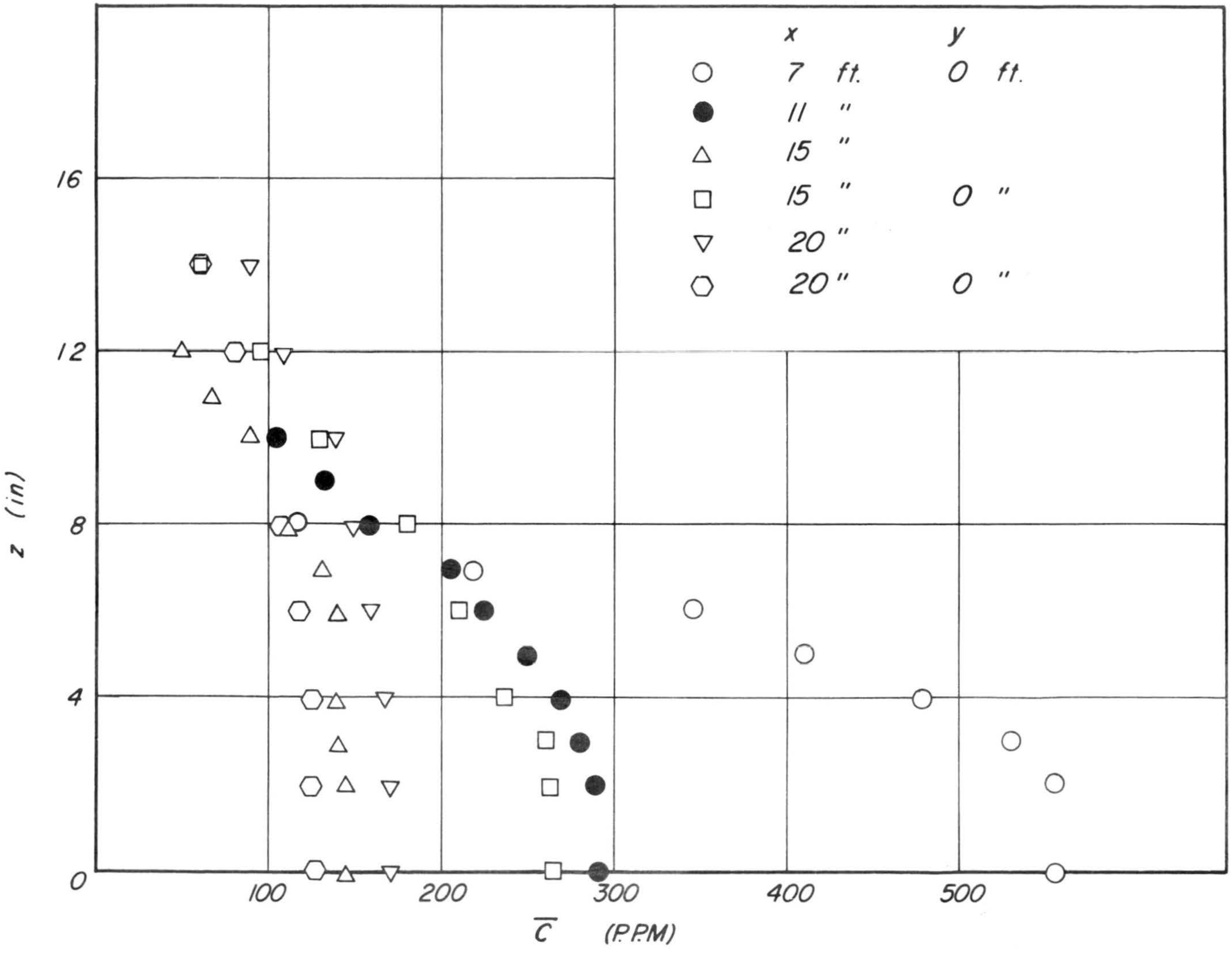


Fig. 58B Vertical gas concentration

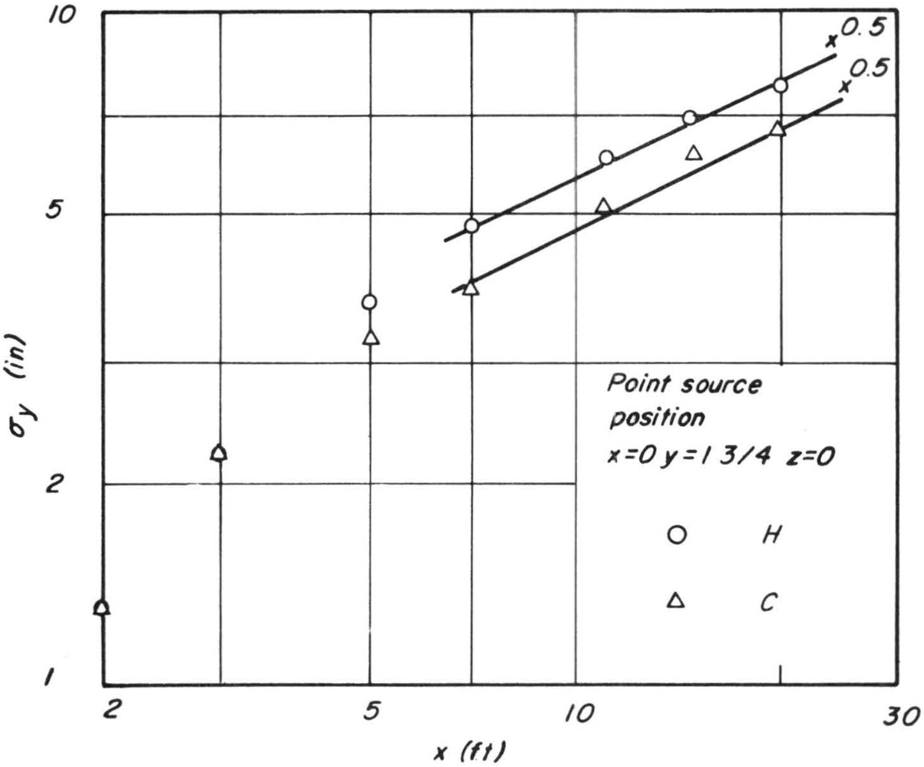


Fig. 59A Standard deviation $\sigma_y$ of horizontal gas diffusion

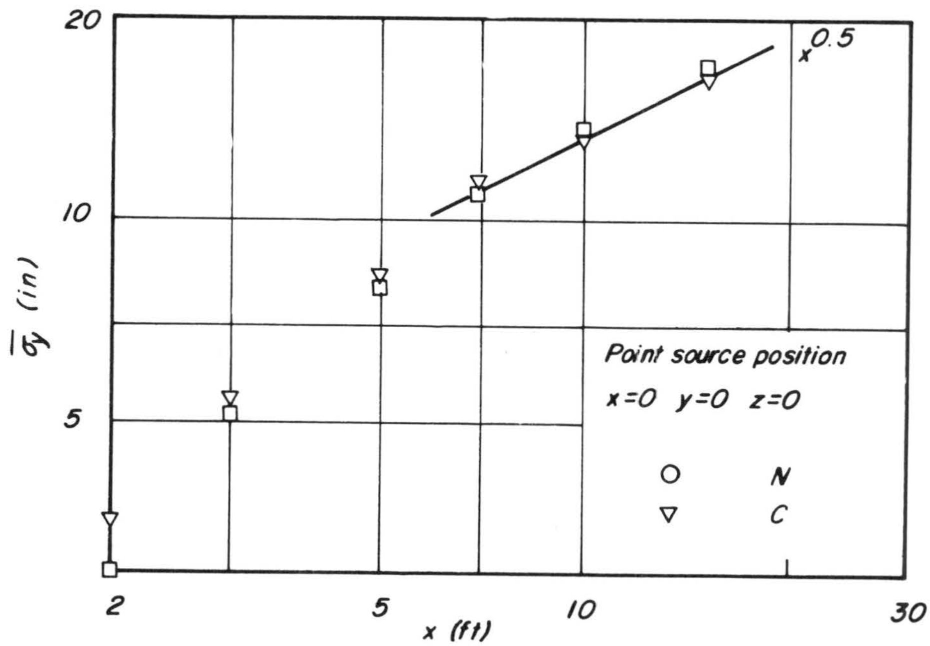


Fig. 59B Width $\overline{\sigma_y}$ between 1/2 $\overline{C}_{max}$ points of horizontal gas diffusion

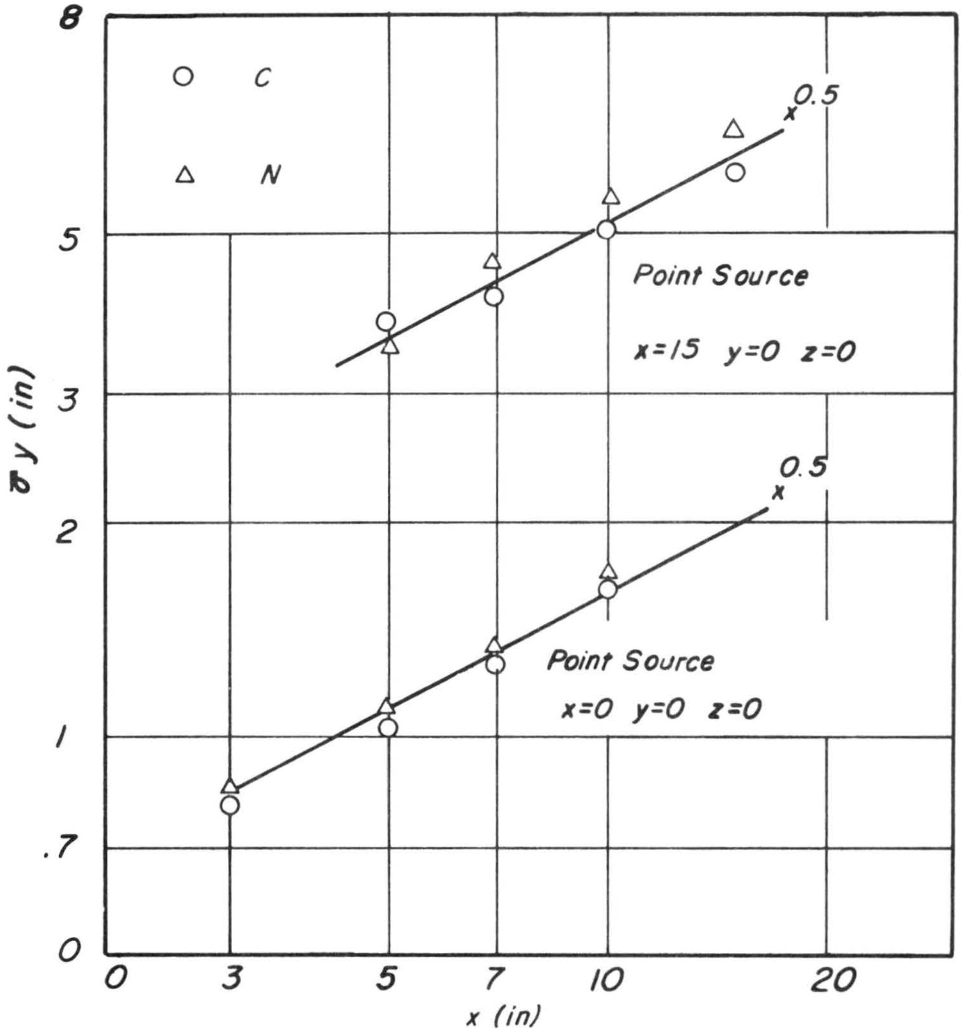


Fig. 60 Width $\overline{\sigma_y}$ between 1/2 $\overline{C}_{max}$ points of horizontal gas diffusion

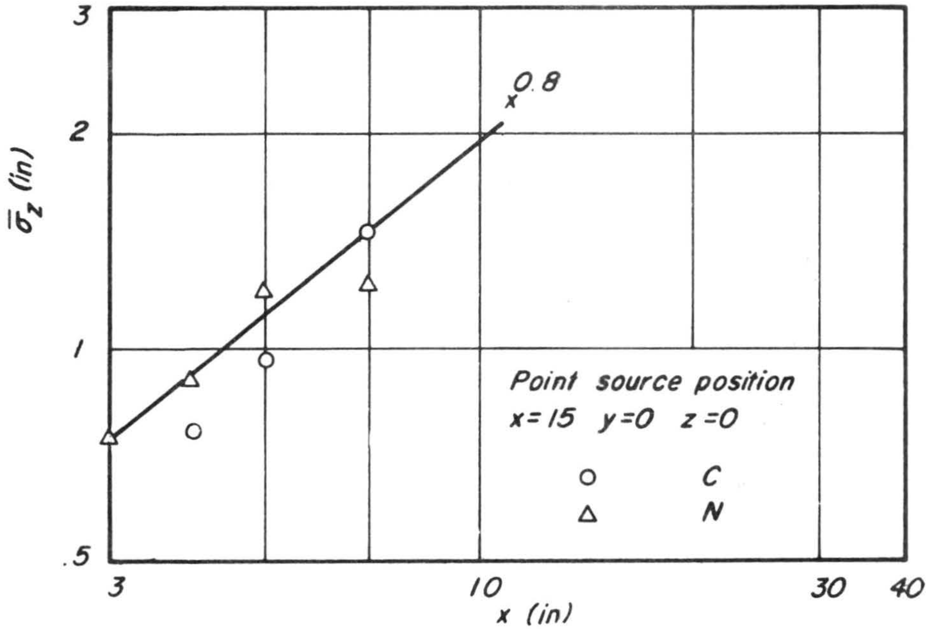


Fig. 61A Width $\overline{\sigma}_z$ between $\overline{C}_{max}$ and 1/2 $\overline{C}_{max}$ points of vertical gas diffusion in unstable (H), neutral (N), and stable (C) cases

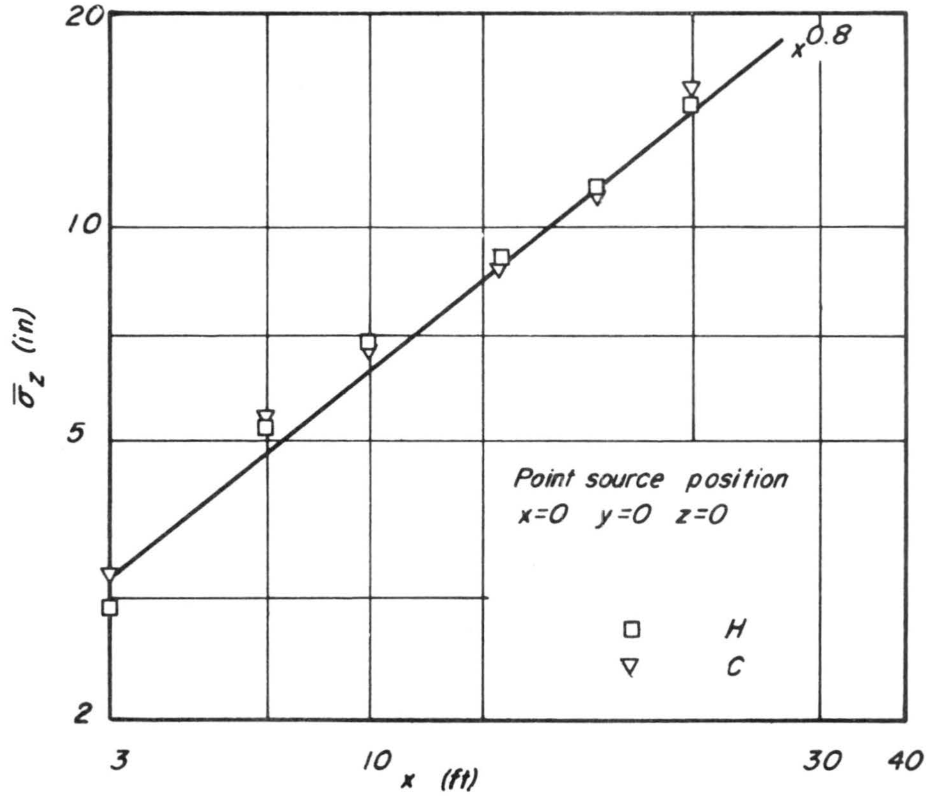


Fig. 61B Width $\overline{\sigma}_z$ between $\overline{C}_{max}$ and 1/2 $\overline{C}_{max}$ points of vertical gas diffusion in unstable (H), neutral (N), and stable (C) cases

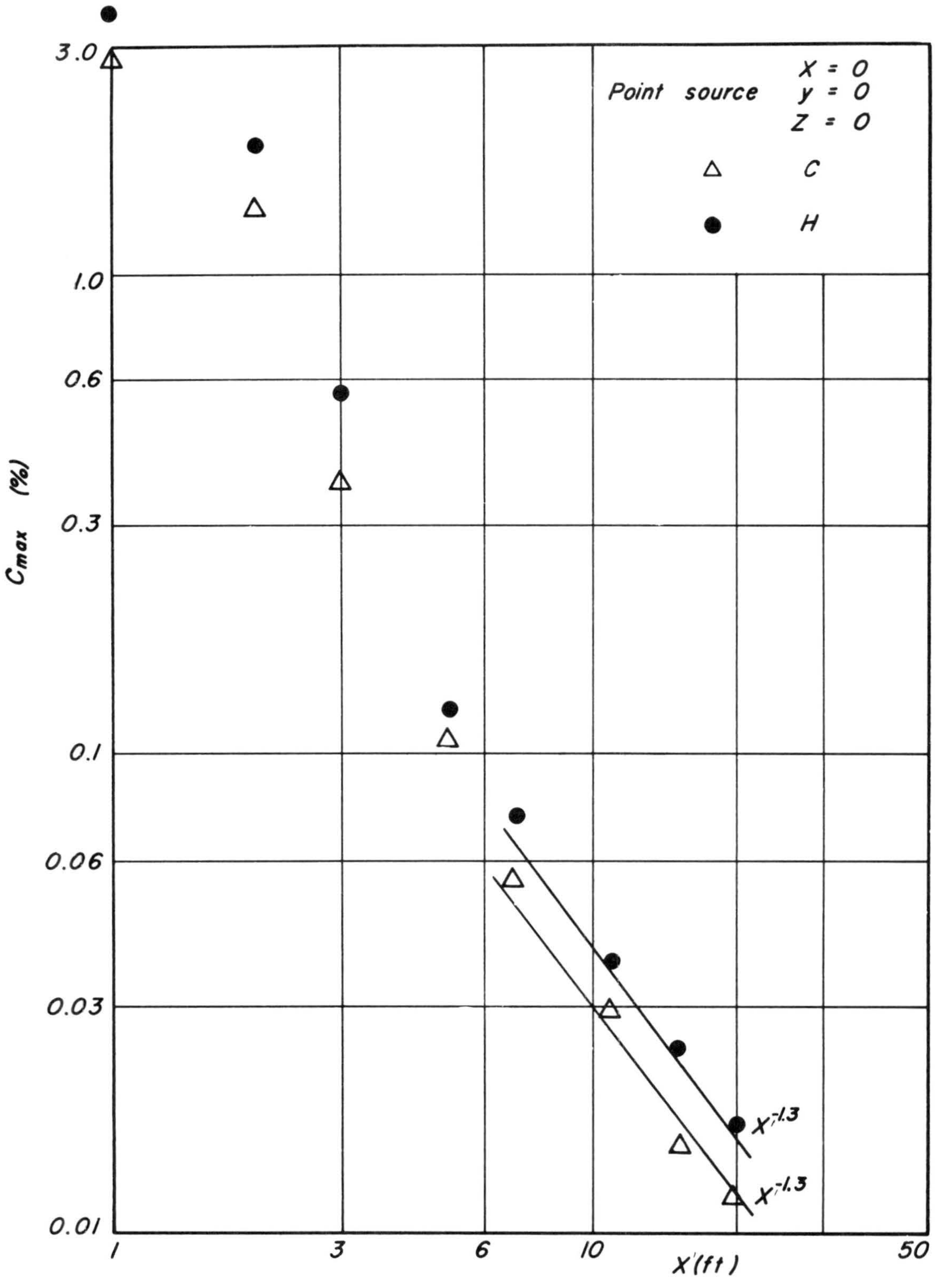


*Fig. 62 Maximum gas concentration in stable (C) and unstable (H) cases*

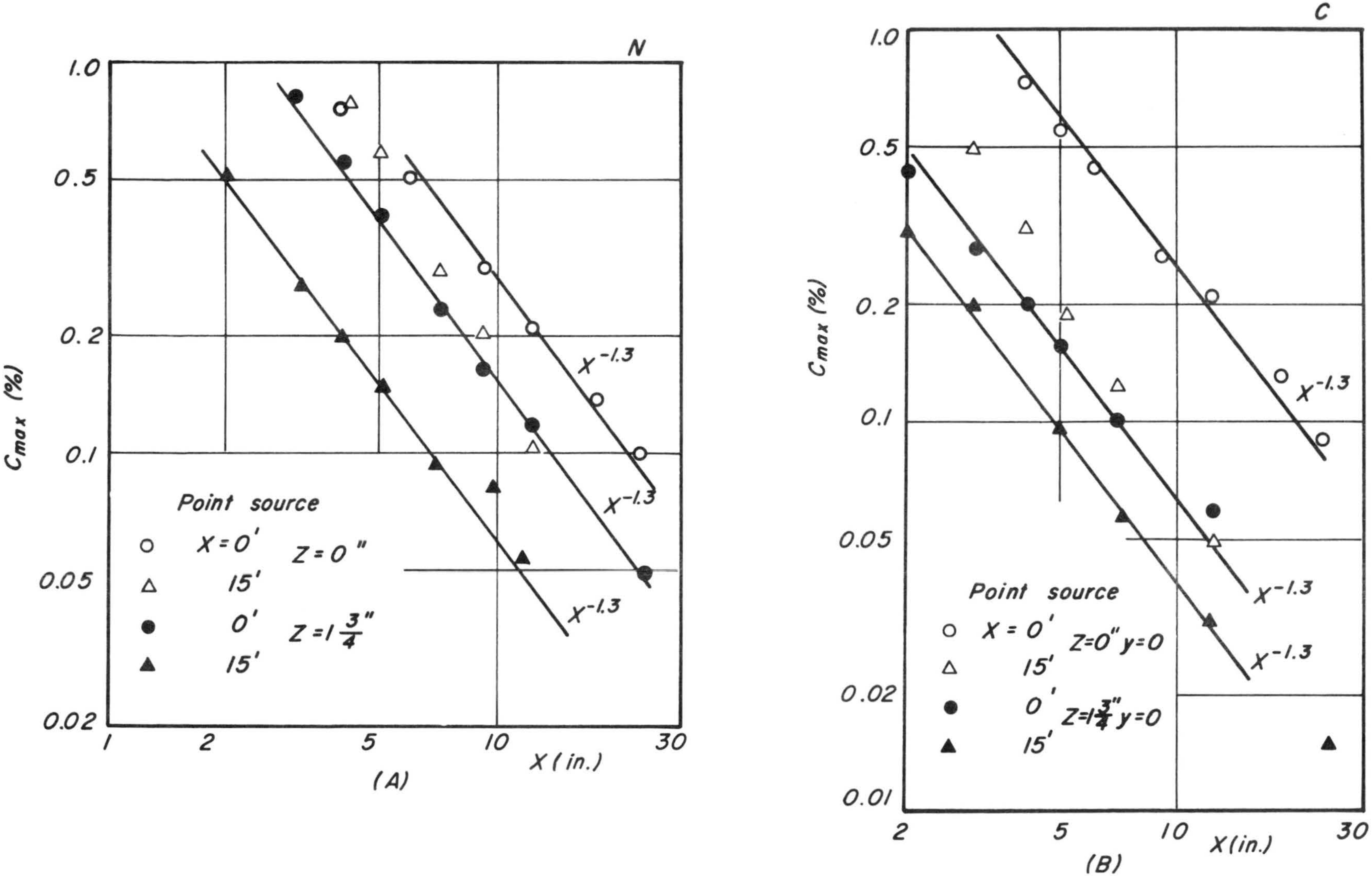


Fig. 63 Maximum gas concentration in neutral (N) and stable (C) cases

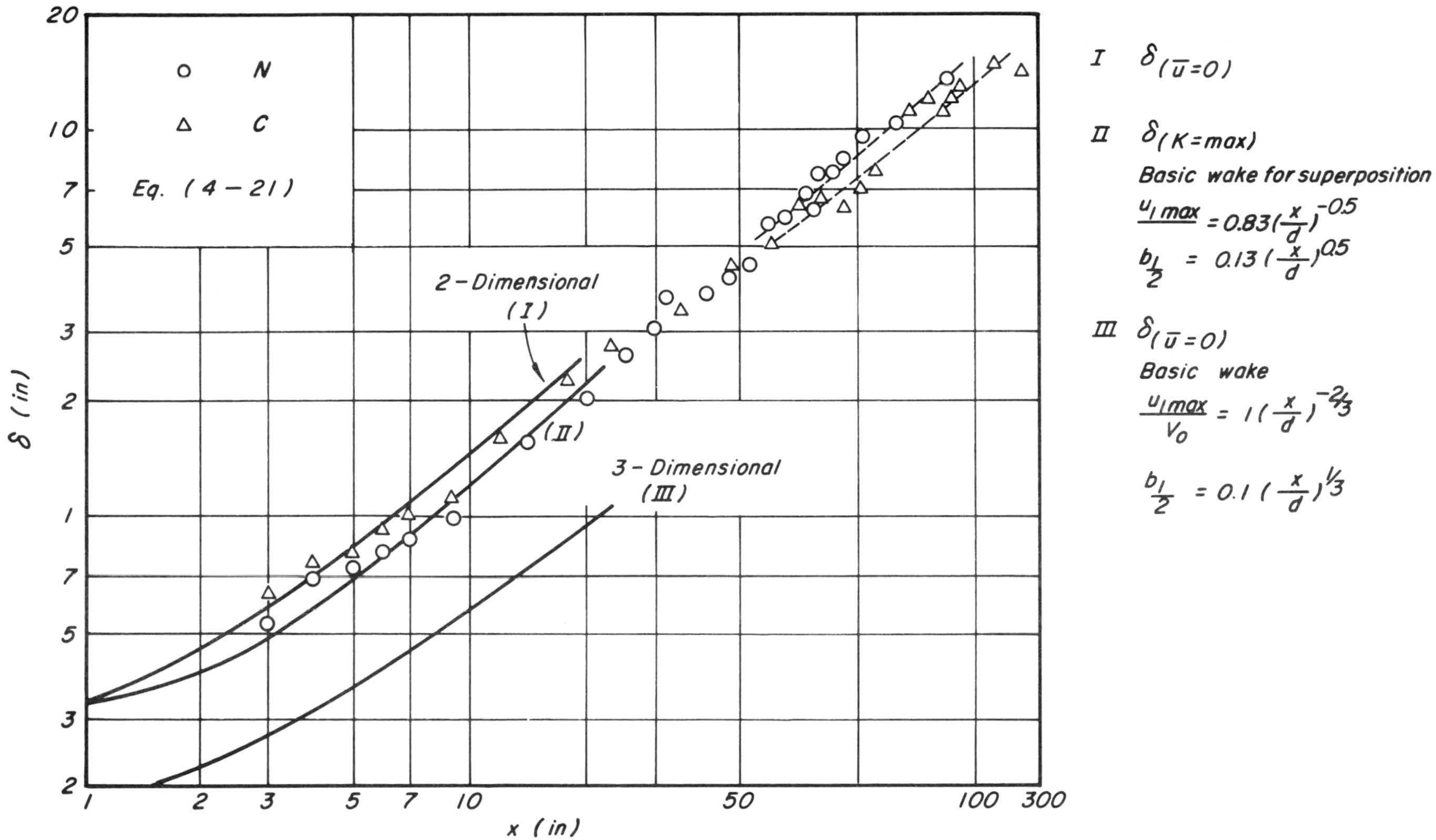


Fig. 64 Internal boundary layer height δ

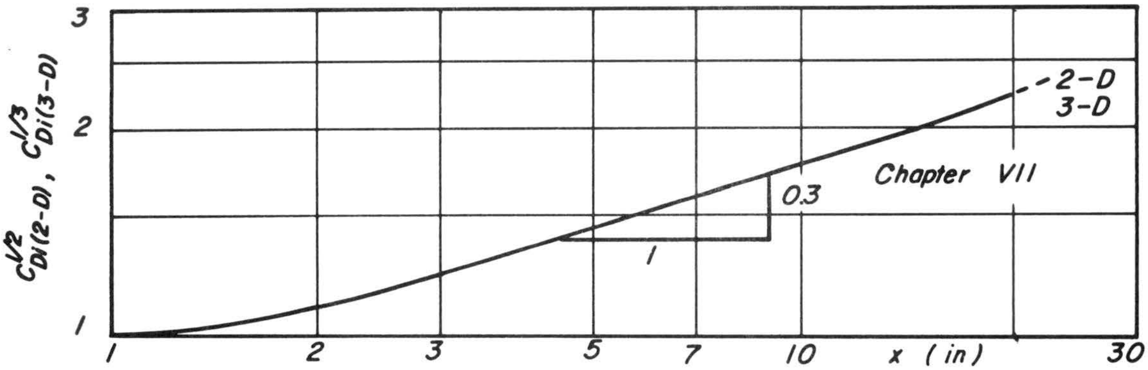


Fig. 65 Equivalent drag coefficients $\left\{C_{Di}^{1/2} = (2-D),\ C_{Di}^{1/3} = (3-D)\right\}$ the internal boundary layer

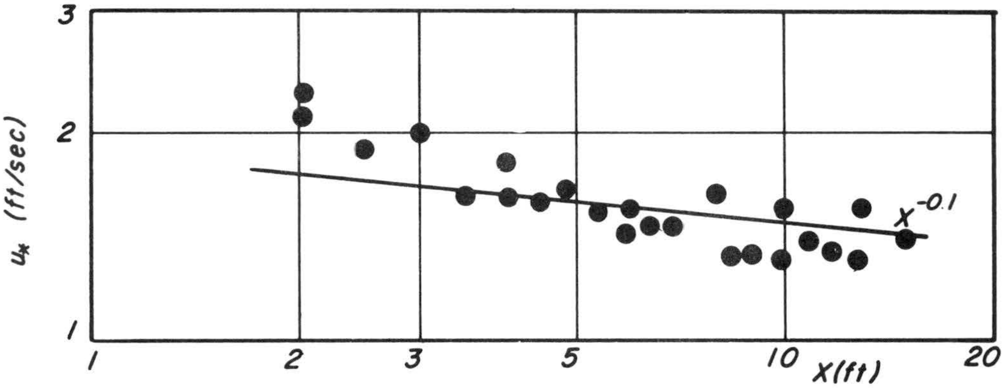


Fig. 66 Experimental data of $u_*$

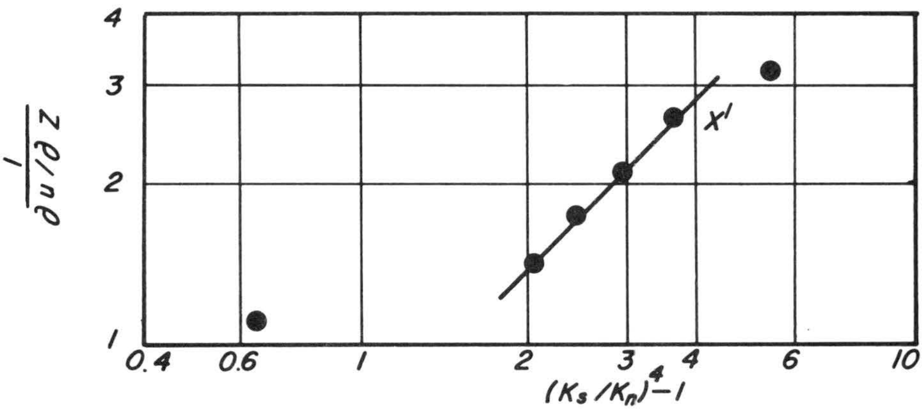


Fig. 67 Relation between $1/\partial u/\partial z$ and $\left[\left(\frac{K(\text{strat.})}{K(\text{neut.})}\right)^4 - 1\right]$ from the analytical $K_1$ and $K_2$ of Fig. 44

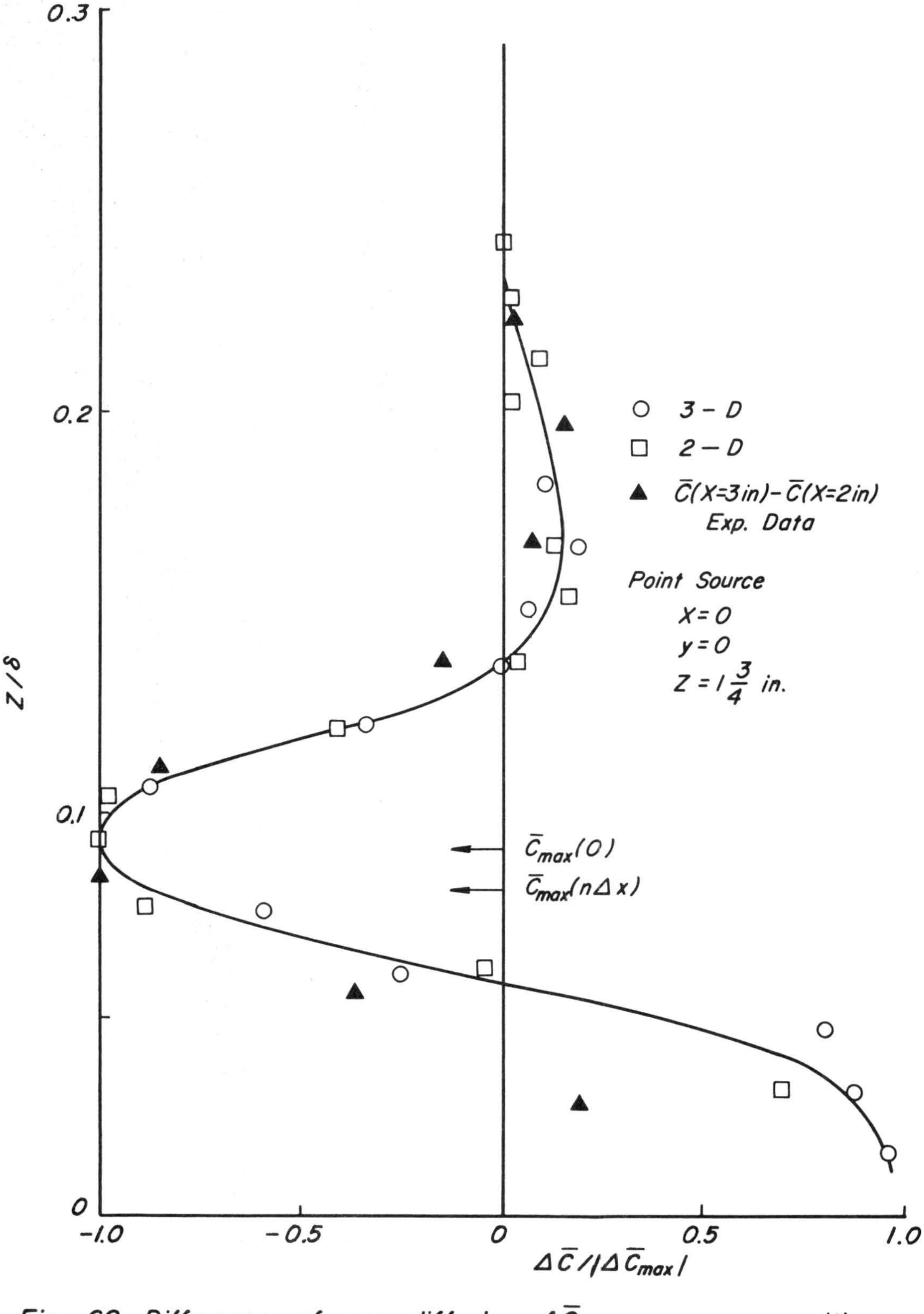


*Fig. 68 Difference of gas diffusion $\Delta\bar{C}$ near source position with analytical and experimental data*

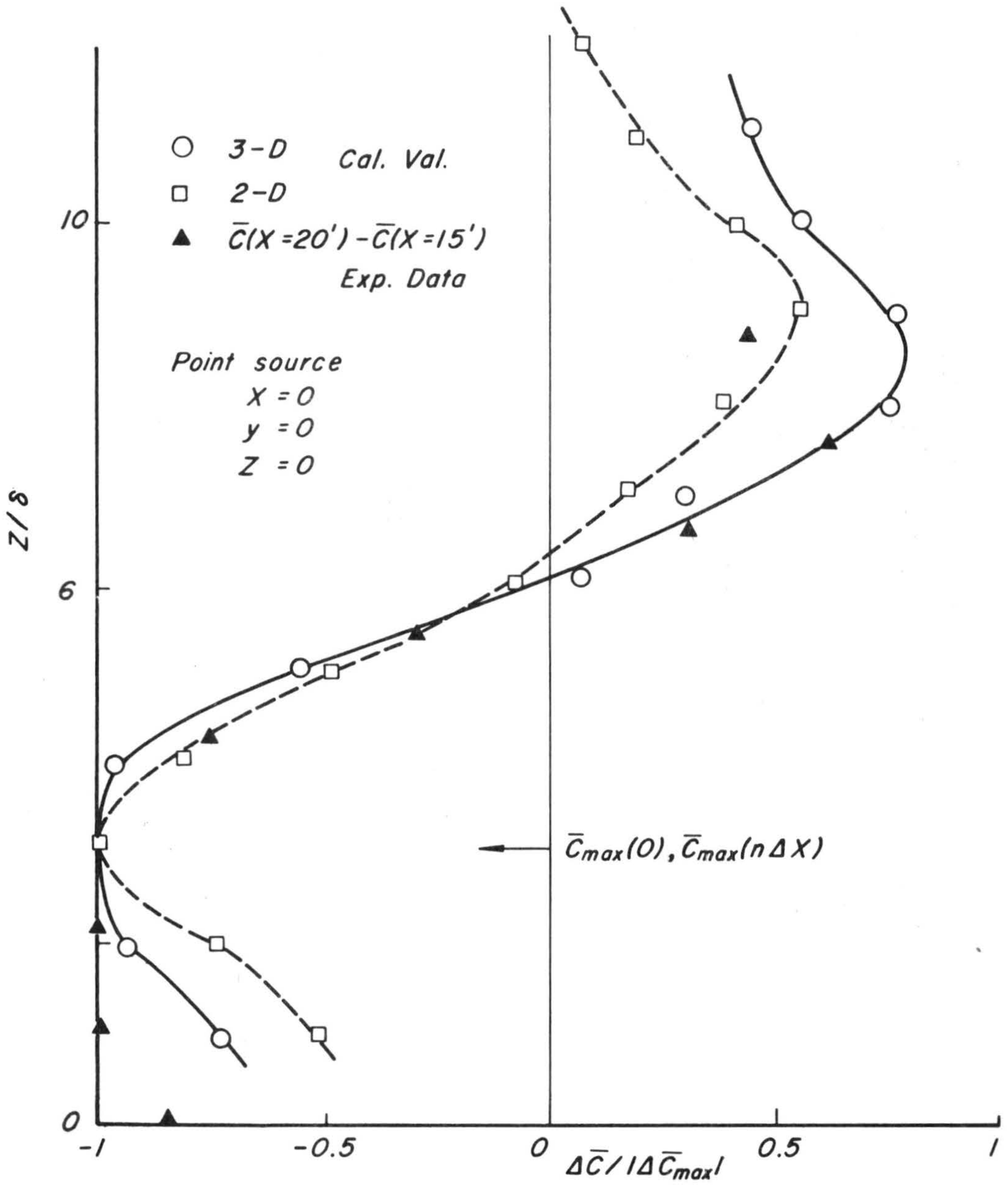


*Fig. 69 Difference of gas diffusion $\Delta\bar{C}$ in large distances from the source position with analytical and experimental data*

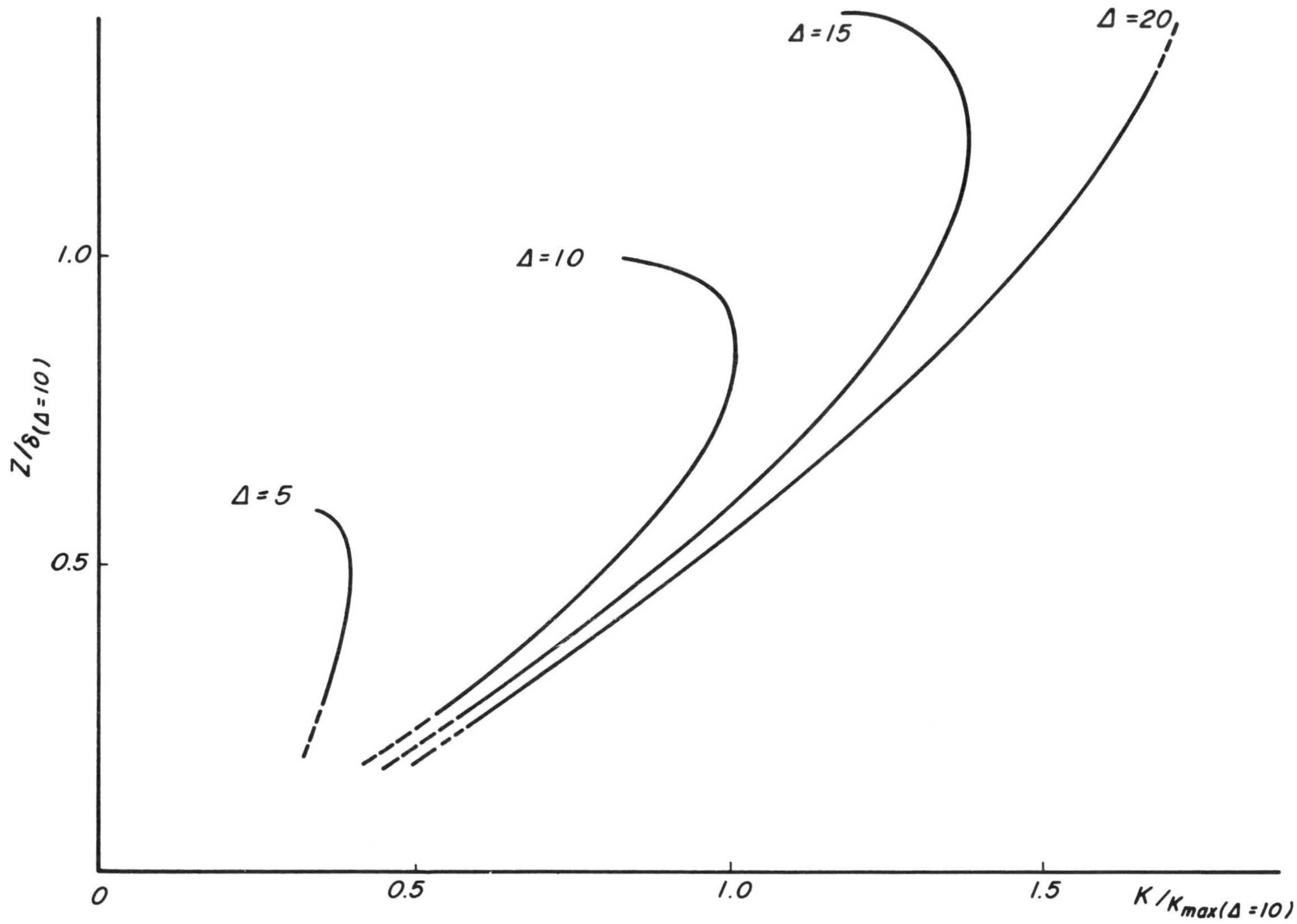


Fig. 70 Variation of coefficient of turbulent diffusion in x-direction